Orthogonal platforms to modulate, monitor, and deliver mRNA *in vivo*

A Dissertation
Presented to
The Academic Faculty

By

Kevin Lindsay

In Partial Fulfillment
Of the Requirements for the Degree
Doctor of Philosophy in Biomedical Engineering

Georgia Institute of Technology and Emory University

August, 2018

Orthogonal platforms to modulate, monitor, and deliver mRNA *in vivo*

Approved by:

Dr. Philip Santangelo, Ph.D., Advisor
Department of Biomedical Engineering
Georgia Institute of Technology

Dr. Krishnendu Roy, Ph.D.
Department of Biomedical Engineering
Georgia Institute of Technology

Dr. Brandon Dixon, Ph.D.
Department of Biomedical Engineering
Georgia Institute of Technology

Dr. Wilbur Lam, M.D., Ph.D.
Department of Biomedical Engineering
Georgia Institute of Technology

Dr. Francois Villinger, Ph.D.
Director of New Iberia Research Center
University of Louisiana Lafayette

Dr. Eric Hunter, Ph.D.
Department of Immunology
Emory University

Date Approved: July 24th, 2018

ACKNOWLEDGEMENTS

The Santangelo Lab is a small, tight knit, and hard-working group of people. I appreciate them for being a willing sounding board to my many bad and sometimes good ideas, and having the technical expertise to guide me forward. Ideas are not shut down without due consideration, and I have felt incredibly supported throughout my years as part of the team. About 8 months ago, something clicked and I felt I have hit my stride as a scientist and researcher. I love what I do, and no small part of that is due to this rich environment.

To put credit where credit is due (which there is a ton of), I will acknowledge people who helped me with each project at the beginning of each chapter. I would like to thank Phil for his openness, intellectual curiosity, technical knowhow that spans diverse disciplines, and writing the grants that allow us to do the cool stuff we do.
In general, though, shouts out to Chiara for taking the time to improve my writing and Daryl with being gracious and gratuitous beyond what is required.

I would like to say after this experience that I'm a useful part of society, or at least useful to my parents, but I doubt that is true. Maybe after the next degree?

TABLE OF CONTENTS

LIST OF TABLES

LIST OF FIGURES

LIST OF SYMBOLS AND ABBREVIATIONS

ABBREVIATIONS

Ψ - pseudouridine

CCL3 - Chemokine (C-C motif) ligand 3

CCL4 - Chemokine (C-C motif) ligand 4

CD80 – Cluster of differentiation 80

CXCL11 – C-X-C motif chemokine 11

ELISA –Enzyme-linked immunosorbent assay

ELISPOT –Enzyme-linked immunosorbent spot assay

i.m. – intramuscular

IL-1β – interleukin 1 beta

IL6 – interleukin 6

Il12b - interleukin 12b

IVT mRNA – in vitro transcribed messenger ribonucleic acid

$M^1\Psi$ - N1-5-methylpseudouridine

MTRIP- multiply-labeled tetravalent RNA imaging probes

mMTRIP-monovalent multiply-labeled tetravalent RNA imaging probes

TLR - Toll-like receptor

UTR- untranslated region

FRT - Female Reproductive Tract

mRNA - messenger RNA

PET - Positron Emission Tomography

CT - Computed Tomography

NHP - Non-human Primate

RM - Rhesus Macaque

CM - Cynomolgus Macaque (aka Crab Eating Macaque)

IM - Intramuscular

SubQ - Subcutaneous

IP - Intraperitoneal

LNP - Lipid Nanoparticle

SUMMARY

Delivering molecular immunotherapies to the necessary organs is a frequent bottleneck in translating drugs to the clinic. We directly associate adjuvants to naked mRNA in an orthogonal fashion so that sufficient and directed immune responses are elicited against the expressed antigen. We then demonstrate two non-invasive approaches - one focused on imaging and the other on mucosal delivery - that attempt to inform the discussion of mRNA delivery in large mammals. To aid in the rational design of mRNA vaccines, we developed a dual PET/near-IR based approach to non-invasively monitor mRNA trafficking longitudinally with high spatio-temporal resolution in non-human primates. This dual imaging modality approach has the potential to link systemic scale events with cellular level details. We use this PET/CT based approach to monitor mRNA trafficking after transfection of the female reproductive tract (FRT) epithelium. Using antibody modifications, we can generate robust levels of the HIV broadly neutralizing antibody PGT121 that reach neutralizing concentrations within hours and persist for weeks in sheep and non-human primate animal models.

PREFACE

Using mRNA in therapeutic and vaccine applications is currently in vogue. Cost effective and robust production methods, excellent therapeutic index profiles, flexible and interchangeable design parameters, and fast production of encoded protein, make mRNA particularly attractive for transgene production *in vivo*. The biotech industry has taken note, and there are numerous independent companies and subsidiaries of larger ones, that focus exclusively on mRNA. While the promise is large and the field is moving quickly (as seen by the increase in mRNA clinical trials), there are numerous gaps in mechanism, design, immune interaction, and delivery that will undoubtedly require attention for downstream clinical applications.

At the Santangelo lab, we bring light to these gaps in knowledge, while providing engineering platforms that assist in investigating them further. With the ability to monitor at the level of single molecules and cells, we are able to provide insight on spatial, temporal, and kinetic determinants of mRNA efficacy, at the cellular level (sub-cellular trafficking, transcript stability, innate immune sensors and activation, and cellular entry mechanisms) and from a systems level (biodistribution, targeted delivery to specific organs, and immune interactions). Because we always keep one eye on translationally relevant questions, a guiding principal of our work is simplification. The more moving parts a technique or formulation has, the probability increases for unforeseen interactions and complications *in vivo*, resulting in downstream regulatory approval hurdles.

This thesis provides a chronological snapshot of some of the work I have pursued during my research. Although the projects are at first glance somewhat disparate, shared principals of simplification (orthogonal labeling of mRNA) and non-invasiveness (whole

body imaging, mucosal delivery) are evident throughout. I believe the implications of the work are quite powerful. As a result, the data and techniques presented here might generate just as many questions as they provide answers.

- The first chapter will discuss a direct means to orthogonally conjugate immune adjuvants onto mRNA based vaccines, without use of carrier particles. Specific and tailored memory immune responses, both humoral and cellular, are elicited.

- I will then describe a positron emission tomography (PET) based approach to monitor mRNA vaccine trafficking in the days following administration in non-human primates (Chapter 2). The sensitivity of the technique is on the order of 10ng of mRNA per mL.

- Lastly, I will discuss my most recent work involving mucosal aerosol delivery of antibody encoding mRNA to the female reproductive tract of sheep and non-human primates. Expression of high concentrations of antibody at the site of infection occurs within a few hours, resides in tissue for at least a month, and functionally neutralizes virus.

I promise to you the reader that I will resist my loquacious side and present the information in a succinct manner. As the third project is still a work in progress, I will also be upfront of what remains to be completed in future studies.

I will start with a quick introduction to mRNA in therapeutic and vaccine contexts.

Synthetic mRNA uses for therapeutic and vaccination purposes

The use of mRNA as a biotechnology for therapeutic purposes has exploded in recent years, directly benefitting from the mechanistic insights garnered from siRNA therapy development and production scale increases through Good Manufacturing Practices (GMP). There are tens of clinical trials that are ongoing or have been completed that use mRNA as a therapeutic, and numerous pharmaceutical companies have entered this blossoming field.

Although they have received the great majority of focus and attention since 1990 when Wolf et al demonstrated in vivo delivery of plasmid DNA and mRNA[1], translational DNA vaccine approaches have been limited by low immunogenicity in humans compared to animal models and AAV initiated immune response against the vector itself. As a vaccine, mRNA has intrinsic advantageous attributes that make it attractive: an excellent safety profile due to transient protein expression with naturally occurring cellular breakdown pathways; no possibility of nuclear insertion; cellular processing that mimics viral transcripts; robust, cell free production methods; rapid manufacturing - on the order of days to respond to need; flexibility in delivery by viral, non-viral, or cellular vectors; focused immune responses to specific epitopes, similar to subunit vaccines[2] ; and perhaps most critically, mRNA vaccines have displayed induction of humoral and cell-mediated immunity in numerous disease models.

Some other benefits of mRNA, include:

→ mRNA can be manufactured without use of cells: this allows rapid mRNA synthesis at scale and cost. This also confers a certain flexibility, as all aspects of the process (i.e. modified nucleotide bases) can be controlled. Compare this to proteins and viruses, which require in vitro expression in cells with downstream purification.

→ Protein expression within 4 hours: this is in contrast to DNA plasmid based methods that have peak expression times around 36 hours. RNA peak expression occurs at around 12 hours.

→ Expression is transient and self-limited: depending on the application, if we don't want the encoded protein expression for months or years.

→ Stable storage at room temperature: in lyophilized form, RNA can be stably stored for years without negatively impacting mRNA function. Compare this to protein, which must be stored in cold chain storage conditions to maintain stability.

→ Glycosylation patterns follow that of the host: since host cells are translating the synthetic mRNA, post-translational modifications will also be included in the final form of the expressed protein.

When IVT mRNA is delivered, a characteristic innate response pattern is elicited. This innate response stimulation is mainly due to mRNA interacting with anti-viral sensors located in endosomal compartments (TLRs) and other receptor families in the cytoplasm (RIG-I-like receptors (RLRs) and NLRs). These pattern recognition receptors (PRRs) vary not only in cellular compartment, but also in the mRNA elements they recognize. Although mRNA is single stranded by design and as such is recognized by ssRNA detectors TLR7 and TLR8, hairpins in the secondary structure can result in dsRNA segments that bind TLR3. In a similar manner, cytoplasmic PRRs recognize both ssRNA and dsRNA elements. The degree of innate immune stimulation can be controlled through the use modified uridine bases. This innate immune abrogation is demonstrated in Chapter 1.

With the ability to tune the intrinsic immunogenicity of synthetic mRNA, it can be used for purposes of protein replacement therapy, or as a vaccine. In the case of protein replacement therapy, the goal is to express the encoded protein, without immune

stimulation, as innate immune responses will shut down translation, decreasing the ultimate amount of encoded protein expressed by cells. Thus, protein expression should be maximized and immunity minimized. In the case of vaccines, a balance between translation of encoded antigen and innate immune stimulation is required. If the innate stimulation is too low, then the immune response will not be robust enough to establish an adaptive immune response. In a similar manner, if innate stimulation is too high, then not enough antigen expression will occur for establishment of adaptive immune responses. Table 1 lists numerous applications where mRNA is being utilized, both as a therapy and for vaccination.

Table 1: Therapeutic mRNA applications. This table lists numerous approaches and applications that are currently being investigated using synthetic mRNA. Table is from: Sahin, U., Karikó, K. & Türeci, Ö. mRNA-based therapeutics — developing a new class of drugs. *Nat Rev Drug Discov* **13,** 759–780 (2014).

Phase	Method	mRNA encoding	Application
Cancer immunotherapy			
Preclinical	Direct injection of mRNA	CEA[4], NY-ESO[98], gp100 (REF. 8), TRP2, tyrosinase[99], PSA and STEAP[62]	Melanoma[8], prostate cancer[62]
	Injection of DCs transfected *ex vivo*	MUC1 (REF. 10), survivin[235], iLRP[236]	Haematological malignancies[235,236]
	Injection of T cells transfected *ex vivo*	CAR-HER2/neo[237], CAR-CD19 (REFS 131,132,238), CAR-mesothelin[129,132]	Ovarian cancer[237], lymphoma[131], leukaemia[131,132,238], mesothelioma[129]
Clinical	Direct injection of mRNA	Melan-A, tyrosinase, gp100, MAGEA1, MAGEA3 and survivin[16] MUC1, CEA, HER2, telomerase, MAGEA1 and survivin[17]	Melanoma[16], renal cell carcinoma[17]
	Injection of DCs transfected *ex vivo*	PSA[12]; telomerase[15]; CEA[13,14]; TriMix, MAGEA3, MAGEC2, gp100 and tyrosinase[18,89,90,239,241]; gp100 and tyrosinase[117]; WT1 (REF. 87)	Prostate cancer[12,15], pancreatic cancer[13], metastatic malignancies[14], colon cancer[14], melanoma[18,89,90,117,239,241], leukaemia[87]
	Injection of T cells transfected *ex vivo*	CAR containing mesothelin-targeted antibody[240]	Mesothelioma
Infectious disease vaccines			
Preclinical	Direct injection of mRNA	Influenza-associated Ag[3,100,133,140], TB-associated Hsp65 (REF. 242), RSV-Ag[101,140]	Influenza[3,100,133,140], tuberculosis[242], respiratory tract infection[101,140], tick-borne encephalitis[7,140]
Clinical	Injection of DCs transfected *ex vivo*	TriMix, HIV-specific Gag, Vpr, Rev, Tat and Nef mRNA[115,134,135]	HIV
Allergy tolerization			
Preclinical	Direct injection of mRNA	Allergens causing type I allergy e.g. peanut Ara h 2.02, ovalbumin, grass pollen Phl p 5, dust mite Der p 2 (REFS 147,148)	Allergies for peanut, egg white, grass pollen and dust mite[147,148]
Protein replacement			
Preclinical	Direct injection of mRNA	Vasopressin[2], AAT[6], EPO[25,26], SPB[25], FOXP3 (REF. 27), HSV1-TK[21], VEGFA[23], BAX[19]	Diabetes insipidus[2], anaemia[25,26], congenital lung disease[25], asthma[27], myocardial infarction[23], melanoma[19]
	Injection of DCs transfected *ex vivo*	IL-4 (REF. 24)	Autoimmune diabetes[24]
	Injection of monocytes, macrophages and MSCs transfected *ex vivo*	IL-10 (REF. 22), P-selectin glycoprotein ligand 1, SLeX[22,28]	Autoimmune myocarditis[22], inflammation[28]
Genome engineering, gene editing			
Preclinical	Transfection *ex vivo*	Sleeping beauty[177,178,181], piggyBac[181,182] and Tol2 (REFS 179,180) transposases	Genome engineering
		Zinc-finger nucleases[172]	Gene editing, engineered animal models
		TALE nucleases[171,244]	Gene editing, engineered animal models
		RNA-guided Cas9 nuclease[170,173–176]	Gene editing, engineered mice[170,173], rats[175], rabbits[174] and macaques[176]
Genetic reprogramming of cells, tissue engineering			
Preclinical	Transfection *ex vivo*	Transcription factors[157–159,161,246,247], progerin[161]	Generating iPSCs[157–159,161,246,247], model diseases[161]

Throughout this thesis, the 3'UTR of the synthetic mRNA is used to anneal oligos that contain adjuvants (Chapter 1), dyes (Chapter 2), or radionuclides (Chapter 2 and 3). This binding to the UTR occurs without inhibition of mRNA translation potential (Chapter 2). We prefer this direct method of RNA labeling because it allows us to work with, but not be dependent on the use of particles and carrier proteins during delivery. In fact, I hope after reading this thesis that it becomes clear these carriers are not nearly as required as might be assumed. In our mind, naked synthetic mRNA facilitates the transition from the bench to translational research, as it's safety is *in vivo* is well established.

CHAPTER 1

Tuning the immune response to synthetic mRNA

The work presented here is under consideration as:

In vitro transcribed messenger RNA vaccines with programmable stimulation of innate immunity. Kristin H. Loomis†[a], **Kevin E. Lindsay[a]**, Chiara Zurla[a], Sushma M. Bhosle, Daryll A. Vanover, Emmeline L. Blanchard, Jonathan L. Kirschman, Ravi V. Bellamkonda††, Philip J. Santangelo*

[a] The authors contributed equally

Summary

In vitro transcribed (IVT) mRNA is an appealing platform for next generation vaccines, as it can be manufactured rapidly at large scale to meet emerging pathogens. However, its performance as a robust vaccine is strengthened by supplemental immune stimulation, which is typically provided by adjuvant formulations that facilitate delivery and stimulate immune responses. Here, we present a strategy for increasing translation of a model IVT mRNA vaccine while simultaneously modulating its immune-stimulatory properties in a programmable fashion, without relying on delivery vehicles, which we believe will allow for more controlled and standardized vaccination studies. Substitution of uridine with the modified base N1-5-methylpseudouridine reduces the intrinsic immune stimulation of the IVT mRNA while enhancing antigen translation. Tethering adjuvants to IVT mRNA through antisense nucleotides boosts the immuno-stimulatory properties of adjuvants *in vitro,* without impairing transgene production or adjuvant activity. *In vivo*, intramuscular injection of tethered IVT mRNA-TLR7 agonists leads to enhanced local immune responses, and to antigen-specific cell-mediated and humoral responses. This system represents a potential

platform compatible with any adjuvant of interest and it enables specific programmable stimulation of immune responses.

Background

Long manufacturing-times associated with current vaccine development impede rapid responses to quickly mutating and emerging pathogens. Synthetic messenger RNA produced via *in vitro* transcription (IVT mRNA) is a platform for next generation vaccines that has the capacity for rapid and large-scale manufacturing. As a vaccine, mRNA presents several attractive advantages: an excellent safety profile due to transient protein expression within hours of delivery, no nuclear insertion, cellular processing that mimics viral transcripts, immune responses to specific epitopes, and, most critically, induction of humoral and cell-mediated immunity [2–5]. IVT mRNA vaccines have recently been investigated in pre-clinical studies for several diseases, including influenza [6], Zika [7], and cancer [8]. Several anti-cancer mRNA vaccines have entered clinical trials, where the ease of manufacturing enables personalized treatment. However, no formulation has of yet significantly improved patient outcomes [8].

IVT mRNA delivered to host cells is translated by the cellular machinery into antigenic proteins. Concurrently, IVT mRNA activates pattern recognition receptors (PRRs) that have evolved as anti-viral RNA sensors to detect single and double-stranded transcripts. In general, PRRs can be classified according to their location within the cell: Toll-like receptors (TLRs) 3, 7, and 8 bind ssRNA and dsRNA in the endosomal compartment [9,10], while cytoplasmic detection largely relies on RIG-I like receptors (RLRs) and Nod like receptors (NLRs).TLR signaling causes translocation of pro-inflammatory transcription factors (ie NF-kappaB, IRF7, IRF3) to the nucleus, ultimately releasing Type 1 IFNs and pro-inflammatory cytokines [3,11]. These secreted IFNs and cytokines act in an autocrine and paracrine fashion to sensitize nearby cells to nucleic acids.

TLR expressing antigen-presenting cells (APCs) such as dendritic cells (DCs) and macrophages are the orchestrators of the innate immune response and are also responsible for linking the innate and adaptive immune responses upon migration to draining lymph nodes and activation of T and B cells. The type of antigen specific effector and memory responses that are generated largely depend on the cytokine profiles released by cells during the innate response: for example IL12 and IFNγ promote T_H1 and cytotoxic T lymphocyte (CTL) pathways, while IL4 and IL6 promote humoral responses [12].

mRNA has characteristic innate immune response profiles with a demonstrated intrinsic adjuvant ability. Unmodified IVT mRNA has been shown to elicit robust type I interferon responses [13,14], which can activate protein kinase R (PKR) and 2'-5'-oligoadenylate synthetase like (OAS-L), resulting in reduced antigenic protein levels [15] as a consequence of protein translational inhibition and RNA decay. High interferon responses have also been linked to weak cell-mediated immunity using both an interferon alpha receptor knockout animal model [13] as well as an animal model treated with an interferon receptor-blocking antibody [14].

As the innate immune responses elicited for an IVT mRNA vaccine influence the yield of antigenic protein as well as the nature of specific memory immune responses, there has been a significant effort to study the intrinsic immunogenicity of IVT mRNA and the use of adjuvants in vaccine formulations to modulate immunogenicity. Substitution of uridine with the modified bases pseudouridine (Ψ) [16,17] or N1-5-methylpseudouridine ($M^1Ψ$) [18,19] in IVT mRNA has been shown to reduce innate immune activation and to increase transgenic protein synthesis. However, reduced innate immune responses to modified IVT mRNAs often required the use of specific adjuvants to grant supplemental immunogenicity by

controlling innate cytokine release [20]. The potential benefits of utilizing adjuvants include dose and frequency reduction, vaccine response broadening, rapid response, and overcoming immune senescence [21].

To date, the prevailing approach for complexing adjuvants with nucleic acids is using cationic carriers such as protamine or nanoparticles. For example, researchers at CureVac demonstrated the efficacy of an influenza vaccine consisting of a naked antigen encoding mRNA (unmodified RNA) and mRNA associated with protamine, which resulted in both B and T cell-mediated responses [22,23]. Another recently reported $M^1\Psi$ modified IVT mRNA vaccine against the Zika virus utilized a cationic lipid nanoparticle as a delivery vehicle. Different disease target for IVT mRNA vaccination may require the development of unique adjuvant and delivery formulations to yield protective immune responses. The main challenge in the successful design of IVT mRNA vaccines is the development of a versatile platform able to grant high antigenic protein expression while inducing controlled and specific robust memory immune responses. Ideally, this strategy should not rely on any delivery vehicle formulation to allow for a controlled and uniform stimulation of the immune system.

In this study, we describe an IVT mRNA-based vaccine platform that enables modular tethering of small molecule adjuvants for a programmed stimulation of innate immunity that does not solely rely on delivery vehicle formulations. An IVT mRNA encoding for the well-established cytoplasmic ovalbumin antigen (OVA) was selected as a model vaccine. To tether small molecule agonists to IVT mRNA, we modified the multiply-labeled tetravalent RNA imaging probes (MTRIPs) design pioneered by Santangelo *et al.* [24]. MTRIPs (multiply labeled tetravalent RNA imaging probes) consist of four RNA-targeting 2'-O-Methyl based oligonucleotides assembled on a neutravidin core. MTRIPs were

utilized in the last decade to study endogenous [24–31] and exogenous RNA [15,32] dynamics via fluorescence microscopy without hindering translation or affecting stability [15]. Here, we generated monovalent MTRIPs (mMTRIPs) by covalently linking single RNA-targeting oligonucleotides to free amines on a Neutravidin core. Four different oligos were selected, each targeting a different region in the 3' UTR of the IVT mRNA. We confirmed that mMTRIPs hybridization to IVT mRNA did not significantly influence transgene production nor alter innate immune activation. Previous studies demonstrated that the available biotin binding sites can be utilized to perform an array of reactions, such as strand displacement and exchange [33]. Here, the four available biotin binding sites on the neutravidin core were utilized to conjugate biotinylated adjuvants, offering a flexible platform for the delivery of small molecule agonists. To selectively stimulate TLR2 and TLR7 pattern recognition receptors we utilized two well-characterized small molecule agonists. The TLR2 agonist PAM2CSK has been found to drive development of Type 2 helper T cell responses [34], promote T helper cell longevity, and reduce the activation threshold for T cell receptor activation [35–37]. TLR7 agonists – in this case CL264 - enhance Type 1 helper T cell and cytotoxic T cell responses [38,39]. TLR7 activation has been shown to enhance the immunogenicity of influenza [40,41] and other vaccines [39,42,43].

First, we abrogated the intrinsic innate response profile of OVA mRNA *in vitro* through $M^1\Psi$ base incorporation, which also led to enhanced production of the transgene protein. Next, we demonstrated that tethering TLR agonists to mRNA can stimulate either the extracellular PRR TLR2 or the endosomal PRR TLR7 *in vitro* in transfected RAW264.7, a murine-derived macrophage cell line used as a model system, as it produces robust inflammatory responses when challenged by agonists [44].

Last, we monitored the cellular and humoral immune responses following murine intramuscular (i.m.) injection of TLR7 agonists tethered to IVT mRNA. Since APCs, which should ideally be targeted and activated, have a strong proclivity for naked mRNA uptake upon intramuscular or intradermal injection, no carriers or formulations were utilized for delivery. We demonstrated that agonist-tethered mRNA increased innate immune responses and resulted in OVA antigen specific cell mediated and humoral responses.

Our results indicate that this strategy enables stoichiometric control of the nucleic acid to adjuvant ratio, offering a more robust innate immune stimulation than mRNA and adjuvants delivered as a cocktail (*i.e.* untethered), likely because of a local increase of the adjuvant's concentration at the site of injection. This promotes a stronger and longer-lasting localized effect. This system enables specific programmable stimulation of immune responses and represents a platform potentially compatible with any adjuvants of interest for future IVT mRNA vaccine design readily applicable to intramuscular delivery.

Effects of modified uridine base substitutions on protein expression and immunostimulatory properties of IVT mRNA

We first aimed to attenuate the innate response profile induced by mRNA transfection, while maintaining high protein expression *in vitro*. Substitution of uridine with the modified bases pseudouridine (Ψ) [16,17] or N1-5-methylpseudouridine ($M^1Ψ$) [18,19] in IVT mRNA can reduce innate immune activation and increase transgenic protein synthesis. We therefore synthesized three OVA expressing IVT mRNAs identical in sequence but incorporating either unmodified bases, or substituting Ψ or $M^1Ψ$ for uridine. To evaluate innate immune activation, RAW 264.7 macrophage cells were transfected with IVT mRNA using Lipofectamine 2000 (L2K), and total RNA was isolated and assayed for gene expression using a mouse antiviral qRT-PCR array. This array consists of primer assays for genes

associated with immune responses to exogenous RNA, such as viral RNA. As expected, IVT mRNA composed of unmodified bases led to the highest upregulation of interferon signaling and stimulated genes, while IVT mRNA incorporating $M^1\Psi$ was less immune-stimulatory than IVT mRNA incorporating Ψ (Figure 1.1 A-C). Specifically, broad and potent interferon signaling and response genes, including IFNα2, IFNβ1 and Mx1, were greatly downregulated using $M^1\Psi$ modified bases.

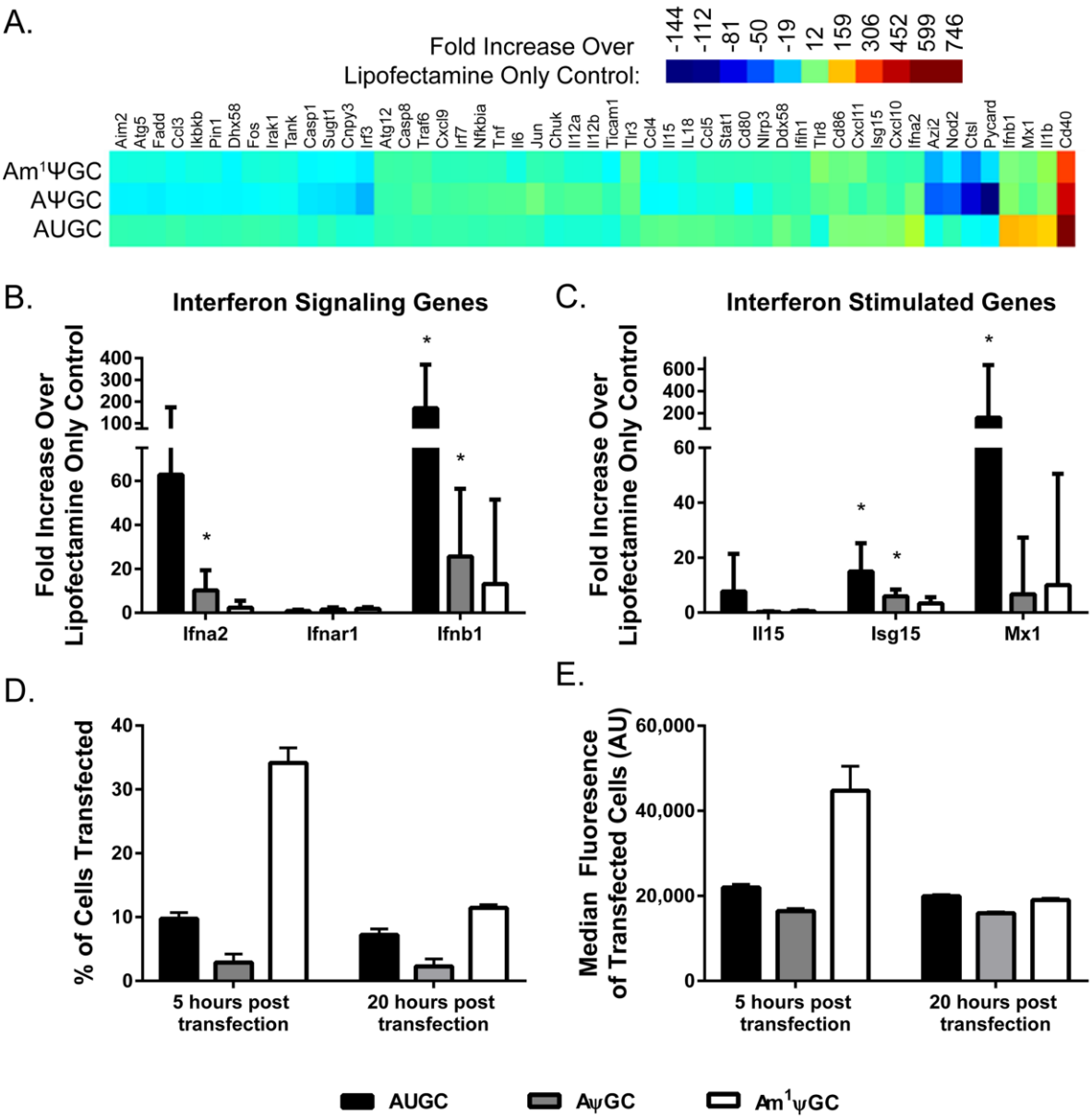

Figure 1.1: Effects of modified uracil base substitutions in IVT mRNA on cellular innate immune responses and transgene production. (A) Heat map showing gene expression of RAW264.7 cells following transfection with OVA IVT mRNA composed of unmodified bases (AUGC), and incorporating either pseudouridine (AΨGC), or 1-methyl pseudouridine ($Am^1ΨGC$). IVT mRNA was delivered using Lipofectamine-2000. Gene expression for each condition is shown as a fold increase over cells treated with lipofectamine only (L2K). Fold increases of (B) common interferon signaling genes: interferon alpha 2 (Ifna2), interferon alpha receptor 1 (Ifnar1), interferon-beta 1(Ifnb1) and (C) interferon stimulated genes: inerleukin-15 (Il15), Ubiquitin-Like Modifier (Isg15), and MX Dynamin-Like GTPase 1 (Mx1). 95% confidence intervals are shown and * indicates that expression was significantly different from L2K control. (D and E). RAW264.7 cells were transfected with OVA IVT mRNA with the indicated nucleobase composition using Lipofectamine 2000. At the indicated time points, cells were stained for the ovalbumin

protein and analyzed with flow cytometry. (D) shows the percentage of cells expressing ovalbumin protein and (E) shows the median fluorescence of the cells positive for protein expression. Error bars indicate standard deviation (n=3)

We used flow cytometry to determine the impact of uridine substitution on ovalbumin protein expression following transfection (Figure 1.1D-E). The highest percentage of cells positive for transgene protein production and the highest median fluorescence intensity were observed upon transfection of $M^1\Psi$ IVT mRNA. While the majority of studies indicate that substitution with Ψ enhances transgene protein production [16,17,45], we found that Ψ IVT mRNA led to slightly less transgene protein levels compared to unmodified IVT mRNA. The influence of modified bases, particularly Ψ, may depend on the gene of interest, codon optimization algorithms, as well as particular experimental conditions, such as the transfected cell type. The ability to achieve a minimal level of mRNA-induced innate immune activation is advantageous to address the effect of specific TLR agonists and to modulate activation of innate receptors, while retaining enhanced protein expression. Therefore, $M^1\Psi$- IVT mRNA was utilized for all subsequent studies.

Assembly and *in vitro* characterization of adjuvant-tethered IVT mRNA

As innate responses in vaccination are important for driving the nature of memory immune responses, we devised a strategy to supplement the intrinsic immunogenicity of the $M^1\Psi$-IVT mRNA molecule by tethering to it a payload of adjuvants. The overall approach is described in Figure 1.2. mMTRIPS were synthesized by designing four 2'O-methyl RNA/DNA chimeric oligonucleotides complementary to the 3'UTR of the ovalbumin IVT mRNA. These oligos contained terminal thiol groups, which were covalently bound to free amines present on Neutravidin using Solulink chemistry. The reaction was optimized to yield an oligonucleotide:Neutravidin molar ratio of 1:1, as determined by bicinchoninic acid assay (BCA) protein assay and nucleic acids absorbance at 260 nm. Biotinylated small

molecule agonists were conjugated to the Neutravidin-oligo complexes, the resulting mMTRIPS were purified via filtration, and hybridized to the IVT mRNA. To determine the efficiency of small molecule tethering, we used a biotinylated fluorescent dye. Following purification, the overall fluorescence and 260 absorbance of the sample were measured and compared to a standard curve of known molar concentration of pure dye. We determined that, on average, 10 fluorescent molecules were bound to an IVT mRNA, which indicates that each RNA is labeled by approximately 2.5 mMTRIPS. The inclusion of modified bases in the IVT mRNA did not significantly affect mMTRIPS tethering efficiency [15].

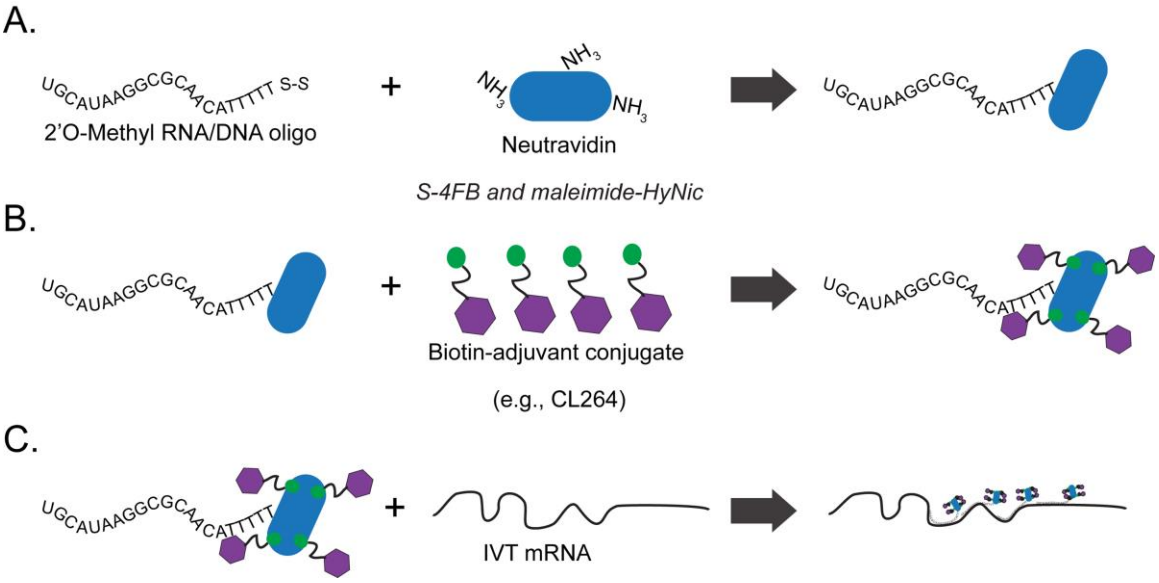

Figure 1.2: Schematic procedure for tethering small molecule agonists to IVT mRNA. (A) 2'O-Methyl RNA/DNA chimeric oligonucleotides complementary to the 3' UTR of IVT mRNA and bearing a 5' thiol group were covalenty linked to Neutravidin via Solulink chemistry to generate mMTRIPS. Unbound oligonucleotides were removed with centrifugal filtration. (B) mMTRIPS were incubated with biotinylated small molecule agonists (purchased commercially). Unbound biotinylated adjuvants were removed by centrifugal filtration. (C) Adjuvant-tethered oligonucleotides were hybridized to IVT mRNA. Unbound oligonucleotides, small molecules, or free Neutravidin, were removed by filtration.

While mMTRIPs are composed of 2'OMethyl RNA/DNA chimeric nucleic acids, which typically abrogate immune responses [46,47], they could potentially alter the secondary

structure of the IVT mRNA leading to TLR7 activation. Thus, unmodified or $M^1\Psi$ modified IVT mRNA were delivered to RAW264.7 cells with or without tethered mMTRIPs and TLR7 activation was quantified. Upon activation, TLR7 forms a protein complex termed the myddosome, which includes myeloid differentiation primary response gene 88 (MYD88), and interleukin-1 receptor-associated kinase proteins (IRAK1, IRAK2, IRAK3, and IRAK4), that initiates signaling cascades. TLR7-IRAK4 interactions were quantified with a proximity ligation assay [48] (PLA) as an indication of TLR7 activation after IVT mRNA delivery (data not shown). As expected, unmodified IVT mRNA upregulated TLR7 with respect to the L2K only control condition, while the $M^1\Psi$ IVT mRNA did not. However, no statistically significant differences in TLR7 activation were observed between unlabeled and mMTRIP-labeled mRNA, indicating that mMTRIPs hybridization does not affect TLR7 activation. Thus, we expected that innate immune activation observed upon delivery of adjuvant-tethered mRNA would be solely reflective of the agonist payload.

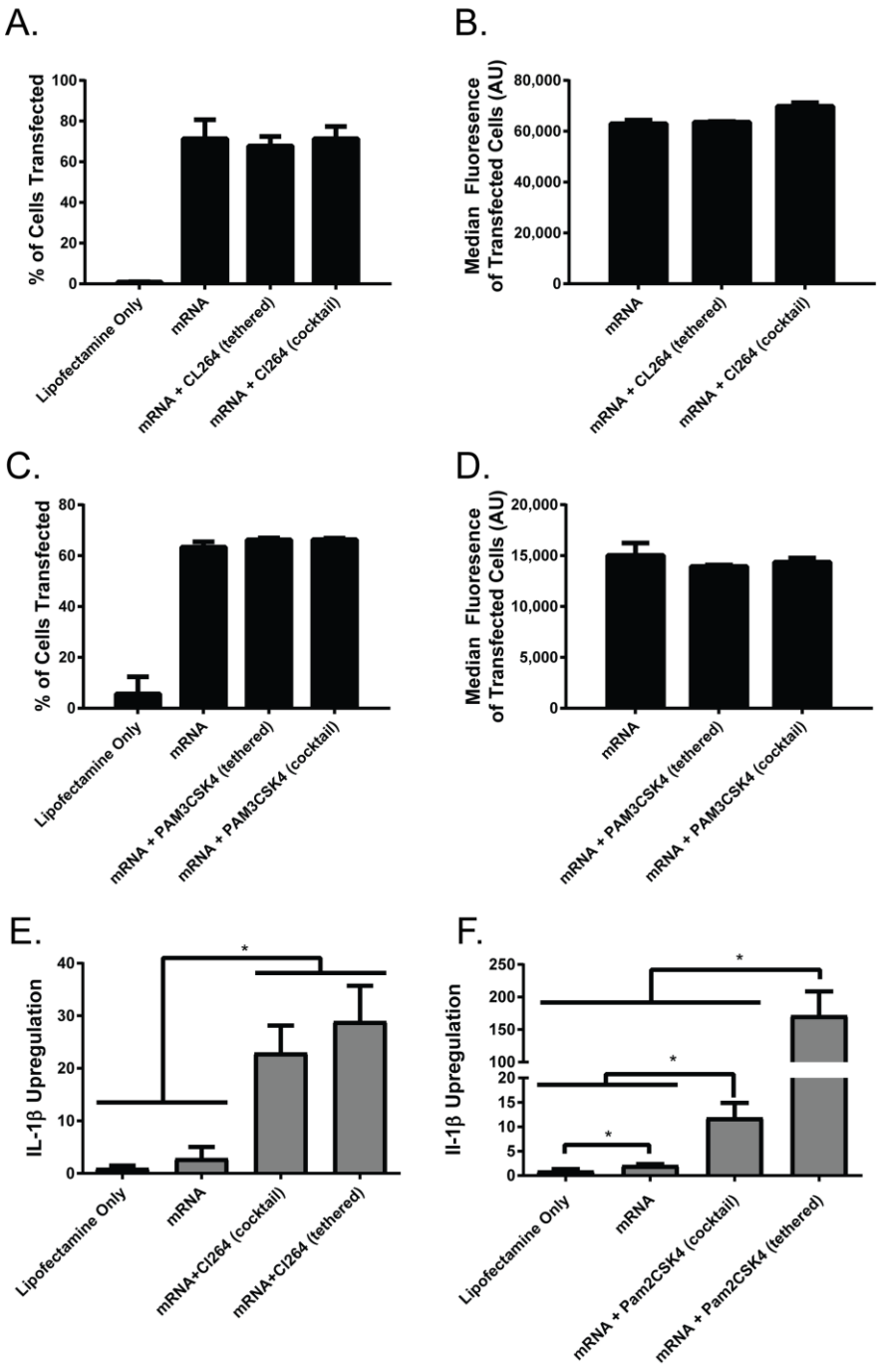

Figure 1.3: Tethering TLR2 and TLR2/6 adjuvants to IVT mRNA does not alter adjuvant and IVT mRNA functionality. RAW264.7 cells were transfected with $M^1\psi$ OVA IVT mRNA and small molecule agonists using Lipofectamine 2000. Five hours following transfection, cells were fixed, permeabilized, stained for the genetically delivered ovalbumin protein, and then analyzed with flow cytometry (A-D) The percent of cells transfected as well as the median fluorescence intensity of cells positive for ovalbumin are shown. Error bars indicate standard deviation, (n=3). Each experiment was repeated at least twice with similar results. cellular responses to tethered adjuvants were assayed

using a RT-qPCR assay for IL-1β (E-F) Tethered and cocktail delivery of (E) CL264 and (F) Pam2CSK4 led to a marked upregulation of IL-1β transcripts compared to controls. Fold changes are shown normalized to a Lipofectamine only condition and are calculated using β- Actin as reference. (n=3). Error bars show 95% confidence intervals. *Indicates significant ($p<0.05$).

The ability of adjuvant-tethered IVT mRNA to interact with its respective pattern recognition receptors while maintaining its translational efficiency was then assessed in L2K transfected RAW264.7. To demonstrate the flexibility of this platform two representative small molecule TLR agonists were chosen: CL264 (TLR7-specific) and PAM2CSK4 (TLR2-specific). TLR7 is expressed in the endosomal compartment and is a natural sensor of exogenous mRNA, while TLR2 is expressed on the plasma membrane where it binds extracellular lipopeptides common in bacteria and fungi. As expected, tethering either CL264 or PAM2CSK4 to IVT mRNA did not affect the translational efficiency of the IVT mRNA with respect to a cocktail formulation (untethered adjuvants) in transfected cells, as assayed via flow cytometry (Figure 1.3A-D). To verify that mRNA tethering did not inhibit agonist function, we measured IL1β mRNA production as an indicator of TLR signaling five hours post-transfection using RT-qPCR (Figure 1.3E). CL264-tethered IVT mRNA led to increased IL1B gene expression compared to mRNA alone, and to comparable levels than a cocktail delivery (not tethered). Instead, PAM2CSK4-tethered mRNA induced a dramatic upregulation of IL-1B expression, compared to the cocktail formulation. The IVT mRNA likely acts as a scaffold, concentrating PAM2CSK4 at the cell surface, facilitating receptor binding and increasing downstream signaling responses. Additionally, the inherent immune-stimulation profile of IVT mRNA may act synergistically with TLR2 activation to enhance innate immune signaling. In the case of CL264, the comparable levels of IL1B mRNA between cocktail and tethered conditions may be due to TLR7 localization in the endosomal compartment,

where reagent concentration is intrinsically increased by the entrapment into endocytic vesicles.

Tethering adjuvant to IVT mRNA induces an acute innate response upon intramuscular injection

We investigated if agonist-tethering to IVT mRNA would lead to stronger innate immune responses than a cocktail formulation following i.m. injection in a murine model system. We reasoned that, upon i.m. injection, a cocktail formulation would elicit an effectively weaker immune response, because the small molecule adjuvants should readily diffuse away from the injection site, given their negligible molecular weight (e.g. CL264 is 413.43 Da and PAM2CSK4 is 1271.85 Da). On the contrary, tethering to IVT mRNA, whose uptake is mediated by clathrin-mediated endocytosis [49], may promote its retention at the site of injection, and increase interactions with endosomal TLRs upon internalization, eliciting a stronger and longer-lasting localized effect.

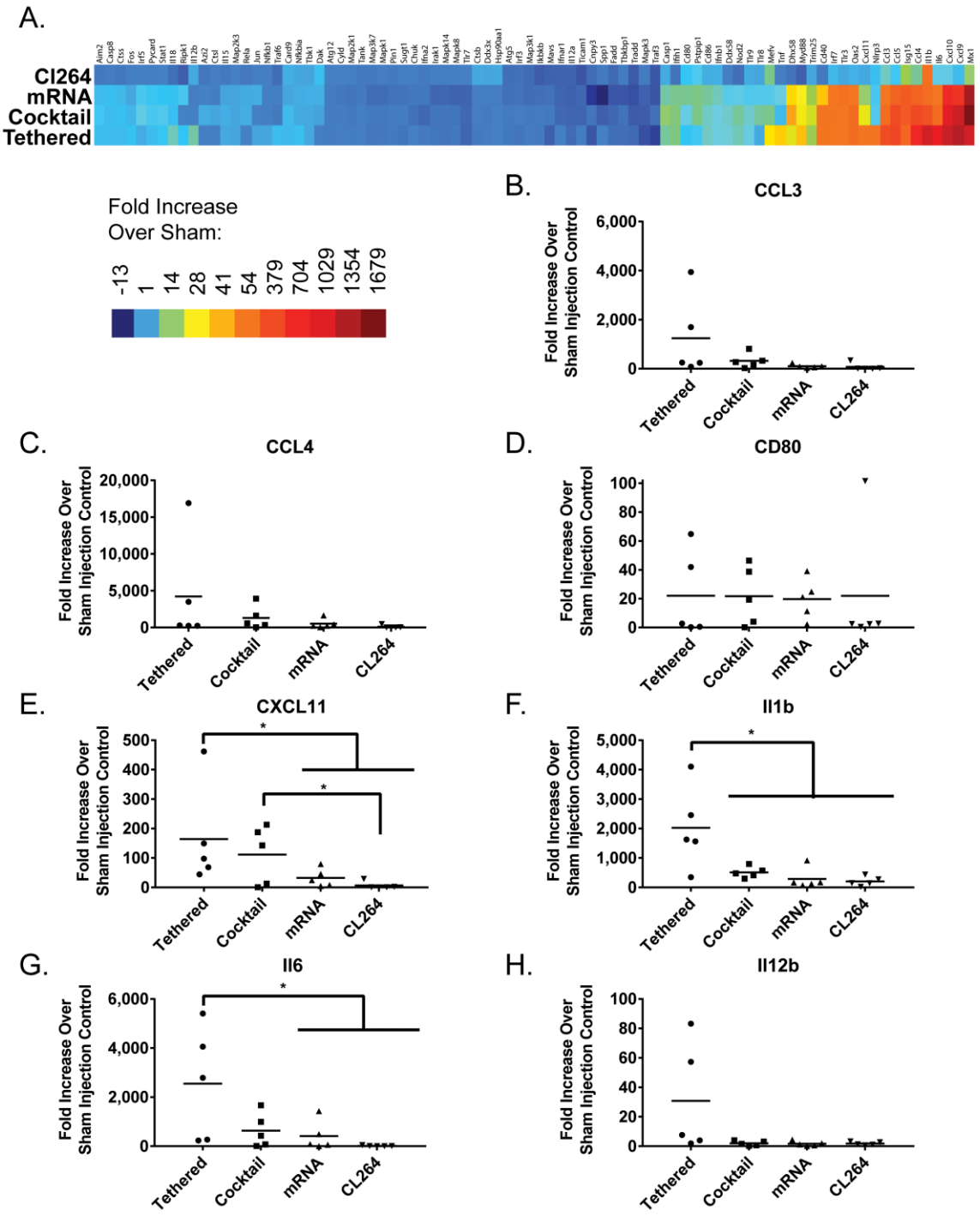

Figure 1.4: Gene expression in mice anterior tibialis muscle five hours following IVT-mRNA injection. (A) Heat map showing fold changes of gene expression over a sham injection control. (B-H) Fold increase of gene expression of Toll-like responsive genes. Each data point indicates expression levels in an individual animal. Lines indicate the mean expression level. * indicates $p<0.05$, Student's t-test based on the $2^{-\Delta CT}$ values for each gene. (n=5)

To assess this, we injected i.m. $M^1\Psi$ IVT mRNA with tethered Cl264 or as a cocktail (five mice were used per experimental condition). $M^1\Psi$ mRNA and CL264 were also injected independently as controls. Five hours post injection, muscles were isolated and analyzed for local gene expression using a mouse antiviral qRT-PCR array (Figure 1.4 and Supplementary Figure 1.3). The heat map of gene expression in Figure 1.4A shows that injection of $M^1\Psi$ IVT mRNA alone and with Cl264 administered either in a tethered or cocktail formulation led to substantial but comparable upregulation of antiviral genes. As CL264 is a TLR7 agonist, we examined the expression of the Toll-like responsive genes in the array to gain insight into CL264's role in upregulating gene expression (Figures 1.4B-H). Contributions to the local immune response due to either CL264 or $M^1\Psi$ IVT mRNA stimulation relative to a sham control are reported in Figure 1.5A-B. To highlight how delivery of CL264 (tethered or cocktail) affected gene expression, results were normalized by the $M^1\Psi$ mRNA control (Figure 1.5C-D). IL1β and Nlrp3, displayed a significant upregulation that was not observed in control conditions. IL1β promotes canonical pro-inflammatory mechanisms at the site of injection, including vasodilation, neutrophil and monocyte recruitment, and activation of matrix proteases [50]. NLRP3 associates with caspase-1 and adaptor proteins to form the inflammasome, a multiprotein complex that proteolytically activates pro-IL1 β, and is also directly involved in sensing cytoplasmic mRNA [51]. Slight expression increases, although not statistically significant from the cocktail formulation, were also observed for pro-inflammatory cytokines IL6 & Il12β and chemokines CXCL11 & CCL3.

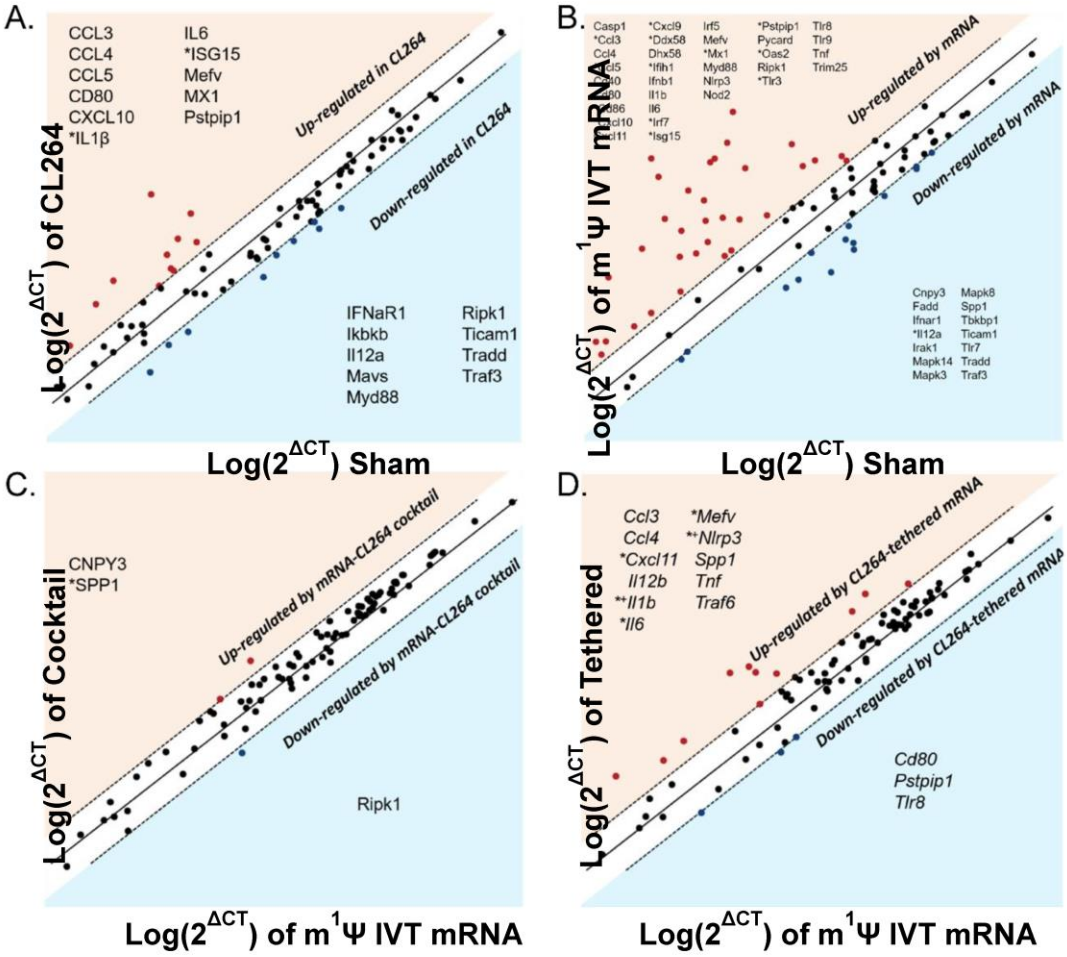

Figure 1.5: Gene expression in the mice anterior tibialis muscle five hours after i.m injection of CL264-tethered IVT mRNA. These data, summarized in Figure 4(A), are presented here to better visualize differences between individual treatment groups. Dashed lines indicate a fold regulation cut-off of 3. Listed genes are 3-fold over or under expressed with respect to control condition. * indicates gene expression was statistically different between the groups, $p<0.05$, Student's t-test based on the 2-ΔCT values for each gene (n=5). + indicates gene expression is significantly different between Cl264 –tethered m1Ψ IVT mRNA and cocktail delivery.

Adaptive responses to adjuvant-tethered mRNA indicate robust Th1 mediated and humoral immunity

We hypothesized that a localized innate immune stimulation at the site of injection via CL26-tethering to IVT mRNA would facilitate the development of memory immune responses. To assess this, we immunized mice with $M^1\Psi$ IVT OVA mRNA with and without tethered CL264 via i.m. injection. Mice also received a sham injection of the vehicle-only or $M^1\Psi$ IVT mRNA alone as control conditions. Mice were immunized on day zero and a booster was administered on day 23. On day 41, murine splenocytes and serum were collected to assess antigen-specific memory immune responses. To evaluate the development of cell-mediated immune responses, an OVA-specific enzyme linked immunospot assay (ELISPOT) was utilized. The OVA peptide SIINFEKL, a potent MHCI epitope commonly used to detect potent CD8+ cytotoxic T cell responses, was tested as a positive control. Ex vivo splenocytes from tethered Cl264-mRNA vaccinated animals demonstrated a significant ($p = 0.035$) cell mediated response, as indicated by IFNγ release (Figure 1.6a). Splenocytes stimulated with whole ovalbumin yielded a less substantial ($p = 0.09$), yet similar T_H1 cell-mediated response (Figure 1.6b). Accordingly, the number of IL-4 producing cells decreased, although non-significantly, suggesting a concurrent inhibition of the T_H2 immune response (Figure 1.6c), which corroborates the inverse relationship between T_H1 and T_H2 immune responses. Next, we analyzed the humoral immune response in the serum extracted from the same animals by measuring the concentration of anti-OVA specific IgG in sera using enzyme-linked immunosorbent assay (ELISA). All 5 animals that received tethered Cl264-mRNA formulations contained detectable levels of anti-OVA IgG, with an average concentration 8-fold higher than those treated with a cocktail formulation (Figure 1.6d). The elicited OVA-specific adaptive responses suggest that tethering adjuvants to IVT mRNA strongly increases mRNA immunogenicity and adjuvant activity *in vivo*.

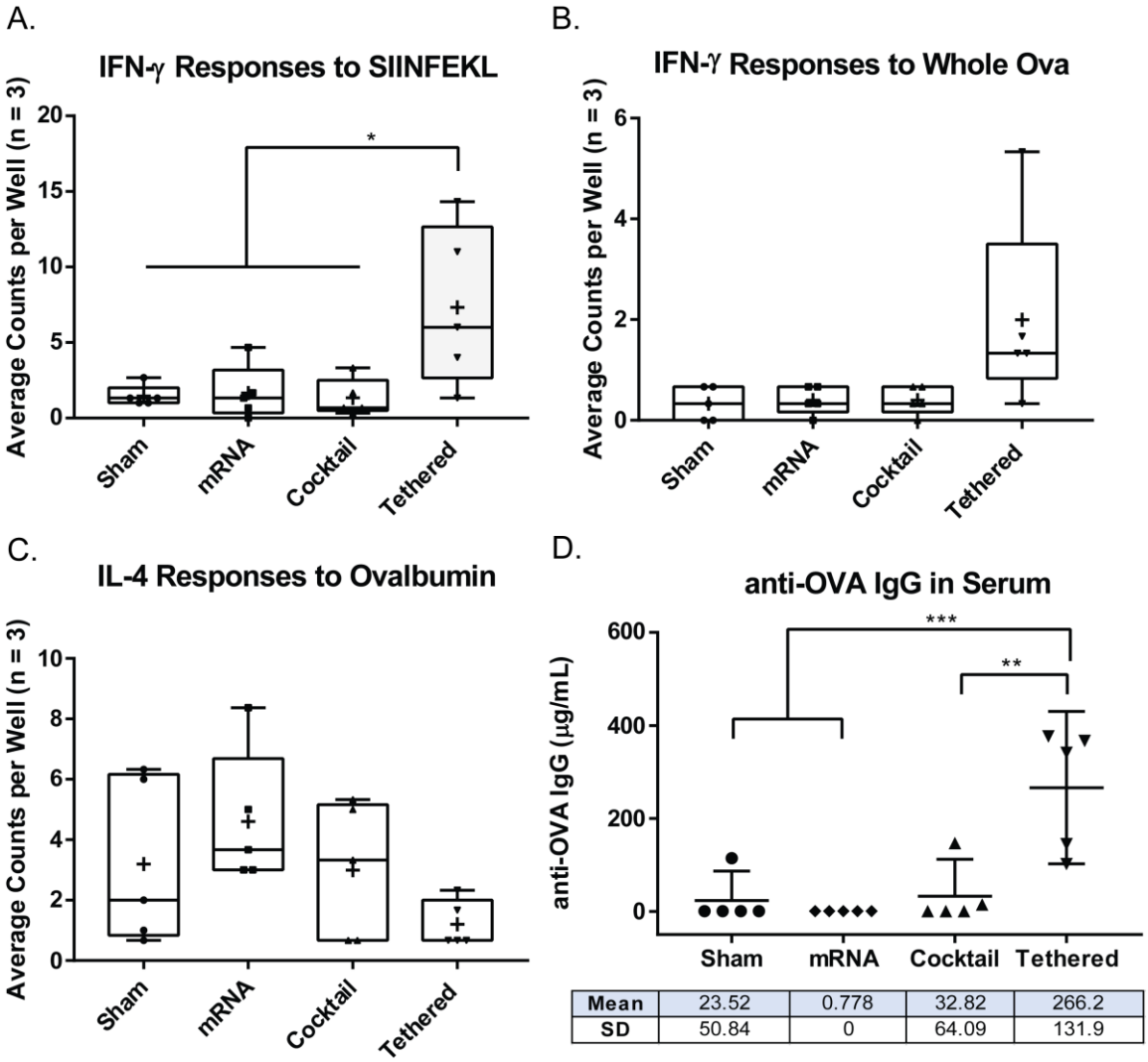

Mean	23.52	0.778	32.82	266.2
SD	50.84	0	64.09	131.9

Figure 1.6: Cellular and humoral immune responses elicited by IVT mRNA tethered to CL264 agonists. Mice were vaccinated i.m. twice with CL264-IVT mRNA (week 0 and week 3). On week six, splenocytes and serum were harvested for analysis. (A-C) OVA specific cell-mediated immune response as measured by ELISPOT. Dissociated spleenocytes were plated in wells containing capture antibodies for either IFN-gamma (A-B) or Il-4 (C) and tested for antigen specific immmune responses via stimulation with $OVA_{257-264}$ SIINFEKL peptide (A) or whole OVA (B-C). Boxes represent the IQR, horizontal lines the median, and crosses the mean. *, $P < 0.05$. (D) anti-OVA specific IgG (ug/mL) in the serum at the time of sacrifice. Values were calculated from a standard curve via direct ELISA with plates coated with OVA. Values represented as mean with 95% confidence intervals. **, $P < 0.01$. ***, $P < 0.001$. Serum samples ran in triplicate.

Conclusion

Here, we described a novel approach for the development of IVT mRNA-based vaccines that does not rely on delivery vehicles for immune stimulation. While delivery vehicles provide control over vaccine characteristics (e.g. conferring IVT mRNA protection from nucleases or cell-type specific delivery), they are not immunologically inert. Moreover, carrier's delivery characteristics and efficiency are intimately tied to their immunological stimulation properties. For example, size, shape, and charge of delivery vehicles have been found to affect both cell type uptake and immunological stimulation [52,53]. Critically, activation of the innate immune response should be finely controllable, because it directly determines the nature of subsequent downstream adaptive responses.

We demonstrated that naked $M^1\Psi$ IVT mRNA, characterized by an intrinsically low immunogenicity, can be delivered i.m. with a tethered payload of adjuvants *in vivo* leading to an enhanced local innate immune response at the injection site that ultimately results in enhanced antigen-specific cell-mediated and humoral immunity. Tethering small molecules adjuvants to the much larger mRNA likely decreases its diffusion away from the injection area, while raising its local concentration at the injection site and promoting interactions with PRRs. This potentially may represent a strategy to lower the systemic toxicity associated with numerous adjuvants [54].

In summary, we present an orthogonal mRNA vaccine platform that directly associates adjuvants with IVT mRNA, with no loss of function of either molecule. We believe that, by rationally choosing adjuvant-mRNA combinations, this modular platform can help standardize vaccine studies and allow for specific and directed immune responses in streamlining the design and improvement of mRNA-based vaccines.

Methods

Preparation of IVT mRNA

To synthesize IVT mRNA encoding for cytoplasmic ovalbumin, a DNA template was prepared from the PCL-neo-cOVA plasmid from Addgene (Plasmid #25097). The Kozak consensus sequence and 3' UTR from murine alpha globin was modified with overlap extension PCR and was verified with Sanger sequencing (MWG Eurofins). The DNA template was amplified using the Q5 high-fidelity DNA polymerase (New England Biolabs), purified using the QIAquick PCR purification kit (QIAGEN), digested with the restriction enzyme NOTI to create a 5' overhang, and then purified again. The T7 mScript Standard mRNA Production System was used to generate IVT mRNA (Cellscript), add a Cap-1 structure, and a poly(A) tail. Manufacturer's instructions were followed; the RNeasy mini kit (QIAGEN) was used to purify IVT mRNA when necessary. To incorporate modified bases, pseudouridine-5'-Triphosphate, 5-Methylcytidine-5'-Triphosphate, and N1-Methylpseudouridine-5'-Triphosphate (TriLink Biotechnologies and USB) were replaced in the 25mM ribonucleotide cocktails. Cytosine triphosphate was purchased from Affymetrix. IVT mRNA was treated with Antarctic Phosphatase (New England Biolabs) for 30 min to remove residual 5′-triphosphates, and then purified with the RNeasy kit, quantified using the Nanodrop 2000 (Thermo Scientific), and then stored at -80ºC.

Preparation of Neutravidin-labeled targeting oligonucleotides

Figure 2 describes the overall schematic procedure for tethering small molecule agonists to IVT mRNA. 2'O-Methyl RNA/DNA chimeric oligonucleotides were purchased from Biosearch Technologies with the following sequences, which are complementary to the 3’ UTR of the IVT mRNA: 5’-TTTTTTT**GCAAGCCCCGCAGAAGG**-3, 5’-TTTATTT**AGAGAAGAAGGGCAUGG** -3’, 5’-TTTTTT**ACCAAGAGGUACAGGUGC**-3’, 5’-TTTTTTT**CUACUCAGGCUUUAUUC**-3’where the boldface indicates 2’-*O*-Methyl RNA. Each oligonucleotide contained a

disulfide C6 5' modification, which was used for conjugation to Neutravidin using Solulink chemistry. The 5' disulfide was reduced by incubation with tris(2-carboxyethyl)phosphine (TCEP) (5mM) (Thermo Fisher Scientific). Oligonucleotides were then filtered (3kDa MWCO, Millipore) to remove the reducing agent. Oligonucleotides were then modified with a HyNic functional group by overnight incubation with 20 µg Maleimide HyNic (Solulink) and 0.3 mM ethylenediaminetetraacetic acid (EDTA) (Sigma). The modified oligonucleotides were individually buffer exchanged into conjugation buffer with centrifugal filtration (3kDA MWCO). Separately, Neutravidin (500 µg) was labeled with succinimidyl-4-formylbenzamide (S4-FB, 20 µg) (Solulink) in Solulink's modification buffer for 2 hours at room temperature. Neutravidin was then buffer exchanged into Solulink's conjugation buffer with centrifugal filtration (30kDA MWCO, Millipore). To conjugate Neutravidin to the oligonucleotide, the reagents were incubated for two hours at room temperature at a 1:2 molar ratio in the presence of 1x Turbolink catalyst (Solulink). Unconjugated oligonucleotides were removed by centrifugal filtration (30kDA MWCO). The final neutravidin concentration was determined by bicinchoninic acid assay (Pierce) against a standard curve. The nucleic acid concentration was determined by measuring the absorbance at 260 nm using the Nanodrop 2000 (Thermo Scientific). The reaction was optimized to yield approximately a 1:1 molar ratio of Neutravidin:oligonucleotide for each mRNA targeting sequence. The resulting probes were stored at 4ºC.

Preparation of agonist-tethered IVT mRNA

Biotinylated adjuvants (Pam2CSK4 biotin, and CL264 biotin) were purchased from Invivogen and were incubated with oligo-conjugated Neutravidin at room temperature for 1 hour in PBS at a 5:1 molar ratio. The resulting mMTRIPS were purified from unbound agonists by centrifugal filtration (30 kDA MWCO, Millipore).

To anneal the adjuvants to IVT mRNA, the latter was first incubated at 75ºC for 5 minutes to remove secondary structures and immediately placed on ice. Each mMTRIP was then added to the solution and incubated with IVT mRNA at a 1:1 molar ratio for approximately 12 hours at 37ºC for hybridization. Unbound targeting oligonucleotides were removed by filtration (200 kDA filter, Advantec) and then concentrated using a 30 kDa centrifugal filter. The nucleic acid content was quantified by measuring the absorbance at 260 nm. To confirm removal of unbound adjuvant, a mock reaction without IVT mRNA was prepared as described. The number of adjuvants bound to IVT mRNA was estimated using biotinylated Atto 565 dyes. Conjugation was performed as described. Following purification, the dye fluorescence and RNA 260nm absorbance were measured. IVT mRNA fluorescence was compared to a standard curve of Atto 565 dye to determine IVT mRNA degree of labeling.

Cell line and transfection

The RAW264.7 mouse macrophage cell line (ATCC TIB-71) was maintained in High Glucose Dulbecco's Modified Eagle's Medium (DMEM) (Lonza) with 10% FBS (Hyclone) and 100 U/ml penicillin and streptomycin (Invitrogen). Approximately 60,000 cells were seeded in a 24 well plate the evening prior to transfection with Lipofectamine 2000 (Invitrogen) according to the manufacturer's protocol.

Proximity ligation assay to measure TLR7 activation

Cells were transfected with 250 ng of modified RNA or 500 ng of unmodified mRNA either unlabeled or labeled with MTRIPS. At the indicated time points, cells were fixed with 1% paraformaldehyde in PBS for 10 minutes, permeabilized with 0.2% Triton X100 in PBS for 5 minutes, and TLR7 -IRAK4 interactions were quantified by a proximity ligation assay according to manufacturer's instructions (Sigma Aldrich). Primary antibodies utilized were rabbit anti-TLR7 (Novus, cat# NBP2-24906), and mouse anti-IRAK4 (LS Bio, cat# LS

BIO452). Images were acquired using an UltraVIEW spinning disk Zeiss LSM 510 Meta confocal microscope with a Hamamatsu Flash 4.0v2 CMOS camera and a 63×, NA 1.4 Zeiss Plan-Apochromat oil objective. Imaging was controlled by the Volocity acquisition software (PerkinElmer). Image stacks were recorded at 350 nm intervals. PLA punctae were counted using the Volocity analysis software, which identified punctae over a signal intensity threshold. The number of punctae per cell was counted for each condition (thirty to forty cells per sample).

Quantitative reverse transcription-polymerase chain reaction (qRT-PCR) on cell culture samples

Six hours following cell transfection, total RNA was collected with the RNeasy mini kit according to manufacturer's protocols, including homogenization using the QIAshredder and an on-column DNAse treatment. RNA content was quantified by absorbance at 260 nm and 1 ug of RNA was retro-transcribed to cDNA using the RT2 First Strand kit (SA Biosciences). qRT-PCR was performed in triplicates using the StepOnePlus real-time PCR system (Applied Biosciences) with 15 ng of cDNA and SYBR green master mix (SA Biosciences), according to manufacturer's instructions. Gene-specific primers for ACTB (as a reference gene), IFNβ-1, and IL-1β and IL-6 were designed by and purchased from Fluidigm. Fold changes and 95% confidence intervals were calculated using the ddCT method on the StepOne software in reference to beta-actin. Significant differences were determined by an ANOVA test followed by Tukey-Kramer's post analysis. Each experiment was independently repeated at least two times.

Flow cytometry analysis of protein expression

Cells were transfected with IVT mRNA as described. Cultured cells were resuspended using Versene solution (Thermo Fisher Scientific), washed in PBS + 2% FBS, fixed with 4% paraformaldehyde for 10 minutes, washed two times with PBS + 2% FBS, and then

permeabilized with 0.2% triton X-100 in PBS. Cells were then stained for transgene expression using an anti-ovalbumin FITC antibody (Abcam) diluted 1:50 in PBS with 2% FBS and 0.1% triton X-100 for 30 minutes at 4°C. Cells were washed twice with PBS + 2% FBS and 0.1% triton X-100 and then analyzed using an BD Accuri C6 Cytometer. Samples were gated to remove debris, doublets and to demarcate the ovalbumin+ population for determination of median fluorescence.

Murine intramuscular injections

Female BALB/c mice (Charles River, Wilmington, MA) were anesthetized with 2.5% isoflurane and then injected in the anterior tibialis with 40 µl of indicated treatment (10 µg of IVT mRNA and/or 0.314 nmol CL264 diluted in RiLa) using a 29-gauge needle. Five mice were immunized per condition. For adaptive immunity experiments, mice received the vaccine once on day 0 and once on day 23. Mice were euthanized on day 41, blood was collected by cardiac puncture for anti-ovalbumin analysis and spleens were harvested for ELIPSOT analysis. Mice were housed and manipulated under specific-pathogen-free conditions in the animal care facilities of Georgia Institute of Technology. All experiments were conducted in accordance with the Institutional Animal Care and Use Committee.

RT-qPCR on mouse muscle tissue

Five hours following intramuscular injection, the muscle was removed and stored in RNAlater (Thermo Fisher Scientific) overnight at 4ºC. The following day, tissue was homogenized using the Bullet Blender and Navy RNAse free stainless-steel beads (Next Advance) in the presence of 1 ml of Trizol (Thermo Fisher Scientific). Samples were extracted with chloroform, mixed with an equivalent volume of ethanol, and then purified according to the RNEasy kit's instructions, which included an on-column DNAse digestion. RNA content was determined by A260 absorbance using the Nanodrop 2000, (Thermo Fisher) and quality was checked by RNA gel electrophoresis. Extracted RNA (1 µg) was

reverse-transcribed to cDNA using the RT^2 PreAMP pathway primer mix (QIAGEN) according to the manufacturer's directions. qPCR was conducted using the Fluidigm system and the mouse antiviral response PCR primer array (QIAGEN) according to the manufacturer's directions with technical duplicates. Five mice were analyzed per treatment condition. QIAGEN's online data analysis center was used for data analysis. Statistical significance was based on a Student's t-test of the replicate $2^{-\Delta CT}$ values for each gene in the control group and treatment groups. The reference genes Gusb, Gapdh, Hsp90ab1, and ActB were used to normalize expression. Heat maps for gene expression were generated in JMP using the multivariate clustering tool.

Enzyme linked immunospot (ELISPOT) assays

Mouse IFN-γ and IL-4 ELISPOT assays were conducted according to the manufacturer's instructions (BD Biosciences). Spleens were removed from the mice and a spleen dissociator kit (Miltenyi) was used to assist harvesting. Splenocytes were treated with red blood cell lysis buffer, washed in PBS, and then resuspended in RPMI (Gibco) supplemented with 10% FBS (Hyclone) and 100U/ml penicillin/streptomycin (Invitrogen). Cell viability and concentration was assessed with trypan blue. Cells were plated in triplicate in 96 well ELISPOT plates at 10^6 cells/ml. Cells were stimulated with either whole ovalbumin protein (for IFN-γ and IL-4 assays) or the SIINFEKL peptide (for IFN-γ assay) overnight (2 mmole/ml). Each assay included a non-stimulated cell negative control as well as stimulation with a PMA/Ionomycin cocktail positive control. Following cytokine staining, plates were imaged with the CTL S6 Core Analyzer ELISPOT plate reader (Immunospot).

Cell spots were counted using the image analysis software Volicity. To quantify cellular cytokine spots, images were background subtracted then thresholded based on the

intensity of the spots observed in the control wells. With this highpass filter applied, the number of cell spots were then counted in each well.

Enzyme-linked immunosorbent (ELISA) assay

Mouse serum was collected on day 41, and assessed for total anti-ovalbumin IgG using a mouse ovalbumin IgG ELISA kit (MyBioSource). Serum samples were diluted 1:100 in the sample diluent supplied, and processed according to the manufacturer's protocol. The mouse monoclonal 6C8 anti-ovalbumin antibody (Abcam) was diluted in serial 2-fold dilutions to generate a standard curve.

CHAPTER 2

Monitoring mRNA vaccine trafficking longitudinally using PET/CT imaging

The work presented here is from:

Evaluating early events of mRNA vaccine delivery in non-human primates using PET/CT and near-IR imaging
Kevin E. Lindsay[1]**, Sushma M. Bhosle[1]**, Chiara Zurla[1], Bruno Pitard[3$], Patrick Baumhof[4], Francois Villinger[2], Philip J. Santangelo[1]*
** Authors contributed equally to work; *corresponding author
Nature Biomedical Engineering **(In Revision)**.

Summary

Understanding the spatiotemporal trafficking of vaccines after delivery can aid in their rational design during preclinical and translational studies. Here we demonstrate a dual radionuclide:near-IR platform to non-invasively monitor non-human primate mRNA vaccine trafficking in a longitudinal, quantitative manner via PET/CT, while preserving the ability to investigate events at the tissue and single cell level. This approach is modular and flexible because the RNA is directly labeled, allowing any vaccine formulation to be utilized, without impeding antigen expression or inducing additional immune responses. We show that at 4 hours post-IM administration, mRNA was present in 3 draining lymph nodes; after 24-hours, the signal increased in the draining lymph nodes by an average of 70%, while it decreased at the injection site by 40%. Cellular analysis of tissues 28 hours post-injection demonstrated that dendritic cells (DCs) and B cells were the primary cells containing the injected mRNA and encoded protein. Due to its non-invasive nature, we believe this approach will reveal critical spatiotemporal determinants of vaccine efficacy in preclinical and translational vaccine studies, particularly in large mammals.

Graphical Abstract

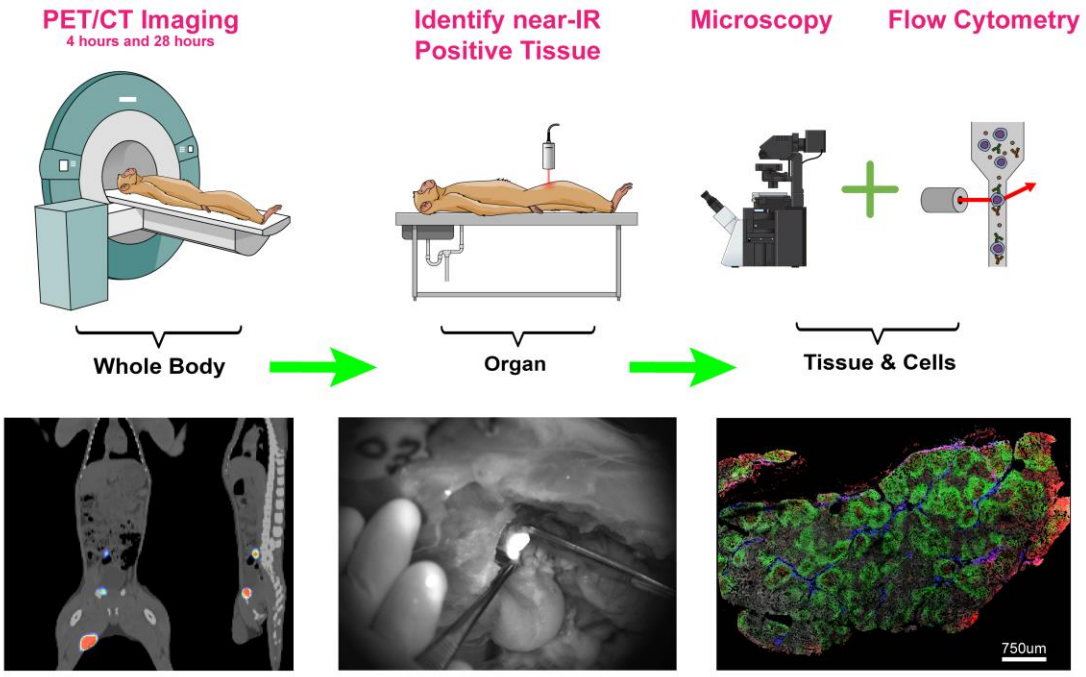

Figure 2.1: Experimental workflow and outline after intramuscular injection of 64Cu:DyLight 680 labeled YF prME mRNA. Whole body PET/CT imaging was performed at 4 hours and 28 hours. Two animals were sacrificed at 28 hours and mRNA positive tissues identified and extracted utilizing a portable near-IR camera. The extracted tissues were then examined at the cellular level with microscopy and flow cytometry. Images along the bottom half of the figure illustrate data collected at each step of the experiment.

Background

Non-invasive approaches to longitudinally monitor vaccine responses and efficacy in a reliable manner are urgently lacking. Current vaccine efficacy prediction metrics (known as correlates of protection) are often dependent on host-responses that take months to develop[55], and are invasive in nature. The requisite gap between administration and evaluation[56] may result in potential infection with the pathogen of concern before vaccine protection is verified.

Synthetic messenger RNA (mRNA) has garnered considerable interest as a biotechnology platform. The short-lived nature of mRNA provides an inherent safety advantage over DNA based approaches as the transcripts are unlikely to enter the nuclear compartment and cannot integrate into genomic DNA. Critically, mRNA-based vaccines are particularly attractive due to their simplicity of design and production, allowing the medical community to respond quickly and at scale to mutating and emerging pathogens. They are also highly amenable to personalized therapy, such as for various cancers[57].

In the context of RNA vaccine development, a balance between expression of the epitopes that host immunity needs to target, and immune stimulation, is required to develop adaptive immunity and protection[54]. Efficacious mRNA vaccines often contain adjuvants that are used in tandem with mRNA to stimulate directed innate responses that drive appropriate adaptive immunity[20,22]. Delivery vehicles such as lipid nanoparticles (LNPs), in addition to protecting mRNA from nucleases, can also be considered adjuvants, as they are not immunologically inert and demonstrate innate stimulating properties independent of the complexed mRNA[58,59]. The use of adjuvants with mRNA to elicit protection has been demonstrated in animal models of Flu[60], Zika[61], and cancer[57], among others. To date however, no mRNA-based vaccine has successfully demonstrated protection in a phase 3 clinical trial[57].

It is apparent that a vaccine or therapeutic agent can only be effective if it localizes to relevant tissues that require the intervention. After intramuscular or intradermal administration of mRNA, dendritic cells (DCs), which when activated migrate to draining lymph nodes, have a strong proclivity for mRNA uptake[62], whether naked[63] or encapsulated in LNPs[20,64]. The complex immune milieu that ultimately develops requires expression and presentation of antigen to lymph node based B and T cells for robust

humoral and cell mediated adaptive immunity to develop[65]. Multiple delivery routes (IP, IV, IM, ID) are typically evaluated for a given adjuvant/delivery vehicle formulation, based on their ability to generate differential correlates of protection[66,67] . Additionally, due to safety concerns, off-target delivery to unintended organs should be thoroughly investigated.

During vaccine development, an assumption is often made that the delivery distributions observed in lower animal models reliably translate to humans. New non-invasive strategies that allow precise monitoring of mRNA after delivery in large mammals (i.e. non-human primates and humans) would prove a useful tool to rapidly screen, evaluate, and compare potential vaccine formulations. For clinical investigations, no such systemic and non-invasive methodology currently exists. In pre-clinical studies, tissue light scattering impedes the utility of commonly deployed optical imaging methodologies, such as luminescence and fluorescence, in larger animal models. Invasive molecular tagging techniques, such as barcoding, are useful tools to investigate drug distribution, but they would be even more powerful if used in combination with an unbiased systemic imaging approach.

Here, we demonstrate the use of PET/CT imaging as a non-invasive means to monitor, in a quantitative manner, the trafficking of a model mRNA vaccine to draining lymph nodes in cynomolgus macaques. We chose yellow fever (YF) prME mRNA as a model system, as the live attenuated 17D virus vaccine provides robust and widespread protection, and as such represents a gold standard to evaluate and compare experimental vaccines. We directly labeled the mRNA with an orthogonal dual PET:near-IR probe, an approach agnostic to formulation, carrier, or route of delivery. The mRNA was complexed with lipid derivatives of natural amino sugars used to deliver RNA structures[68–70] and delivered via

intramuscular injection (IM), the most common route of delivery for vaccines in humans. By choosing ^{64}Cu, a radioisotope with a half-life of 12.7 hours, we reasoned that any vaccine formulation could be precisely tracked for days following administration.

PET/CT was used to monitor the first 28 hours of mRNA trafficking dynamics with high spatiotemporal resolution (Fig. 2.1). Substantial signal in draining lymph nodes was observed in three anatomical regions at 4 hours post-injection and it increased over the next 24 hours by an average of 70%. Subsequently, near-IR fluorescence allowed us to confirm the systemic level events indicated by PET imaging and to investigate mRNA localization within tissues and the cell types involved with vaccine trafficking at the injection site and in the draining lymphoid organs. We believe this study establishes PET imaging as a viable platform to monitor and characterize delivery of mRNA therapeutics and vaccines in large-mammals, and, as such, has potential implications for pre-clinical and clinical mRNA studies.

^{64}Cu:DyLight 680 Labeling of YF prME mRNA and IM Injection

We previously demonstrated orthogonal fluorescent labeling of IVT mRNA through the use of tetravalent NeutrAvidin:oligo nucleotide complexes (MTRIPS) targeting the 3'UTR[49,71,72], achieving sufficient signal-to-noise ratios without comprising translational capacity or stimulating immune responses. Here, in addition to labeling the oligos fluorescently, we conjugated the divalent cationic chelator DOTA to the NeutrAvidin protein core (Fig. 2.2a). The resulting probes contained two components: a) DyLight 680 labeled oligos complementary to the 3'UTR of the mRNA for near-IR imaging and b) NeutrAvidin core labeled with the chelator DOTA for whole-body PET/CT.

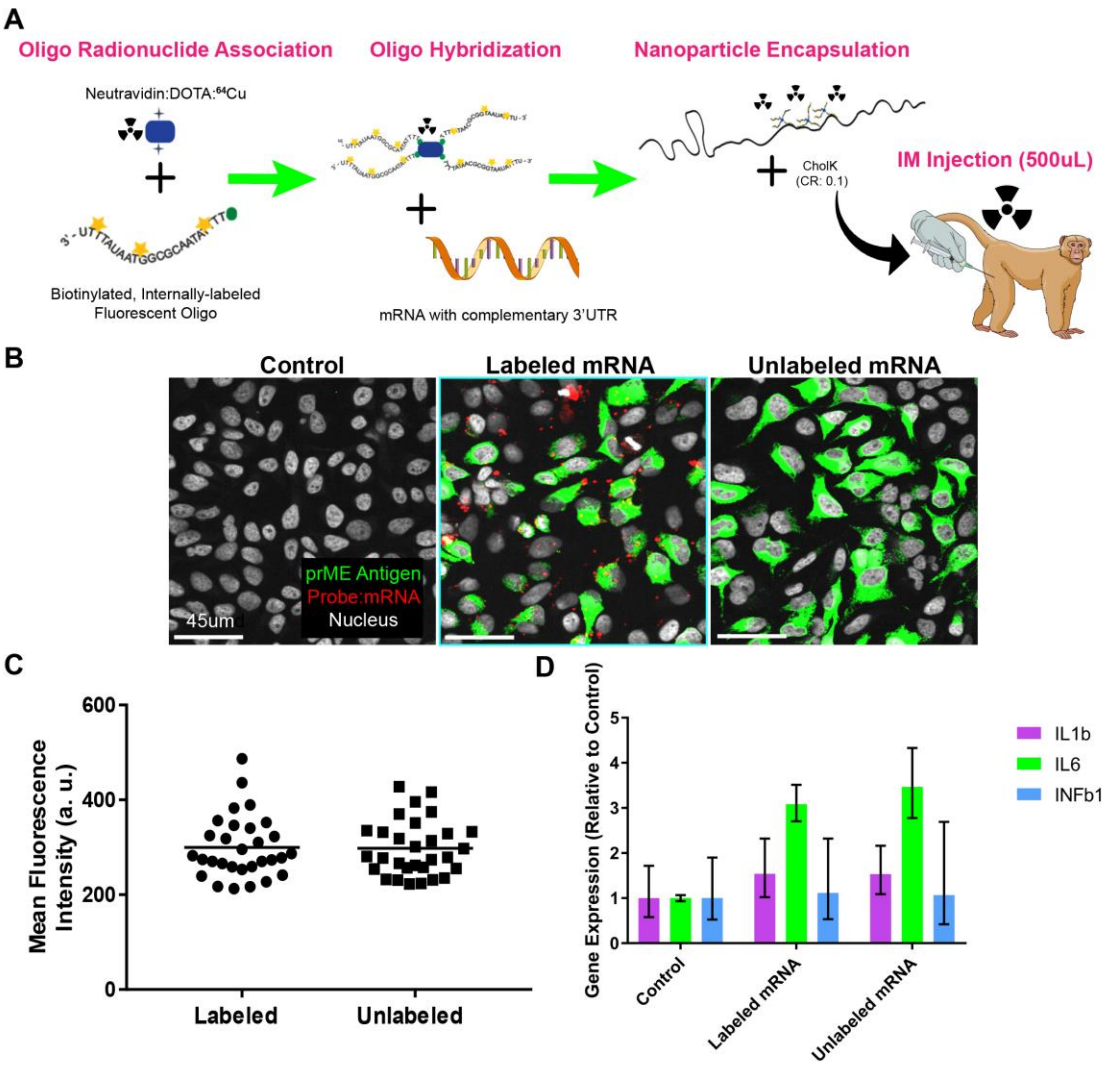

Figure 2.2: Approach to orthogonally label YF prME mRNA with dual radionuclide:near-IR probes. (A) Schematic demonstrating mRNA labeling with radioactive:near-IR probes. (B) immunofluorescence (IF) analysis of protein expression in HeLa cells after Lipofectamine 2000 transfection with YF prME-encoding mRNA. Green represents staining for the YF prME protein, while red designates the fluorescently labeled prME mRNA. (C) Quantification of IF analyses, demonstrating efficient translation of a DOTA:DyLight 680 labeled YF prME mRNA and the corresponding unlabeled mRNA. (D) qPCR analysis of gene expression demonstrates no differential activation of innate immune response genes (IL1b, IL6, and IFNb1) between labeled and unlabeled mRNA in HeLa cells, 24 hours after transfection. Error bars represent 95% CI.

The probes were labeled with the radionuclide PET reporter ^{64}Cu and annealed to the mRNA 3'UTR at a molar ratio of 1:0.5 of mRNA to probe, as optimized through size exclusion HPLC (data not shown). Efficient protein expression and negligible innate immune activation were confirmed via *in vitro* transfection (Fig. 2.2 b-d), with respect to non-labeled mRNA. Before injection, the ^{64}Cu:DyLight680 labeled YF prME mRNA was complexed with the aminoglycoside lipidic derivative CholK containing a kanamycin polar head group and a cholesterol moiety as a hydrophobic portion. We have previously demonstrated that mRNA complexed with CholK, at low mRNA to nanoparticle charge ratios (0.1), entered via clathrin mediated endocytosis, was released from the endosome, and protein was expressed efficiently *in vivo*[49]. Four cynomolgus monkeys (6kg-8kg) were injected with 200ug (0.8mCi in a total volume of 500uL of Ringers lactate) of CholK formulated YF prME mRNA in the right quadriceps. Animals were imaged via whole body PET/CT at 4 hours and 28 hours post-injection, in a clinical grade scanner.

PET/CT reveals a consistent spatial distribution of IVT-mRNA

PET/CT images of AFO32 at 4 hours post-immunization are used to illustrate the general results observed at the a) injection site and b) draining lymph nodes (Fig. 2.3a). mRNA was clearly visible at the site of injection in the right quadriceps, as well as in three draining lymph node regions: inguinal, iliac, and paraaortic. The signal magnitude in a given LN decreased with Euclidian distance from the injection site (Fig. 2.3b). The distance between the injection site and the most distal paraaortic LN was 9.2cm. This observation, combined with known draining patterns, indicates that the order of trafficking from the injection site is inguinal, iliac, then paraaortic, all confined to the ipsilateral side as the injection.

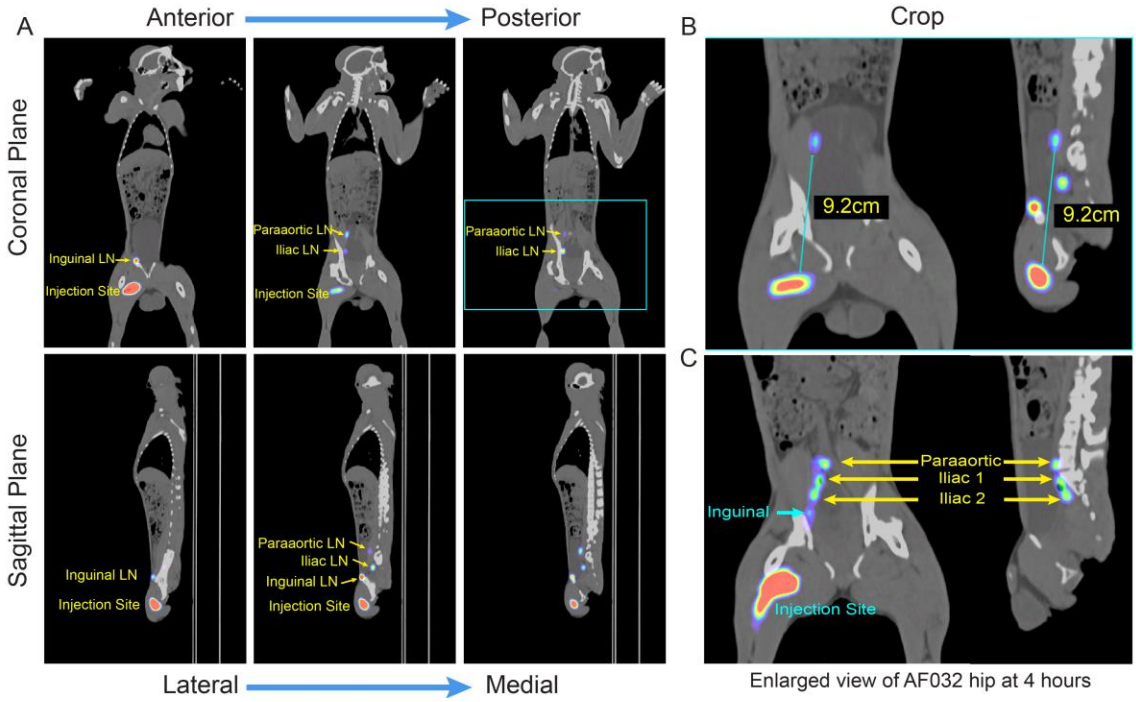

Figure 2.3: Representative PET/CT images of non-human primates 4 hours after 64Cu IM vaccine delivery. (A) Whole body coronal and sagittal PET/CT images for animal AF032, four hours after delivery. The injection site in the quadriceps and 3 lymph node clusters - Inguinal, Iliac, and paraaortic – display standard uptake value (SUV) levels above background. All sections are contrasted equally. (B) An expanded view of the inlet of (A) demonstrates a maximum Euclidian distance between injection site and the most distal node (paraaortic) of 9.2 cm. (C) Individual draining lymph nodes within an anatomical lymph node chain are distinguishable using appropriate contrast enhancement.

The exact number and connections between LNs within an anatomical chain varies per animal. As a result, if signal contrast is appropriately enhanced, numerous LNs within an anatomical region can be resolved: AFO32, for instance, displayed two draining iliac LNs (Fig. 2.3c). For purposes of quantification and comparison, these individual LNs were grouped by anatomical regions into single entities in subsequent analyses (i.e. the two-draining iliac LNs of AFO32 are reported as a single iliac LN).

These consistent trafficking patterns were confirmed at 28 hours post immunization. Figure 2.4 shows the four relevant anatomical regions of each animal, presented from anterior to posterior, all with equal contrast enhancement.

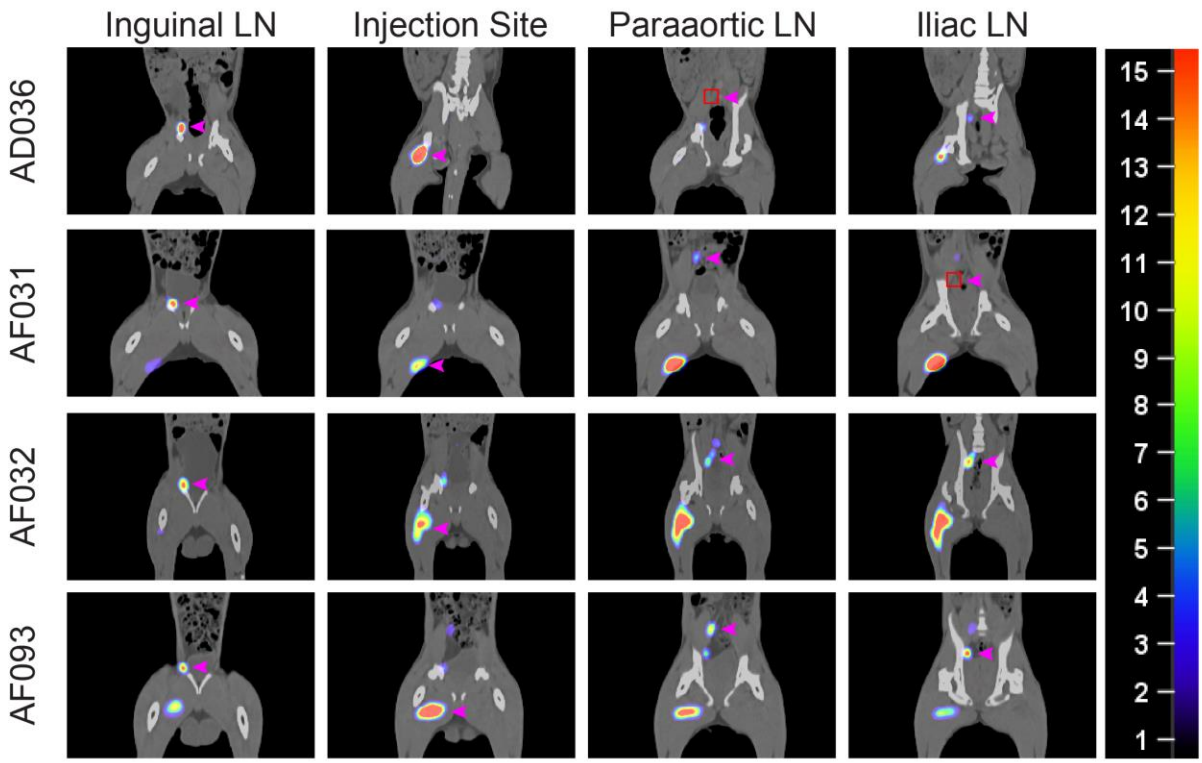

Figure 2.4: PET/CT images of non-human primates 28 hours after 64Cu IM vaccine delivery. PET/CT fusion images of each animal at 28 hours post injection, for all 4 anatomical regions with SUV signal above background. All images are contrasted equally, according to the scale bar. Magenta arrow heads indicate the organ specified by the column header. A red square inscribes the organ of interest in cases when the signal is too low to be visible.

Longitudinal PET/CT monitoring of mRNA trafficking

The mRNA distribution over time was assessed by measuring changes in the PET signal over time, as highlighted through heat map profiling of the maximum standard uptake value (SUV) (radioactivity normalized to dose and body weight) intensity at the injection site and Iliac LN at 4h and 28h, after equal contrast enhancement (Fig. 2.5a). For each anatomical area, a region of interest (ROI) was circumscribed based on high-pass thresholding above the lowest 28% of signal. The integrated SUV values across these ROIs were reported for each organ (Fig. 2.5b). The total signal at the injection site was an order of magnitude higher than in any draining LNs for all time points. In general, the total

SUV of a given LN was inversely correlated with its Euclidian distance from the injection site i.e. inguinal, iliac, then paraaortic LN.

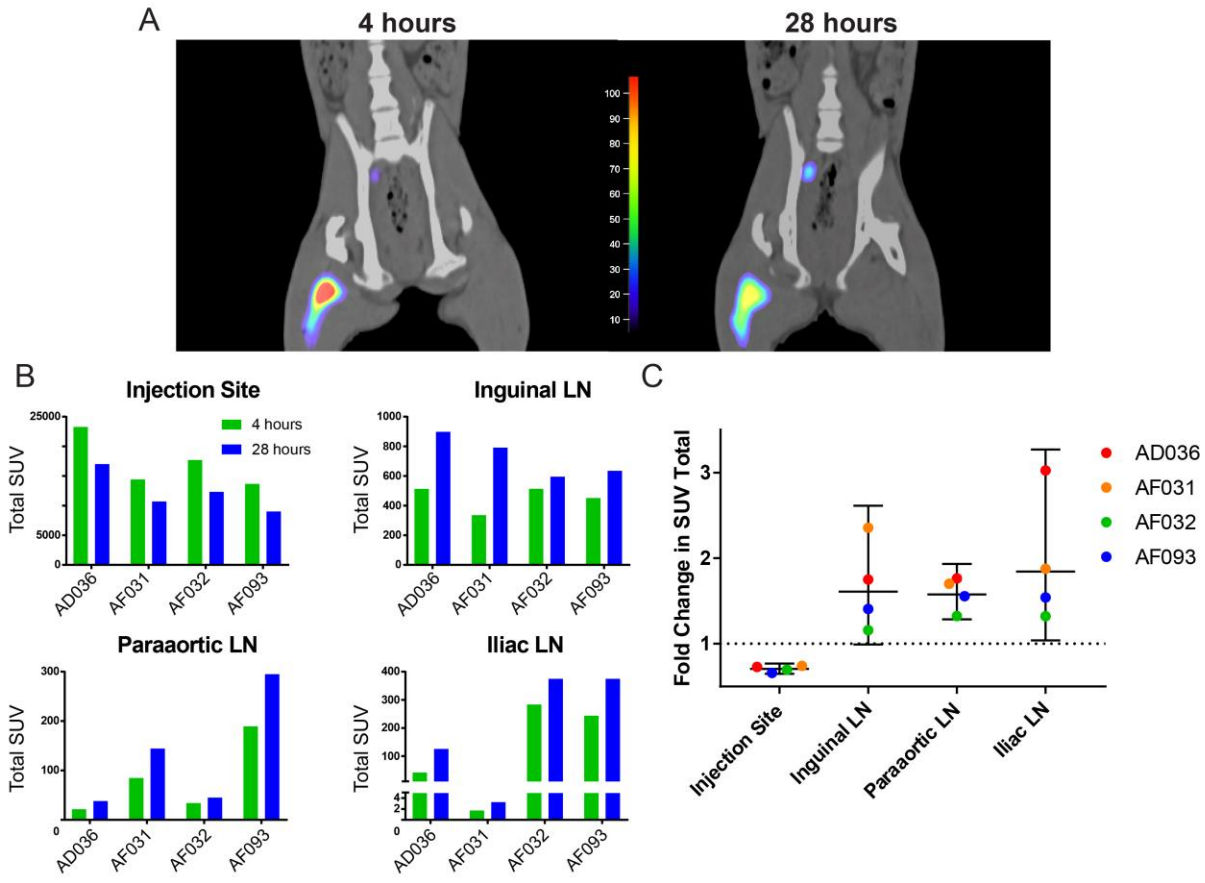

Figure 2.5: Total SUV increases over 24 hours in draining lymph nodes
(A) Visual representation of the SUV signal changes observed from 4 hours to 28 hours in AFO32. The SUVmax decreased at the injection site over time, and increased in a draining iliac LN. (B) Integration of SUV signal in each animal based on each anatomical region at 4 and 24 hours. Note that while absolute values vary across regions, signal generally increased in LNs and decreased at the injection site. (C) Fold change in Total SUV over 24 hours. Horizontal lines designate the median, with error bars representing the 95% CI.

The signal changes over time for each organ were statistically significant ($p < 0.05$). The average decrease in total SUV was 45% in the muscle at the injection site. The draining LNs showed an average increase of 1.5x in the inguinal, 1.9x in the Iliac, and 1.4x in the

paraaortic (Fig. 2.5c). To achieve accurate comparisons across time, background levels in the contralateral muscle were used to normalize absolute SUV and account for any instrument parameter differences during image acquisition.

Of note, the Iliac LN of AF031 was distinct from the other LNs, with detectable, yet extremely low total SUV values. Nevertheless, the sensitivity and high dynamic range of PET imaging allowed for quantification over time. This result is perhaps, in part, due to the intramuscular injection for this animal being markedly medial and peripheral compared to other injection sites (Figure 4). As such, the iliac LN of AF031 was used to estimate the sensitivity of PET/CT imaging to be 15.4 ng of mRNA per cm^3 (see methods for calculations).

In conclusion, *in vivo* imaging of the radiolabeled mRNA by PET/CT demonstrated that upon IM injection, mRNA reaches draining lymph nodes relatively quickly and continues to accumulate for at least 28 hours after injection. We next sought to examine mRNA distribution and protein expression at the tissue and cellular level, to characterize the cell types involved with mRNA trafficking.

mRNA transport and prME protein expression in muscle and lymph nodes

Two animals were euthanized 28 hours post injection and experimentally relevant tissues were selectively extracted during necropsy with the help of a portable near-IR camera. We observed that, in general, for each anatomical region, a single node of a chain was positive for mRNA signal while the other nodes were negative. Interestingly, a dissected inguinal node contained only a well-demarcated portion of its volume positive for mRNA signal (Fig. 2.6a). This result highlights the utility of a reporter system to specifically identify immunologically relevant tissues, as the signal-to-noise ratio in downstream analyses - such as qPCR, IHC, flow cytometry – may be negatively affected without such screening. Portions of the tissues (positive and negative) were cryopreserved as whole tissues or dissociated cells, for IHC and flow cytometric analyses, respectively.

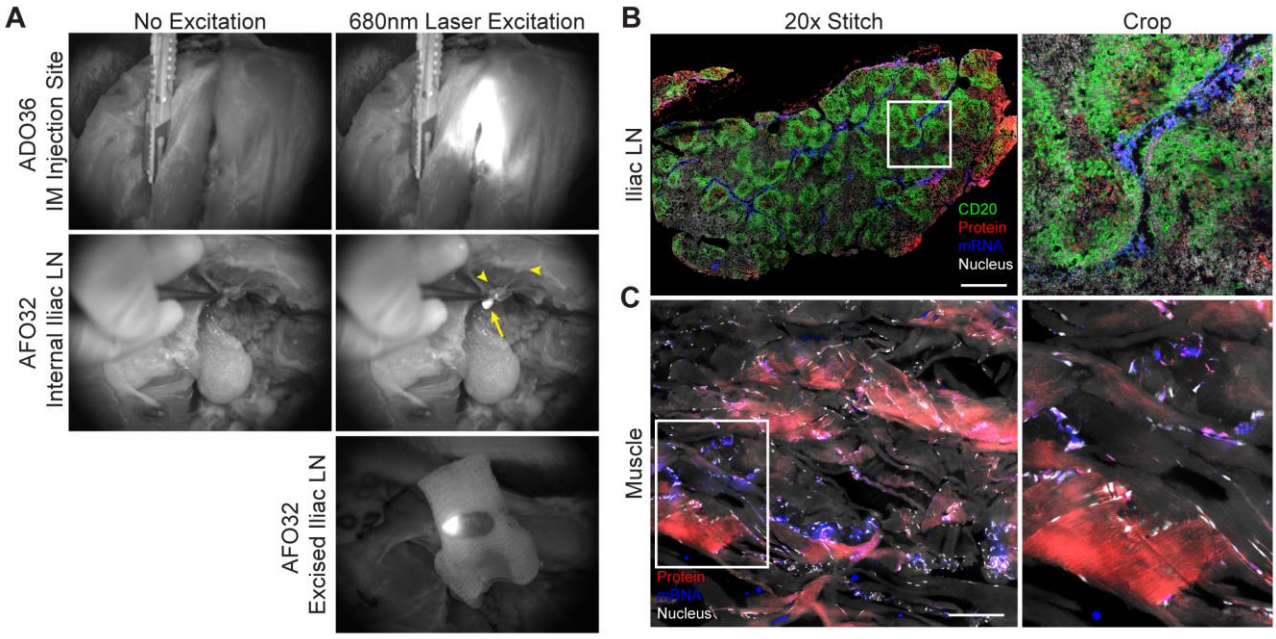

Figure 2.6: Near-IR assisted tissue extraction demonstrates robust mRNA transport and prME protein expression in muscle and ipsilateral lymph nodes. (A) At the time of necropsy, a portable near- infrared imager was used to identify mRNA positive tissues. The arrow represents a positive LN, while arrowheads point to nearby negative lymph nodes. An excised Iliac LN displayed distinct compartmentalization, with only a minor portion containing mRNA. Contralateral organs were processed in parallel as negative controls. All laser power and exposure times were empirically determined by minimizing background on negative controls. (B) A whole organ stitch of an ipsilateral LN from AF032 at 20x magnification. mRNA (blue) appears in central regions of the node, while expressed protein (red) predominately, but not exclusively, is located on the external capsule of the LN. The section was also stained for CD20 (green). (C) Ipsilateral muscle stitch at 40X

magnification demonstrating mRNA and protein distribution in blue and red, respectively; the DAPI signal was purposely contrast enhanced to visualize muscle fibers.

Immunofluorescence staining revealed the spatial distribution of both administered mRNA and expressed prME protein within the extracted organs (Fig. 2.6 b-c and Fig. 2.7). YF prME protein expression in the lymph node was confirmed by staining tissue sections using two different polyclonal antibodies (Fig. 2.8).

Stitched cross-sectional images of iliac LN (Fig. 2.6b) and skeletal muscle (Fig. 2.6c) indicated that, as expected, mRNA retained its translational capacity, as evidenced by protein staining within both tissues. In the iliac LN, prME antigen was mainly concentrated in the region of the subcapsular sinus, while the mRNA was distributed immediately outside the trabecular sinuses, near the periphery of the well demarcated germinal centers (Fig. 2.6b: crop). It is important to note that YF prME is secreted by cells upon translation. Thus, the large amount of antigen detected on the external edges of the LN could be representative of free (i.e. non-cell encapsulated) antigen transport through lymphatics.

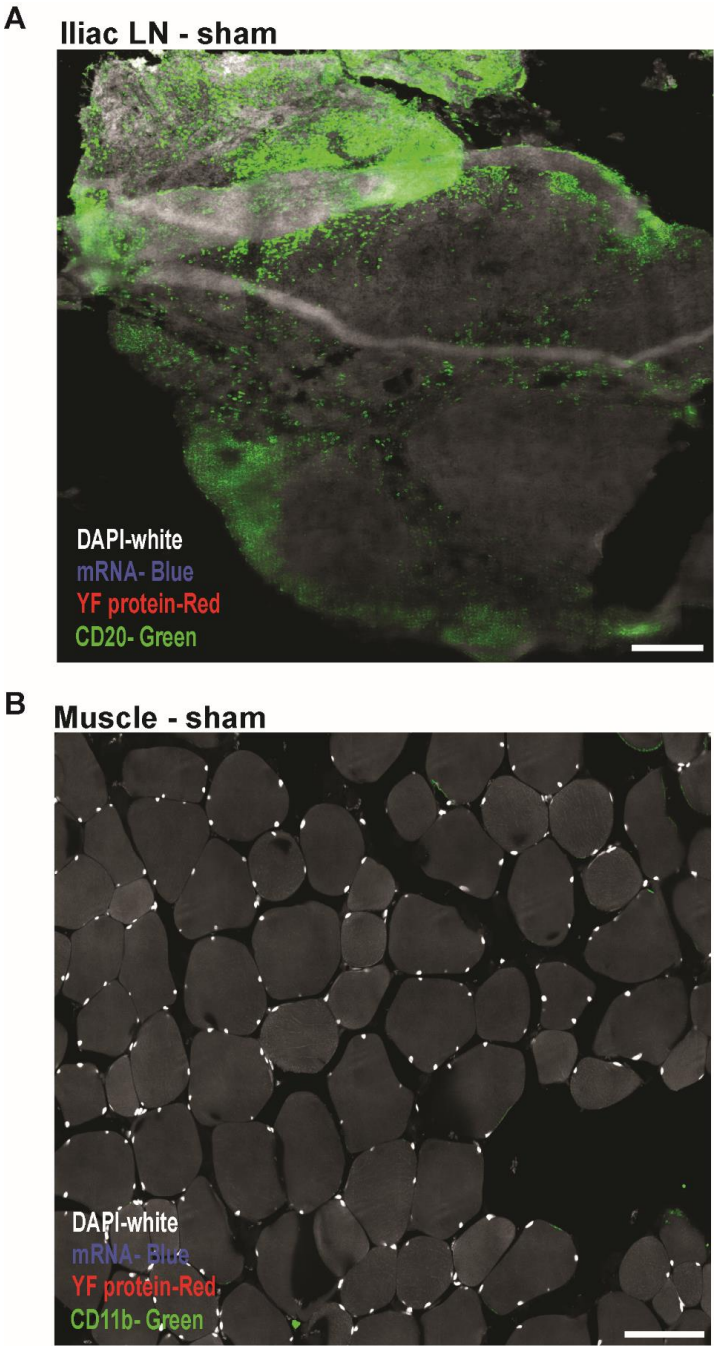

Figure 2.7: Stitches for macaques iliac LN and muscle from uninjected shams. (A) Stitch of sham Iliac LN stained for YF protein (red), cell type marker CD20 (green). Images were taken on an Elyra confocal microscope with 20X objective. Scale bar is 200 µm. (B) Stitch of sham muscle stained for YF protein (red), cell type marker CD11b (green). Images were taken on an Elyra confocal microscope with 40X objective. Scale bar is 100 µm. mRNA is shown in blue and DAPI in white.

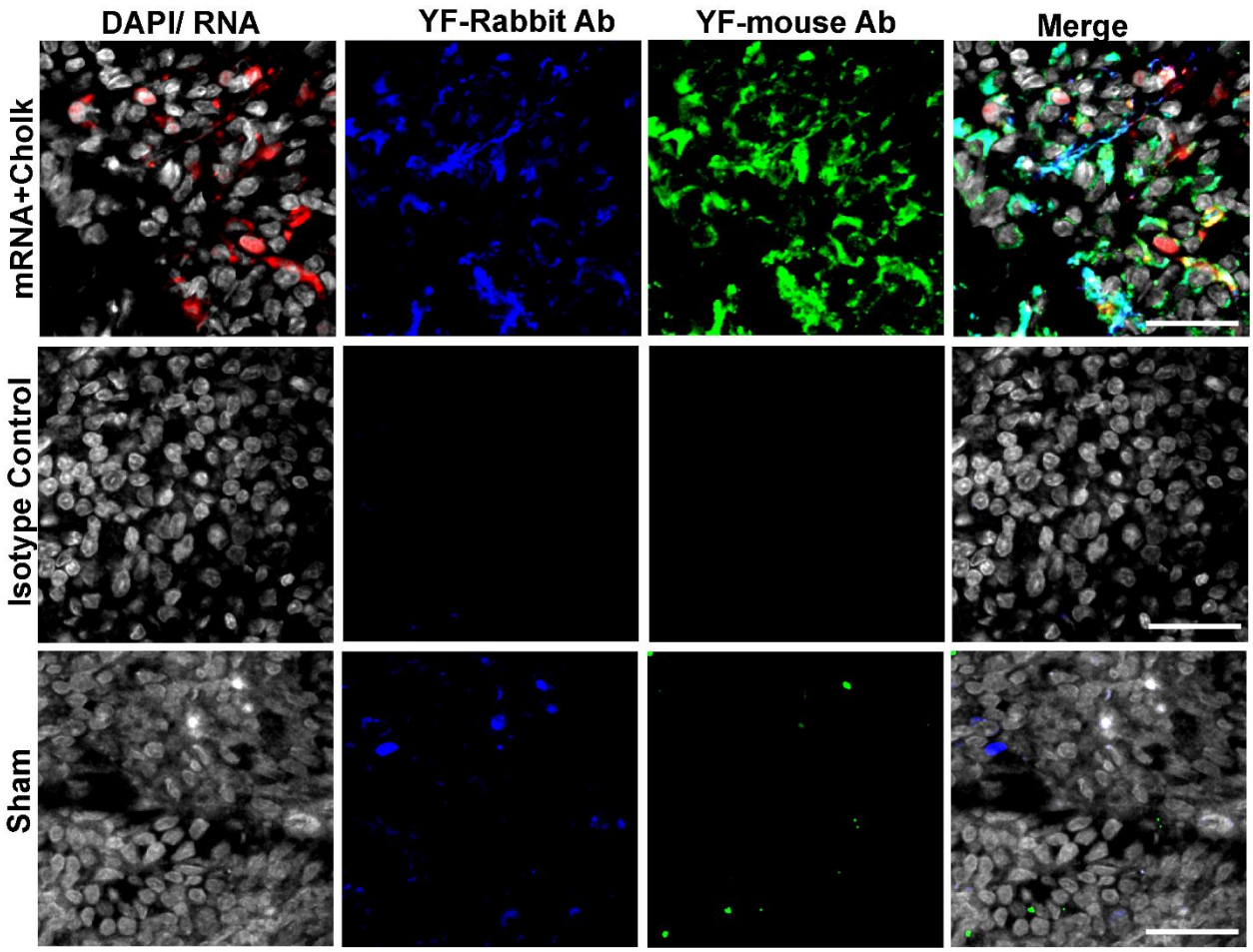

Figure 2.8: Yellow fever prME protein expression with two different antibodies in macaque iliac lymph node. Lymph node tissue stained for YF prME protein with YF antibody raised in mouse (blue) and rabbit (green). mRNA is in red and DAPI in white. Images were taken on an Elyra confocal microscope with 40Xobjective. Scale bars are 30 µm.

APCs are the primary cell type that express synthetic mRNA

First, we aimed to confirm that mRNA co-localized with prME antigen. Line profile analyses on lymph node tissue sections indicated that mRNA fluorescence signal spatially overlapped and correlated with prME antigen staining (Fig. 2.9a and Fig. 2.10). Next, we characterized the cell populations that contained the mRNA and expressed antigen via immunofluorescence co-localization analyses. Tissues were stained with the following immune cell markers: CD86 (APCs), CD20 (B cells), CD11c and CD123 (Myeloid and

Plasmacytoid DCs, respectively), CD4 (predominately T cells, but also DCs) and CD68 (Macrophages). Specific immune cell markers were utilized to measure the fraction of mRNA positive cells or protein positive cells in each tissue section that were positive for a specific immune cell marker (Suppl. Fig. 2.11-2.13). (i.e. we selected for mRNA positive cells, then examined the fraction of these positive cells that co-stained with the immune cell marker stained for in that slide).

The majority of mRNA was found in CD123+ (70%) and CD20+ (20%) cells, specific markers for plasmacytoid dendritic cells and B cells, respectively (Fig. 2.10b). The inducible APC marker CD86 was present in 85% of mRNA positive cells. For the prME antigen, a remarkably similar cell subtype distribution was observed (Fig. 2.10c). mRNA and protein expression were also observed, to a lesser degree, in B cells, perhaps reflective of their capacity to act as professional antigen presenting cells.

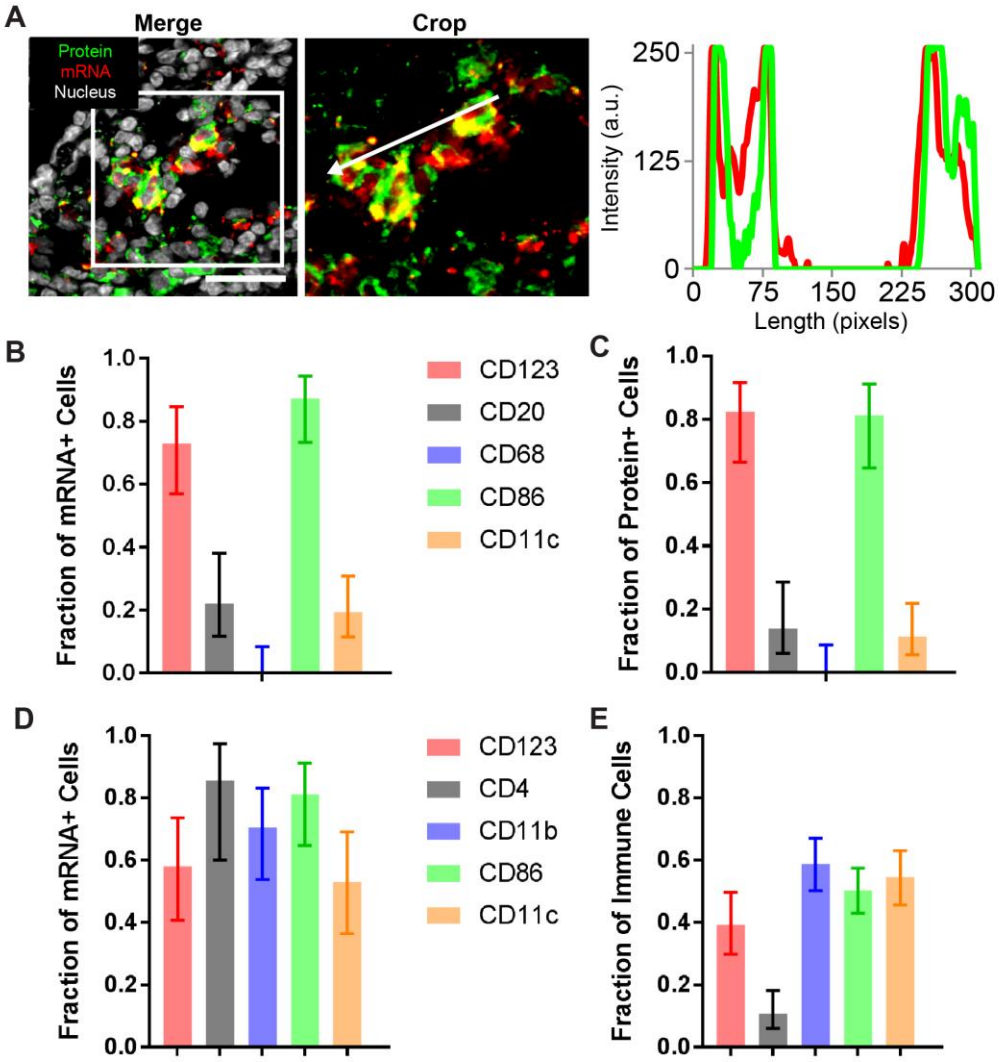

Figure 2.9: APCs are the primary cell type containing mRNA and protein in muscle and LN. (A) Line profile co-localization analysis in LNs was used to confirm spatial correlation between prME antigen (green) and mRNA (red). LN cells with mRNA (B) or protein (C) were phenotyped based on cell surface markers. Plotted values are the proportion of mRNA/protein positive cells containing the immune cell marker indicated. IHC analysis was used to quantify the proportions, with a minimum n >= 40. In *muscle tissue*, the fraction of mRNA+ cells based on cell type (D) and immune cell sub-types out of total number of immune cells (E) are presented. Error bars for all graphs indicate 95% CI.

A similar cell phenotype analysis was performed for muscle tissue. mRNA positive cells were selected and their phenotype determined via line profile co-localization analyses (Fig. 2.10d). We stained for specific cell markers, including dendritic cells (CD123 and

CD11c), B cells (CD20), macrophages and monocytes (Cd11b), APCs (CD86) and T cells (CD4). The predominant population of infiltrating immune cells recruited to the muscle consisted of antigen presenting cells and dendritic cells (Figure 2.10d). However, it proved difficult to identify sufficient prME antigen containing cells on a given tissue section for meaningful statistics. Thus, in lieu of antigen analyses, we characterized the infiltrating immune cell population at the injection site. Approximately 50% of immune cells in muscle were APCs (Fig. 2.10e). We did not observe infiltrating B cells in muscle tissue (data not shown). Flow cytometric analysis of lymphocyte activation suggests increased numbers of cells with activation makers CD25 and CD69 in the draining ipsilateral iliac LN, but not in the contralateral iliac LN (Figure 2.14). Further, these cells proved to be Fas receptor (CD95) positive CD4+ T cells. The CD25+ cells were also Foxp3-/CD127-, indicating that they are not Tregs (data not shown).

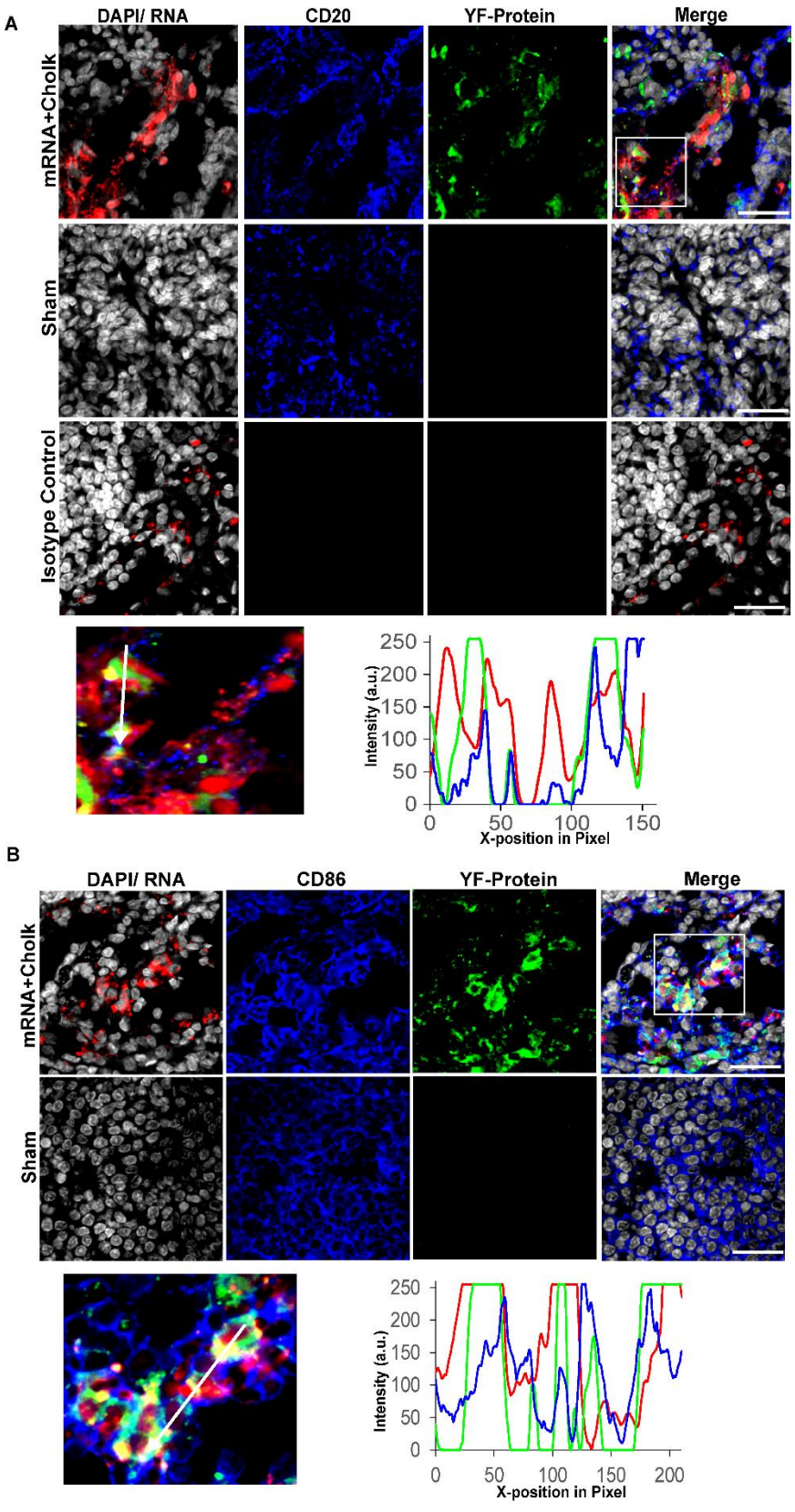
A
DAPI/ RNA
CD20
YF-Protein
Merge
mRNA+Cholk
Sham
Isotype Control
Intensity (a.u.)
X-position in Pixel
B
DAPI/ RNA
CD86
YF-Protein
Merge
mRNA+Cholk
Sham
Intensity (a.u.)
X-position in Pixel

Figure 2.10: Yellow fever prME mRNA and protein expression in immune cells of Iliac lymph node of Macaques. Lymph node tissue sections from sham and monkey injected with 200ug of dylight 680 labeled mRNA (red) complexed with Cholk at charge ratio 0.1 in monkey muscle intramuscularly. Tissue sections were stained with immune cell marker (blue) CD20 (A) and CD86 (B), YF prME protein (green) and counterstained for DAPI (white). Sham from uninjected monkeys and isotype control are shown. Images were taken on an Elyra confocal microscope with 40Xobjective. Scale bars are 30 µm. Line profile for cropped image are shown with mRNA in red, cell marker in blue and protein in green.

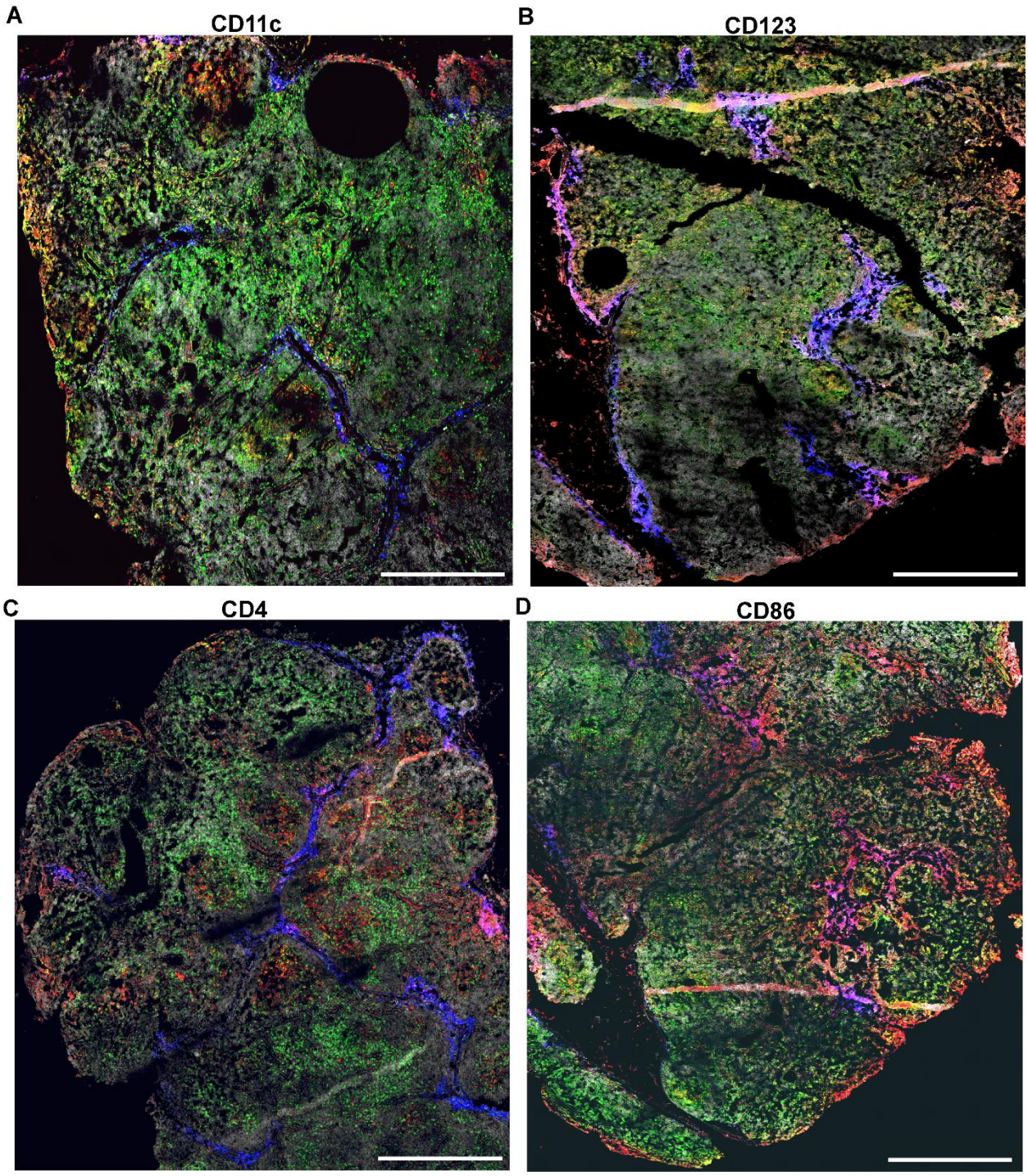

Figure 2.11: Stitches for macaques iliac LN. Stitches of Iliac LN stained for YF protein and cell type marker CD11c (A), CD123 (B), CD4 (C) and CD86 (D). mRNA is shown in blue, protein in red, cell type marker in green and DAPI in white. Images were taken on an Elyra confocal microscope with 20X objective. Scale bars are 30 µm.

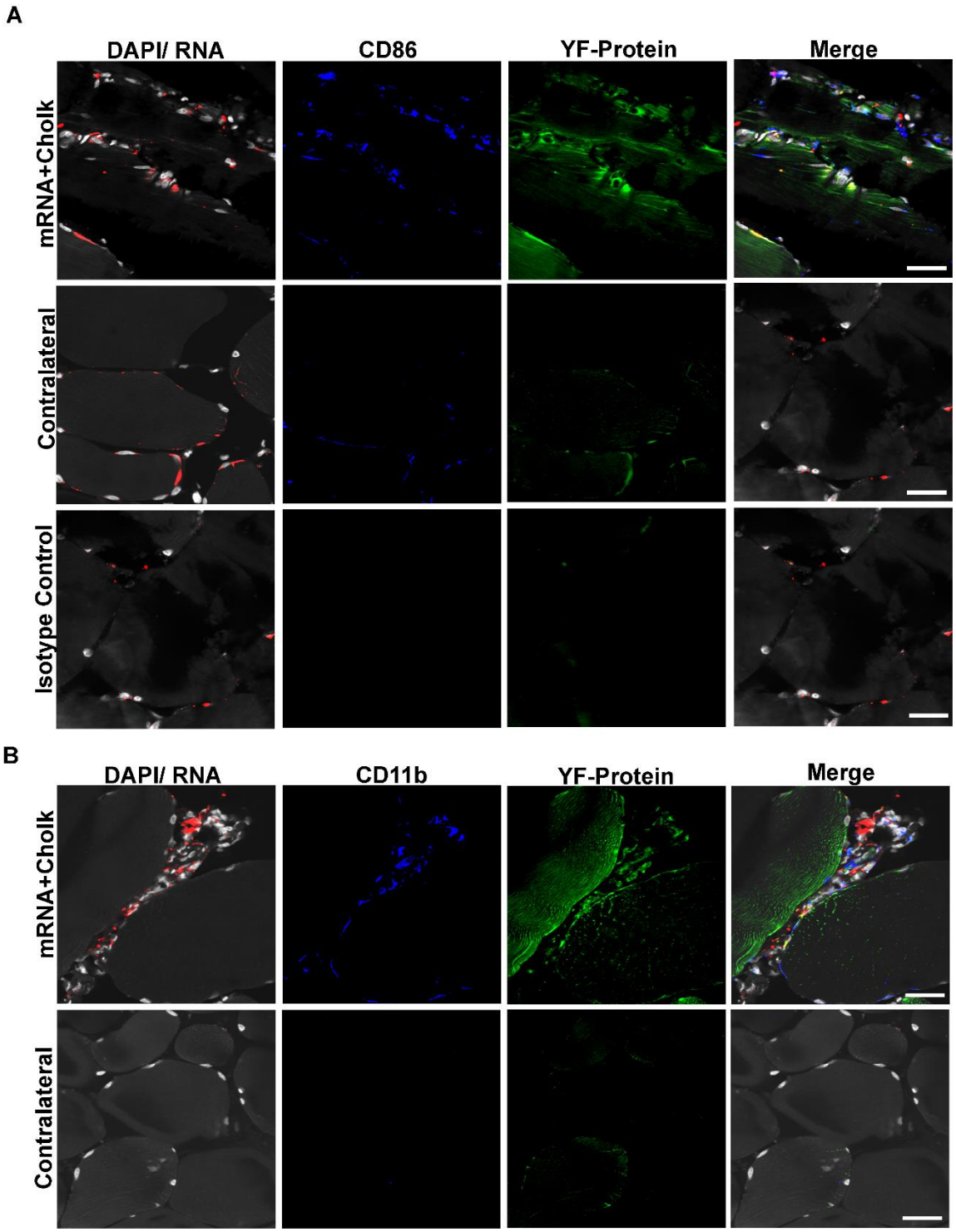

Figure 2.12: Infiltrating immune cells (APCs, Macrophages) and YF prME protein at site of injection. Cynomolgus macaque muscle injected with labeled mRNA and contralateral tissue stained with protein in green, immune cell marker in blue [Cd86 (A) and Cd11b (B)], mRNA in red and DAPI in white. Images were taken on an Elyra confocal microscope with 40Xobjective. Scale bars are 30 µm.

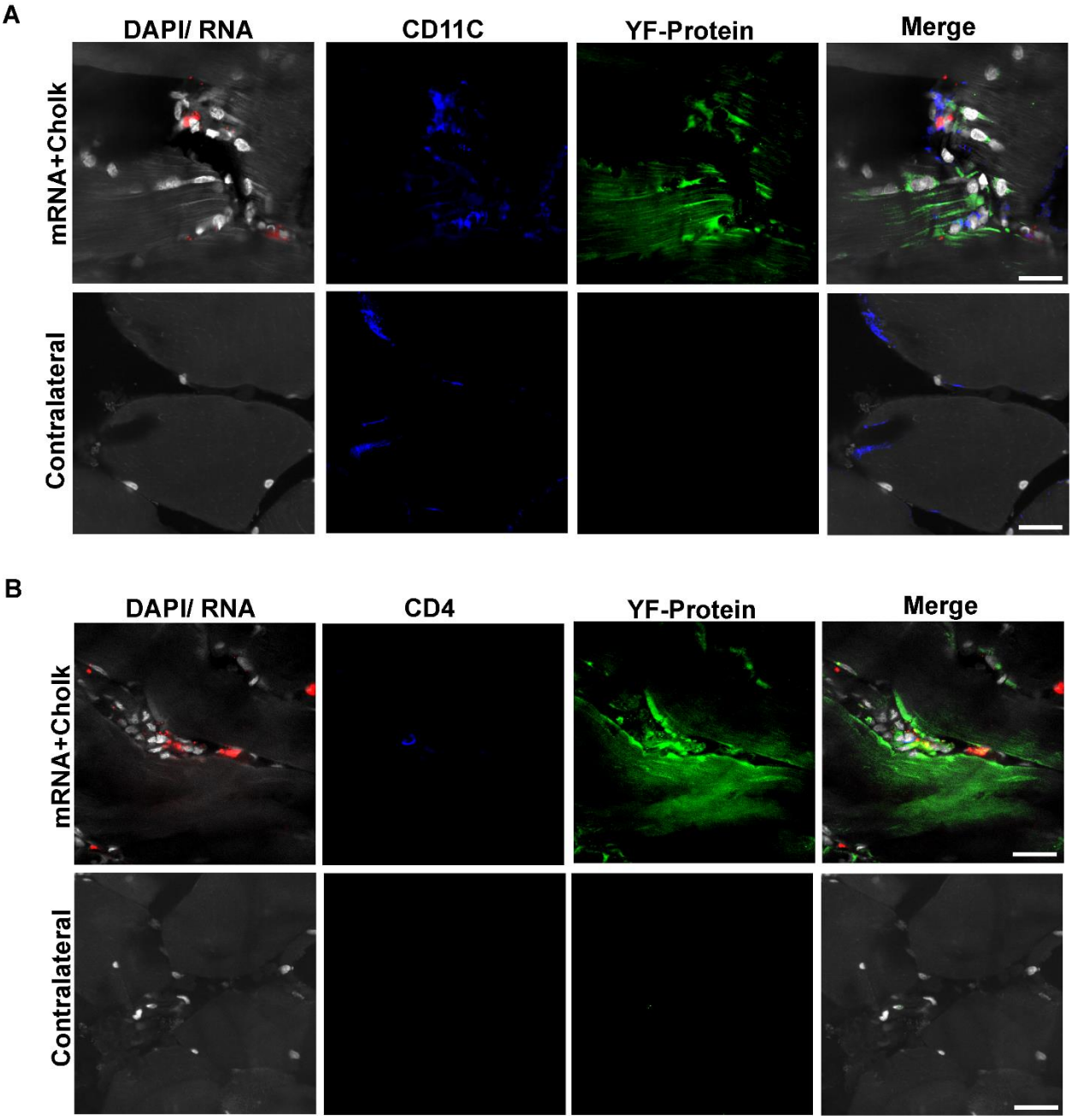

Figure 2.13: Infiltrating immune cells (Dcs, T cells) and YF prME protein in muscle tissue of macaques. Cynomolgus macaque muscle tissue and contralateral stained with protein in green and immune cell marker in blue [CD11c (A) and CD4 (B)], mRNA in red and DAPI in white. Images were taken on an Elyra confocal microscope with 40Xobjective. Scale bars are 30 µm.

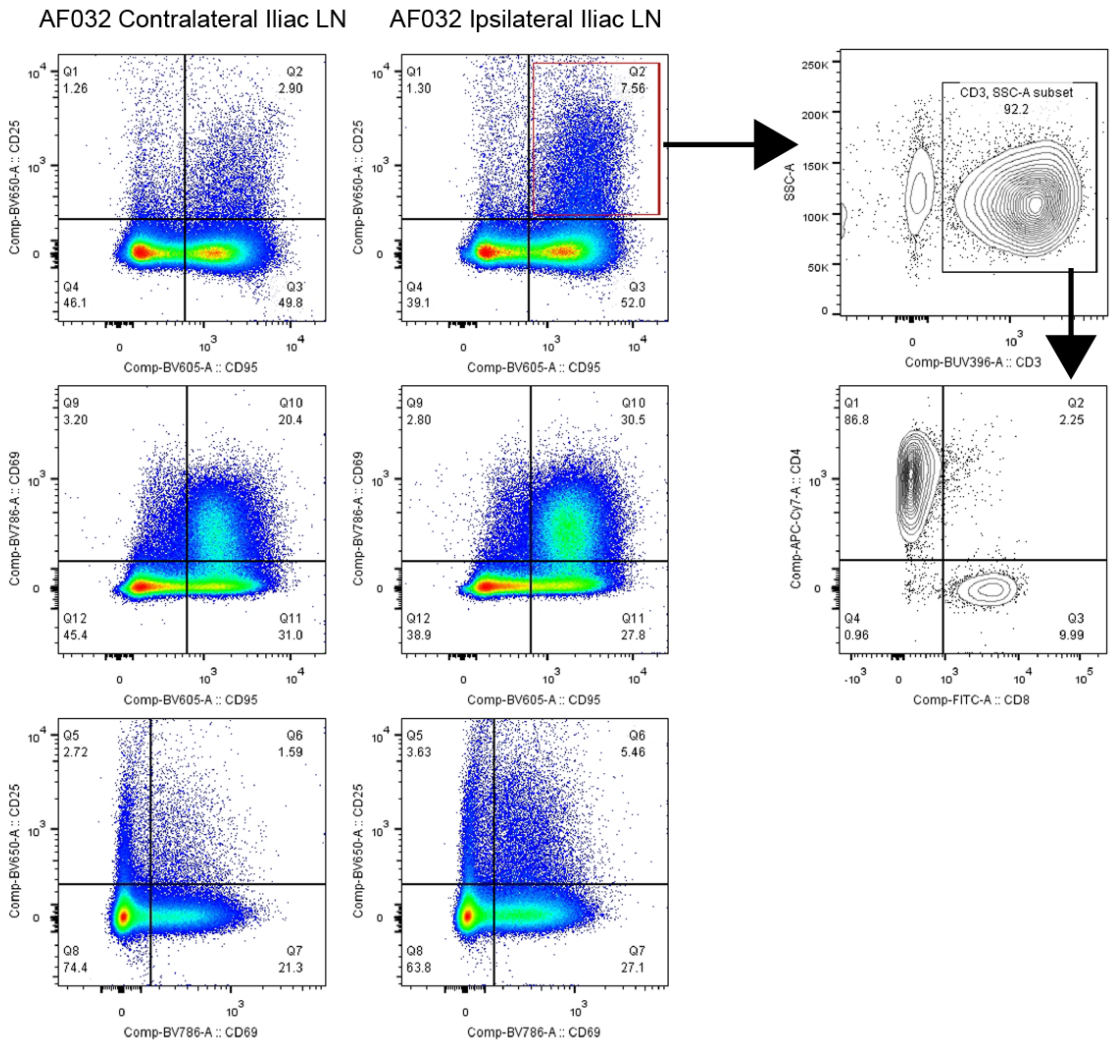

Figure 2.14: Activation of CD4+ T cells in the draining ipsilateral LN. Contralateral iliac LN lymphocytes display an upregulation of early activation markers CD25 and CD69, as well as Fas Receptor CD95, as compared to contralateral (ie non-draining) iliac lymph node primary cells from the same monkey. Further gating of CD25+CD95+ double positive cells reveals these upregulated cells are CD4+ T cells.

Discussion

Current non-invasive whole-body imaging technologies (i.e. luminescence) are less applicable to large mammals, due to size constraints as well as being optically thick. PET/CT data demonstrate a quantitative, tomographic, and *sensitive method to follow mRNA trafficking upon delivery in an in vivo setting longitudinally in non-human primates*. The estimated fundamental resolution limit for clinical and pre-clinical PET scanners is 1.83 mm and 0.67mm, respectively[73]. Based on our experimental data, we estimate the sensitivity to be 15.4 ng of mRNA per cm^3. At 4 hours post-IM administration, mRNA was present in 3 draining lymph node anatomical regions. Over a 24-hour period, the signal increased in the draining lymph nodes by an average of 70%, while mRNA in the muscle injection site decreased by 40%. Cellular analysis of near-IR positive tissues 28 hours post-injection demonstrated translation of encoded protein and that dendritic cells (DCs) and B cells were the primary cells containing the injected mRNA and encoded protein. Critically, the four monkeys in this study displayed remarkably consistent trafficking patterns, hinting at the robust nature of this tracking technology. Based on this sensitivity and ^{64}Cu half-life of 12.7 hours, it is reasonable to expect signal above background for at least 4 days (or 7.6 half-lives) post administration. Additionally, PET scanners are a staple of most hospitals, and as such as a resource are relatively available for translational studies.

During necropsy, near-IR signal from the dual-labeled probes was used to extract only relevant portions of organs that contained the RNA of interest, or at the least the single positive node of a lymphatic chain of nodes. We believe using such a positive screening approach is critical to achieve *high signal-to-noise* and to mitigate sampling errors, particularly in the case where low frequency cell types are being investigated (ie antigen specific CD8 cells and DCs). Whole LN stitched images at 28 hours post IM injection

indicated that the mRNA was spatially located just outside the B cell follicles, while YF prME antigen was observed in the interior of the germinal centers. Moreover, we observed upregulation of T cell activation markers in the lymph nodes, suggesting signaling changes in the LN microenvironment.

The proposed imaging platform is *inherently flexible and modular,* in regard to both the protein that is encoded by the mRNA and the carrier that encapsulates the RNA cargo. Labeling the mRNA directly (i.e. before encapsulation) allows this technique to be used with any carrier or delivery system. In this study, the nanoparticle CholK was selected as aminoglycosides are natural compounds known to interact specifically with RNA structures, but any nanoparticle could be utilized in practice. Furthermore, the technical hurdle to label DNA in an analogous manner is minimal. This allows for head-to-head comparisons between vaccine formulations of interest to be conducted.

Still an open question is the degree to which muscle protein expression is a determining factor in subsequent antigen specific immune responses. Producing an innate immune response in the muscle is beneficial due to potent chemokine and cytokine production that recruits immune cells[74,75], but it is possible that the primary consequence of this in terms of vaccine efficacy is increased antigen transport to lymph nodes, where antigen presentation to T helper cells and costimulatory molecule activation occurs[76–78]. In this study, we observed prME expression in the muscle and general recruitment of APC immune cells to the injection site. In the LNs, plasmacytoid DCs were the primary cell types containing mRNA and expressing prME protein.

The transport of vaccine components to secondary lymphoid tissue can occur in a passive manner that is driven by convective forces or in an active, cell mediated manner by antigen

presenting cells that infiltrate the tissue due to cytokine and chemokine signaling gradients brought about by inflammation[76]. Passive convection occurs in minutes to hours after delivery, while active transport is on the order of hours to days. These two modes of antigen delivery to lymphoid tissue are not equivalent however, and there is evidence that antigen presentation without cellular activation contributes to tolerance[76]. While we are not able to resolve using this approach which transport mechanisms are primarily responsible, the strong draining LN signal we observed at 3.5 hours suggests that imaging within 30-60 minutes after injection could help delineate the transport mechanism.

A barrier slowing down effective vaccine development is the empirical manner by which vaccines are evaluated, in a trial and error fashion, without a detailed understanding of the reasons they worked in the first place[54] . The parameters of a given vaccine, including adjuvant, delivery vehicle, and route of administration each have profound impacts upon the type of immune response generated and subsequent vaccine efficacy[21]. With each vaccination approach having its advantages and disadvantages based on the treatment setting, understanding and reverse engineering the spatiotemporal kinetics of successful vaccines could allow for the rationale development of vaccines that share similar trafficking characteristics. In other words, knowing the 'why' and 'how' of a successful vaccine can aid in improving the efficacy of other, less efficacious vaccines.

Although beyond the scope of this study, linking acute vaccine trafficking events with downstream adaptive immune responses has the potential to shed light on critical spatiotemporal determinants of vaccine efficacy. The early sequelae following injection of vaccine formulations determine the nature and magnitude of downstream adaptive immune responses[4,79,80]. This information could be used to correlate vaccine efficacy with trafficking patterns in the days immediately following injection. Generating such a

predictive model could help save time, financial resources, lower animal numbers, and in the long-term, provide a rapid proxy for vaccine efficacy during emerging outbreaks or military contexts where verifying immunity quickly is vital.

In summary, understanding acute spatiotemporal trafficking in the days following vaccine delivery can aid in the rational design of vaccines during preclinical and translational vaccination studies. We demonstrate a dual radionuclide:near-IR platform to non-invasively monitor non-human primate mRNA vaccine trafficking in a longitudinal, quantitative manner via PET/CT, while preserving downstream ability to investigate events at the level of single cells and tissue. As the RNA is directly labeled, the approach is highly modular and flexible, allowing any vaccine formulation to be utilized. In particular, using PET imaging in combination with cellular/molecular based tagging methods, such as barcoding, could prove powerful. Due to its non-invasive nature, we believe this vaccine monitoring approach can help reveal spatiotemporal determinants of vaccine efficacy in preclinical and translational vaccine studies, particularly in large mammals, where safety is paramount.

Methods

IVT mRNA labeling

IVT mRNA encoding Yellow Fever prME was provided by CureVac AG (Tübingen, Germany). It included a 5’ cap, the 3' untranslated region (UTR) from human albumin as well as a poly(A) tail. MTRIPS for mRNA labeling were synthesized as previously described (1). Briefly, 15-17 nucleotide long 2’ O-methyl RNA-DNA chimeric oligonucleotides, containing three to four amino-modified thymidines, a short poly(T) linker and a 5’ biotin (Biosearch Technologies, Petaluma, CA) were purchased. Three oligonucleotides (termed CV1, CV2 and CV3) complementary to sequences in the human

Albumin 3' UTR of the mRNA were used for annealing. The oligonucleotides were labeled with DyLight 680-NHS esters (Pierce) using manufacturer protocols, and excess dye was removed using 3kDa centrifugal filters (Millipore).

The neutrAvidin core for MTRIPS assembly was conjugated to DOTA NHS ester (5X molar excess) in 0.1M-phosphate chelexed buffer and excess DOTA was removed using 10kDa filters. For radioactive labeling, NeutrAvidin-DOTA (Na-DOTA) was incubated with ^{64}Cu in ammonium acetate for 1 hour. Unbound Cu64 was removed using 10 kDa filters. Finally, Na-DOTA was incubated with each fluorescently labeled oligonucleotide separately for 1 hour at RT, at a 1:5 molar ratio. Excess oligonucleotides were removed using 30kda filters. For mRNA labeling with MTRIPS, 800ug mRNA were first heated at 75˚C for 10 minutes (to remove secondary structure) and immediately placed on ice for 2 minutes. MTRIPS were added to the mRNA and were incubated at 37˚C for 2 hours. The mRNA to MTRIPS ratio was optimized to 1:0.5, which ensured efficient mRNA labeling while avoiding the need for a final purification step by filtration. The resulting labeled mRNA was tested via HPLC (data not shown).

Animals and intramuscular (I.M.) Injection

Cynomolgus monkeys (age, n=4) were used in this study. Macaques were maintained in accordance with the regulations of the Guide for the Care and Use of Laboratory Animal at New Iberia Research Center, University of Louisiana. Each animal was injected intramuscularly in the right quadriceps with 500uL Ringer's Lactate solution formulation CholK (In-Cell-Art, Nantes, France) with Yellow Fever (YF) prME IVT mRNA labeled with MTRIPS composed by DyLight 680-oligonucleotides conjugated to ^{64}Cu NeutrAvidin. The total radioactivity injected was 0.7-0.9 mCi. Radioactive animals were housed in a separate, designated room, according to EH&S policies, with daily radioactivity measures, until 10 half-lives had elapsed (5.3 days for ^{64}Cu).

PET/CT imaging of NHPs and Image Analysis

Animals were imaged at 3.5 and 28 hours post injection on a clinical grade PET/CT scanner (Siemans Biograph 40 at Our Lady of Lourdes Regional Medical Center, in Lafayette, Louisiana). Specific PET parameters used during acquisition can be requested through the corresponding Author.

All quantitative software analysis was completed from DICOM formatted images using MIM Software Inc. (Cleveland, Ohio). A high pass thresholding filter set at 28% (i.e. only the highest 72% of signal within a given region) was used to assign region of interests (ROIs) for each lymph node. These volumetric regions of interest were used to report average, maximum, and total standard uptake values (SUV) values. The volume of the ROIs for a given lymph node never varied by more than 5% across time points. To account for instrument parameters that might have altered between imaging sessions, contralateral muscle SUV average values for a circumscribed ROI (region of interest) were used to normalize readings. The video clip displaying a 3D reconstruction of the PET/CT data was accomplished through Amira software (Thermo Fisher Scientific, California).

PET sensitivity estimation of mRNA

The iliac LN of AF031 was used to estimate the sensitivity of PET/CT to quantify mRNA, as it was the lowest, yet detectable, organ able to be quantified. The calculations that follow are based on the SUV values for this iliac LN and an initial injection quantity of 200ug of mRNA. Assuming a closed system (i.e. no RNA enters the blood circulation), then the amount of mRNA indicated by an SUV of 1.72 is 36.3ng. This iliac LN signal is 11.80-fold greater than that found in an equal volume of control muscle tissue. If we assume a detection sensitivity 2x greater than background, then the sensitivity of detection appears to be 6.16ng for a volume of 0.4mLs, or *15.4 ng/cm^3.*

Tissue extraction and near-IR imaging

Two of the four animals were euthanized at 28 hours post vaccine administration. During necropsy, muscle tissues and lymph nodes were screened for near-IR signal using the Fluobeam near-IR portable camera (Fluoptics Imaging Inc, Cambridge MA). Images were acquired at varying exposure times in low ambient light conditions. Contralateral tissues were also collected as negative controls. Excised tissues were split in half, and dissociated for downstream flow cytometry, or fixed and snap frozen for tissue immunohistochemistry.

For cell dissociation, lymph nodes (and spleen sections) were mechanically dissociated by pressing and grinding the tissue on top of a 70-micron filter, fitted on top of a 50mL conical tube. During this mechanical disruption, the tissue was systematically washed with RPMI media, under sterile conditions. After the lymph nodes appeared as a thin flat layer, the tissue was washed a final time, and the filtered cloudy solution within the 50mL tube was centrifuged at 1000xg for 10 minutes at 4°C. If the resultant cell pellet contained a top RBC layer, RBCS were lysed with addition of JAK solution for 5 minutes, and rewashed with RPMI. Cells were resuspended in 10mLs of RPMI, counted with a hemocytometer, and frozen at a concentration of 10-20 million cells/mL in 20% DMSO in FBS at a temperature gradient of -1°C/minute. Cells were stored and shipped at -80°C, and stored long-term in liquid nitrogen.

For IHC tissue processing, macaque draining iliac or inguinal LNs, muscle (injection site and contralateral) and mouse iliac LN tissues were fixed in 4% PFA overnight at RT. The next day, the tissue was washed once with PBS and incubated with 30% sucrose in PBS overnight at 4°C, followed by OCT embedding. Tissue blocks in OCT were immediately snap frozen in dry ice cooled isopentane, and stored at -80°C. Frozen tissue blocks were sectioned using a cryostat in 10 micron tissue sections. Tissue sections separated by 50-100 microns were used to stain for the specific immune cell markers and antigenic protein.

Macaque LN tissue from a sham animal (uninjected) and contralateral animal were used as controls.

Immunofluorescence tissue imaging

Cynomolgus monkey iliac LN tissue sections were stained for cell surface markers (Table 2) and expressed YF prME antigen. The slides were thawed in a humidified chamber for 5 minutes and washed with 1x PBS twice. The sections were incubated in 1x Dako antigen retrieval buffer for 30 minutes in a steamer followed by cooling at RT for 20 minutes. The slides were washed once with PBS (1x) and permeabilized with PBS with 0.1% Tween 20 for 30 minutes. The tissues were blocked with 10% Donkey serum plus 1% BSA for 45 min followed by incubation with the primary antibodies targeting selected cell type markers and YF prME protein for 45 minutes at RT (the primary antibodies source and dilutions are listed in Table 2). Tissue sections were washed four times with 1x PBST for 10 minutes each followed by incubation with the secondary antibodies (as listed in Table 2) for 30 minutes. Slides were washed with 1x PBST four times for 5 minutes each and incubated with DAPI for 5 minutes at RT. After two final washes with 1x PBS, slides were mounted with 10ul of prolong gold. Muscle tissue sections were incubated with 1x DAKO antigen retrieval buffer for 20 minutes and blocked for 1 hour as previously described. Slides were incubated with primary antibodies for selected immune cells markers overnight. The next day, the tissue sections were incubated with secondary antibodies for 30 minutes, followed by three washings with PBST. The YF prME antibody was added for 1 hour followed by three washings with PBST. Nuclei were counterstained with DAPI and slides were mounted with Prolong Gold.

LN and muscle tissue sections from macaques were imaged with a 40x, oil objective. Three or four slides were imaged for each cell marker and 10-12 images were taken per

slide. Stitching was performed using a 20X objective for LN tissue and a 40X objective for muscle tissue.

Table 2: Immunofluorescence Staining Markers

Cell Marker	Primary antibody Host (source) / Dilution in blocking soln.	Secondary antibody (source) / Dil. In blocking soln.	Primary Antibody cat. No. / clone	Validations
CD86 – Antigen presenting cells	Rabbit (Abcam) / 1:50	Donkey anti rabbit-488 (Invitrogen) /1: 500	ab53004 / EP1158Y	WB, IP, ICC, Flow Cyt, IHC-P, IHC-Fr
CD20- B cells	Rabbit(Abcam) / 1:50	Donkey anti rabbit-488(Invitrogen) /1: 500	ab78234 / EP459Y	WB, IP, IHC-P
CD68- Macrophages	Rabbit (Santacruz)/ 1:25	Donkey anti rabbit-488(Invitrogen) /1: 500	sc-9139 / H-255	WB, IP, IF and ELISA
YF protein	Mouse (Sigma)/ 1:2000	Donkey anti mouse 555 (Invitrogen) /1:500	MAB984 / 2D12.A	Neutralization (BLK) Asibi YF Hemagglutination-inhibition
CD123 – Plasmacytoid DCs	Rabbit (Santacruz) (1:50)	Donkey anti rabbit-488(Invitrogen) /1: 500	Sc-681 / V-18	WB, IP, IF, IHC-P
Cd11c – Myeloid DCs	Rabbit (LS Bio) (1:25)	Donkey antirabbit-488 (Invitrogen) /1: 500	LS C165321 / Polyclonal	WB, Flow Cyt, IF, IHC-P,
CD4 – T Cells	Rabbit (abcam) (1:100)	Donkey antirabbit-488 (Invitrogen) /1: 500	ab133616 / EPR6855	WB, ICC/IF, Flow Cyt, IHC-P

Flow Cytometry

Cryopreserved cells were thawed at 37°C, washed with two volumes of fresh RPMI, resuspended in 2 mLs 1x PBS, and counted with a hemocytometer. One million cells were chosen and stained with the lymphocyte activation panel indicated Table 3. Live dead staining was performed first, followed by surface cell staining, and finally permeabilization (saponin) followed by intracellular staining (All staining steps occurring in FACS Wash – 2% FBS in 1x PBS. Cells were fixed with 1% PFA in FACS Wash at 4°C until data acquirement. In all cases, cells were gated for single cells via FSC-H vs FSC-A → SSC-A vs FSC-A for lymphocytes → Live/Dead stain. All samples were acquired using a Fortessa Cell Cytometer equipped with 405, 488, 560, and 640 laser lines (BD Biosciences). All analysis was performed using the FlowJo software package (Tree Star, Ashland, OR, USA). A total of at least 300,000 events were recorded for each organ.

Table 3: Lymphocyte Activation Panel for Flow Cytometry

Cell Marker	Indicates	Dye	Clone (Company)
CD3	T cells	V450	SP34-2 (BD)
CD4	T cells	APC-H7	L200 (BD)
CD25	Activated T cells	BV650	BC96 (Biolegend)
CD8	T cells	FITC	RPA-T8 (Biolegend)
CD69	Activated T cells	BV786	FN50 (BD)
CD20	B Cell	BV711	2H7 (Biolegend)
CD95	Fas Receptor	BV605	DX2 (Biolegend)
Ki-67	Proliferation	PerCp Cy5.5	B56 (BD)

Statistics and Image Visualization

For the comparisons of total SUV across time, the fold change in total SUV for a given lymph node was calculated. Both estimation (95% confidence interval) and null hypothesis significance testing via multiple comparison student T-tests were conducted at 95% significance to evaluate differences from a baseline fold change of 1x. For both CIs and student T-tests, the Bonferroni correction was applied. All statistical tests and graphical figures were generated using GraphPad Prism (La Jolla, California).

RT-PCR for cytokine expression *in vitro*

Hela cells (ATCC) were cultured in DMEM (Lonza) with 10% FBS (Hyclone), 100 U/ml penicillin, and 100 µg/ml streptomycin (Invitrogen) and were plated one day prior to experiments. Cells were transfected with 500ng unlabeled or MTRIP-labeled mRNA in duplicates using Lipofectamine 2000 (L2K, ThermoFisher Scientific) following the manufacturer instructions. Vehicle only controls were included. 24h post transfection cells were processed for total RNA extraction using the RNeasy mini kit (Quiagen). Total RNA was checked for integrity via agarose gel electrophoresis and quantified via Nanodrop2000. 1ug of total RNA was used for cDNA synthesis using the RT2 first strand kit (Quiagen) according to manufacturer instructions. 1ul of the reaction product was used for qRT-PCR using the Real-time RT2qPCR primer assay (SYBR green) in the presence of gene-specific primers for IL6, INF1B, IL1B and GAPDH (Quiagen). qRT-PCR was performed using the ABI StepOnePlus real time PCR system (Applied biosciences).

Data Availability

The authors declare that [the/all other] data supporting the findings of this study are available within the paper [and its supplementary information files]. PET/CT scanner acquisition settings can be attained by writing to the corresponding author PJ Santangelo.

CHAPTER 3

Aerosolized mRNA transfection of the FRT mucosa to express antibodies targeting HIV

Much of the preliminary anchored antibody and aerosol delivery in this chapter was developed in: Tiwari PM*, Vanover D*, **Lindsay KE**, Bawage SS, Kirschman JL, Bhosle S, Lifland AW, Zurla C, Santangelo PJ. **"**Engineered mRNA-expressed antibodies prevent respiratory syncytial virus infection." *These authors contributed equally to this work. *Nature Communications* (In Revision).

Key Points

- The whole of the FRT can be transfected with naked mRNA and H_2O
- Expression occurs quickly, within 4 hours
- Anchoring can retain antibody in tissue and secretions for at least 28 days
    - Antibody is detected throughout the FRT, including in the Uterus
- Genitally expressed antibodies neutralize virus *ex vivo* and protect cervical biopsy explants from SHIV Challenge
- Aerosolized mRNA reaches distal lymph nodes within 80 minutes after transfection

Background

Human immunodeficiency virus (HIV) remains a large public health burden worldwide, with 36 million people infected and 1.8 million new cases per year[81]. The portal of virus entry can vary based on the route of transmission and geographic location, but in general, genital mucosal entry is most common, followed by i.v. drug use and mother to child transmission. In the case of heterosexual serodiscordant couples, the estimated

probability of infection of the female genital tract (FRT) is 1 in 200-2000 per coital act, although this probability is dependent on the current viral burden in the donor, which is highest during the acute and late stages of infection[82,83]. Recipient factors providing protection include mucus, antimicrobials present in genital secretions, intact tight junctions between epithelial cells, and protective mutations in the CCR5 co-receptor[84]. The increased use of anti-retroviral therapy (ART) to reduce the risk of transmission, both in the donor and receiver, has led to dramatic decreases in nascent HIV infections, with a protection rate of 90%. Both pre-exposure (PrEP) and post exposure prophylaxis regimens consist of a required daily use regimen, potential for nephrotoxicity, expensive cost, and a lack of coverage against other STIs. As such, alternative and potentially patient-applied approaches to treatment and prevention of HIV could prove useful, especially in regions where access to ART therapy is difficult to access.

The mechanisms and kinetics underlying HIV acquisition in humans is inherently difficult to study. As a result, the simian immunodefiency virus (SIV) and chimeric simian-human immunodeficiency virus (SHIV) models in non-human primates (NHPs) are powerful models to examine acute infection, as the disease progression reliably follows the course of human HIV infection [Refs]. The only protein on the virion surface is the *Env* glycoprotein, a trimer of two non-covalently associated sub-units, gp120 and gp41, responsible for binding CD4 receptors on target immune cells and mediating membrane fusion, respectively. The HIV genetic variants most likely to successfully infect the host enrich for *Env* on the virion surface, increasing the probability of binding CD4+ cells[85,86], which are located with varying frequencies throughout the entire submucosa of the lower FRT. These consist of predominately CD4 high expressing CCR5+ T cells[87,88], but also CD4 low expressing dendritic cells and macrophages. Epithelial cells are not able to support productive infection. It is likely that inflammation, whether caused by co-infection

with other sexually transmitted infections, genital ulcers, hormonal birth control, or physical trauma, increases the risk of HIV transmission by recruiting T cells and dendritic cells (DCs) to the area[89], while also activating T cells[90].

When virus is introduced into the FRT lumen via ejaculate, it rapidly permeates the vaginocervical epithelium by passive diffusion, perhaps as quickly as within 30 minutes[91]. After initial productive infection in CD4+ T cells, clonal amplification occurs and virus is able to spread more generally within the mucosa, and systemically to lymph nodes and mucosal associated lymphoid tissue (MALT)[92]. Alarmingly, there is also evidence that virus can reach systemic lymph nodes in under one day, suggesting that mucosal amplification is not necessarily required for HIV to reach systemic organs[93]. Dendritic cells don't support productive infection themselves, but facilitate HIV transmission and dissemination by transferring CD4-bound-HIV to T cells located the mucosa and lymphatic organs[94,95]*. Thus, it is critical that any intervention strategy counteracts initial virus seeding and replication in the lower FRT and regional lymph nodes.*

Active (vaccination) and passive (topical) immunization strategies are being deployed to protect patients from HIV. While not underplaying the importance of CTL and T helper cell responses for control and protection from HIV at mucosal surfaces, humoral immunity plays a considerable role against genital pathogens by providing a first line of defense at mucosal surfaces[96]. Antigen specific immunoglobulins present in the genital mucosa of vaccinated animals are a mixture of systemically derived[97] and locally produced antibodies[98]. Local production occurs in the form of IgG+ cells[99] consisting of sub-epithelial plasmablasts and ectopic follicles[100,101], while systemic IgG reaches the FRT compartment by neonatal Fc mediated transport from the serum[96].

Due to tight association with cervicovaginal mucus[102], immunoglobulins (predominately IgA and IgG) mediate protection through neutralization[103,104], along with a variety of Fc mediated mechanisms, including: slowing virion diffusion through mucus[105], antibody dependent cellular cytotoxicity of infected cells, activating complement pathways, virus opsonization, transcytosis inhibition[104], cellular phagocytosis, and in the case of IgA, agglutination. For genital IgG in particular however, it appears neutralization of *Env* plays an outsized role in affording protection, compared to other antibody-associated mechanisms[106]. That said, certain non-neutralizing antibodies play a role in controling[107] and impacting viral seeding following vaginal challenge[108], due to their diverse Fc mediated anti-viral activities[109] .

Binding of a neutralizing antibody to a single monomer of the *Env* trimer is sufficient to prevent the conformational changes required for membrane fusion, effectively neutralizing the entire spike in a single binding event[82]. Broadly neutralizing antibodies (bNAbs), which are characterized by their ability to neutralize a broad assortment of HIV strains with high potencies, correlate strongly with chronic viremic control, but only a minor fraction of infected individuals develop them[110]. Unfortunately, to date, no HIV vaccine has elicited host generated broadly neutralizing antibodies in uninfected inviduals[106], although directed antibody evolution through engineered immunogens is an area of active research. Due to this, passive immunoprophylaxis by parenteral administration of bNAbs is a current stopgap, until HIV vaccines progress sufficiently.

Human clinical trials involving passive transfer of bNAbs are promising, displaying control of viral loads in human patients[111,112] and suppression of viral rebound after ART treatment

interruption[113]. Passive infusion of the CD4 binding site bNAb 3NBC117 even increased host generated antibody responses to HIV-1[114]. NHP studies demonstrate protection from mucosal SHIV challenge[115–117], along with control of viral replication[118–120]. In one study, administration during acute SHIV infection led to long lasting CD8+ T cell immunity that suppressed virus long after administered antibody titers were undetectable[121]. In these passive immunotherapy based approaches, virus breakout occurs if serum antibody titers drop below threshold levels[111] or antibody-resistant provirus strains evolve in the individual[111–113]. Escape viruses that emerge during passive therapy remain sensitive to bNAbs that target other non-overlapping domains[112]. LS-mutations in the Fc region of antibodies increase circulation half-life, and in a phase 1 clinical trial VRC01LS remained in circulation 4 fold longer than wild type VRC01[122].

To protect patients from acquiring HIV, ectopic antibodies delivered parenterally must reach the genital compartment through transudation from the serum. It has been estimated based on empirical measurements that around 1/90th of the concentration of antibody in the serum is achieved in vaginal secretions[82]. The amount of bNAb required in genital secretions to prevent infection decreases with higher binding affinities. For the bNAb PGT121, with a relatively high binding affinity (k_D = 0.086nM), genital secretion concentrations of as low as 30 ng/mL are estimated to provide neutralizing protection[82]. There also appears to be a time delay between the peak serum concentration of injected antibody (which is almost immediately) and the peak concentration in the vaginal secretions, although the magnitude of this delay is dependent on the specific antibody[117,123]. In effect, systemically administered bNAbs have demonstrated promising anti-viral properties. However, the large doses administered and uncertain time required for genital secretions to reach sufficient neutralization concentrations, suggests that local

application of bNAbs could prove useful. Direct vaginal application of bNAbs prior to challenge provided protection in NHPs[124], but the half-life of such an approach is likely on the order of several hours[125].

In this study, we explored the potential use of the cervicovaginal mucosa as a platform to express mRNA encoded bNAbs locally, at the site of infection. Specifically, we demonstrate in sheep and rhesus macaques, the use of aerosolized naked mRNA to express PGT121 at high concentrations in the vagina and cervix. To promote the retention of bNAbs in the FRT, we incorporated a glycophosphotidyl inositol (GPI) membrane anchor to the heavy chain Fc domain of PGT121. *In vitro* data confirms that this membrane anchored PGT121 (termed aPGT121) leads to an outward facing cell surface display of PGT121 that is functionally able to bind SHIV virions. We detected aPGT121 in FRT tissue at the longest time point we measured, 28 days. In comparison, secreted PGT121 levels were comparable in the short term, but dropped off substantially by three weeks. The expressed PGT121 retains neutralizing capacity in secretions and in cervical biopsy explant SHIV challenge models.

Aerosolized transfection deposits mRNA directly into the cytoplasm

Pilot experiments in rhesus macaque genital mucosal surfaces and other comprehensive studies in mice lungs illustrate that aerosolized delivery to these mucosal surfaces results in robust protein expression. There is some evidence that hypotonic solutions increase transport from luminal spaces[126]. For this reason, and translational simplicity, we use a formulation of H_20 with naked nucleic acids. However, the mechanism underlying this transfection method remains uninvestigated.

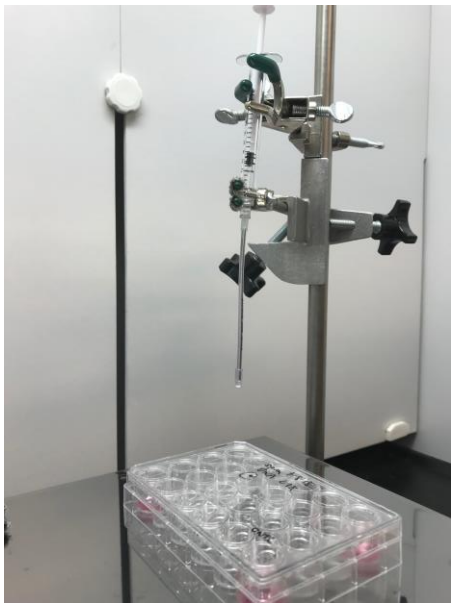

Figure 3.1: The in vitro transfection setup using the MADgic Teleflex aerosolizer attached to a high-pressure syringe. Media is removed directly prior to application of spray to plated on coverslips in 24 well plates.

To investigate how naked mRNA is leading to robust protein expression via aerosol, we used a vertical *in vitro* setup (Figure 3.1) to transfect monolayers of adherent cells. The ideal distance to prevent cell dissociation from the applied pressures were sprayer dependent, and were determined to be 4.5 inches for the Teleflex and 1 inch for the microsprayer. After delivery with dye labeled mRNA, the fraction of nucleic acid not in the endosomal compartment or nucleus was estimated using microscopy at discrete time points after spraying (Figure 3.2). The markers CD63, Clathrin, Caveolin, EEA1, LAMP-1 were used to demarcate early through late stages of the endosomal compartment, while DAPI stained the nucleus.

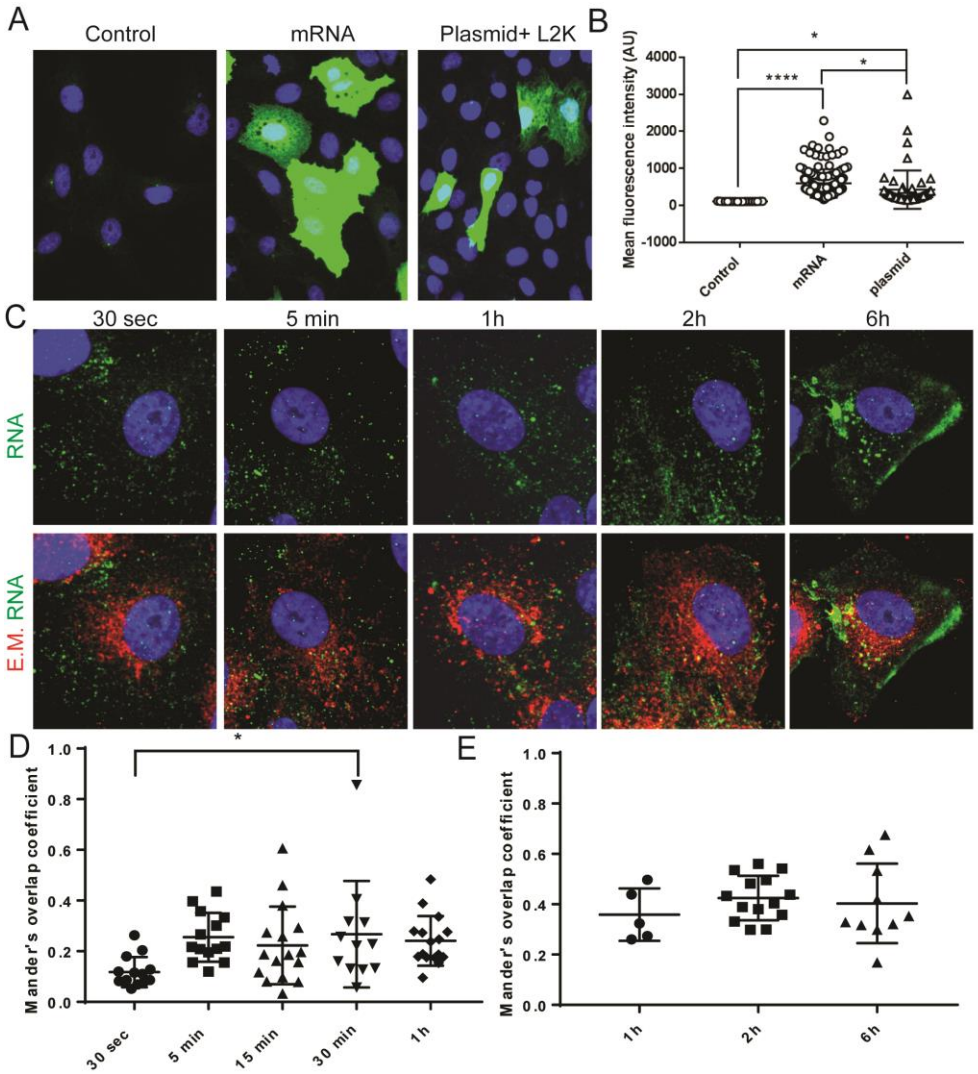

Figure 3.2: Aerosol transfection of cells localizes the mRNA directly to the cytosol of cells. (A) Spraying of mRNA and pDNA in lipofectamine 2000 (L2k)resulted in GFP protein production at 24 hours. (B) mRNA led to more GFP production and more cells transfected than pDNA + L2k. (C) In vitro fluorescent imaging of dye labeled Mrna (green) alone and costained with endosome markers (red). (D) Less than 70% of the mRNA colocalizes with the pan stage endosomal markers CD63, Clathrin, Caveolin, EEA1, LAMP-1. (E) The proportion of mRNA in the cytosol does not change from 1 hours to 6 hours post transfection. * $p < 0.05$; **** $p < 0.00005$.

The results indicate that GFP encoding mRNA is reaching the cytoplasm almost immediately upon delivery. Around 70% of the cellular mRNA is cytosolic at 15 minutes post-delivery (Figure 3.2D). There is a slight pattern of increased endosome localization over time (up to 6 hours), but these changes are not significant (Figure 3.2E). These

results suggest aerosol transfection is depositing naked nucleic acids directly into the cytosol. For mRNA, this results in access to translational ribosomal machinery, leading to protein expression. Preliminary data with aerosolized naked pDNA suggests direct deposition into the cytosol, with no transport to the nucleus, and thus no subsequent protein production (data not shown).

Aerosolization of naked mRNA is required to transfect the cervix

To explore the physico-temporal parameters of FRT transfection, we used sheep, an animal model that is used in contraceptive and vaginal implant trials due to a geometry that closely mimics the human FRT (as a point of reference, the sheep in our studies weigh ~80-110 lbs). From the vaginal vestibule to the cervix is 8-10 inches. To visualize transfection, we delivered 250ug of Firefly Luciferase mRNA via the MADgic Teleflex aerosolizer to the FRT. After 24 hours, the entire FRT was removed, D-Luciferin substrate applied, and IVIS used to record bioluminescence signal (Figure 3.3). As an alternative delivery method, mRNA was squirted by high-pressure syringe onto the cervix. Robust transfection of the cervix was observed by aerosolization, but no signal was detected when simply applying the fluid out of a syringe at high pressure.

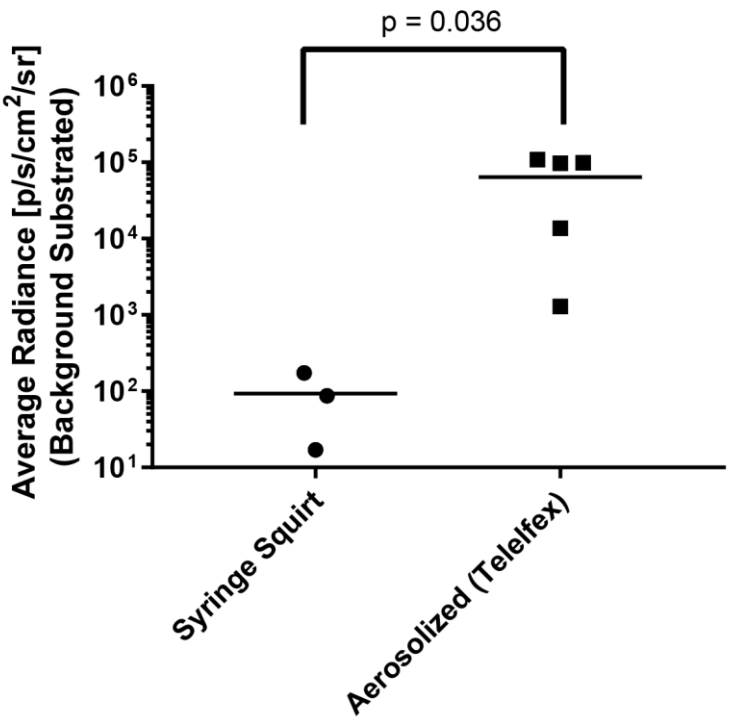

Figure 3.3: Aerosolized naked luciferase mRNA transfects the sheep cervix. 250ug of Firefly luciferase encoding mRNA was sprayed in a single dose onto the cervix. Statistical comparison was completed using two tailed Mann-Whitney non-parametric analysis.

PGT121 antibody anchored to the membrane of cells functionally binds SHIV

In work that was is covered in Tiwari & Vannover et al., Nature Communications, I have modified the heavy chains (HC) of antibodies with the post-translational modified GPI anchor. GPI anchors, in this case for decay accelerating factor (DAF), are commonly used in nature to associate proteins to the outside surface of the plasma membrane. There is as of yet no published literature on using GPI anchored antibodies for *in vivo* purposes.

In both Palivizumab and PGT121 heavy chains, correct association with the light chain (LC) and binding to target antigen is still retained after addition of the DAF GPI anchor on the 3' end of the primary HC transcript (5' terminal DAF anchors inhibited folding with the

light chain). Whole antibody localizes to the surface when aHC (anchored HC) and the light chain mRNA are both delivered (Figure 3.4). The delivery of a single chain alone does not lead to abundant protein expression.

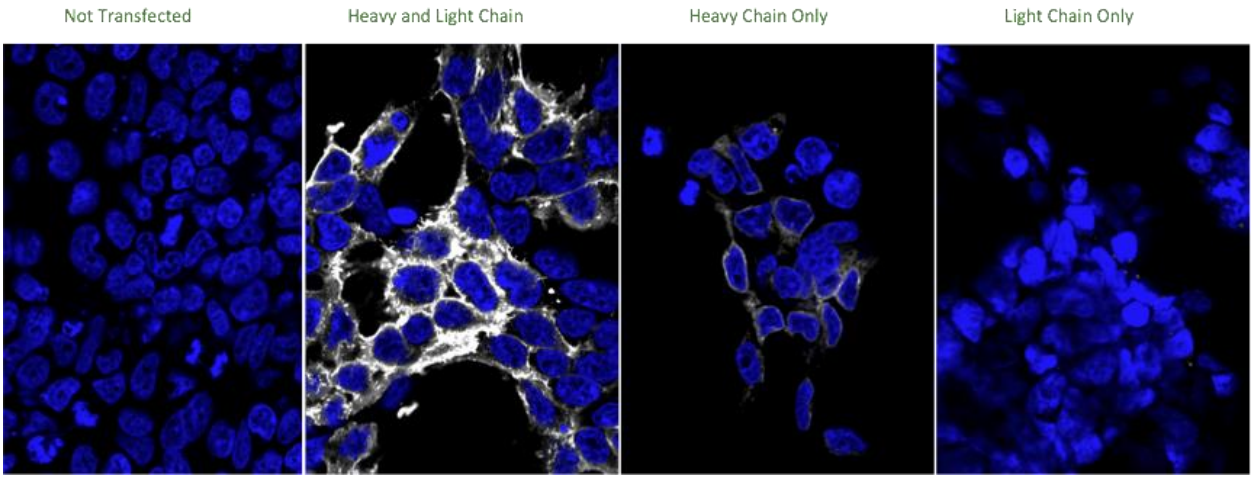

Figure 3.4: aPGT121 is displayed efficiently on the surface of transfected cells only when both heavy and light chains are expressed. mRNA encoding for each antibody chain were delivered via L2k transfection and fixed 24 hours post transfection. Blue – DAPI ; White – anti-human secondary

We next tested whether aPGT121 (anchored PGT121) is *functional* while on the outside surface of cells. Fluorescently labeled SHIV virions were added to cells transfected with aPali or aPGT121. Only aPGT121 transfected cells bind SHIV and capture it at the cell surface (Figure 3.5)

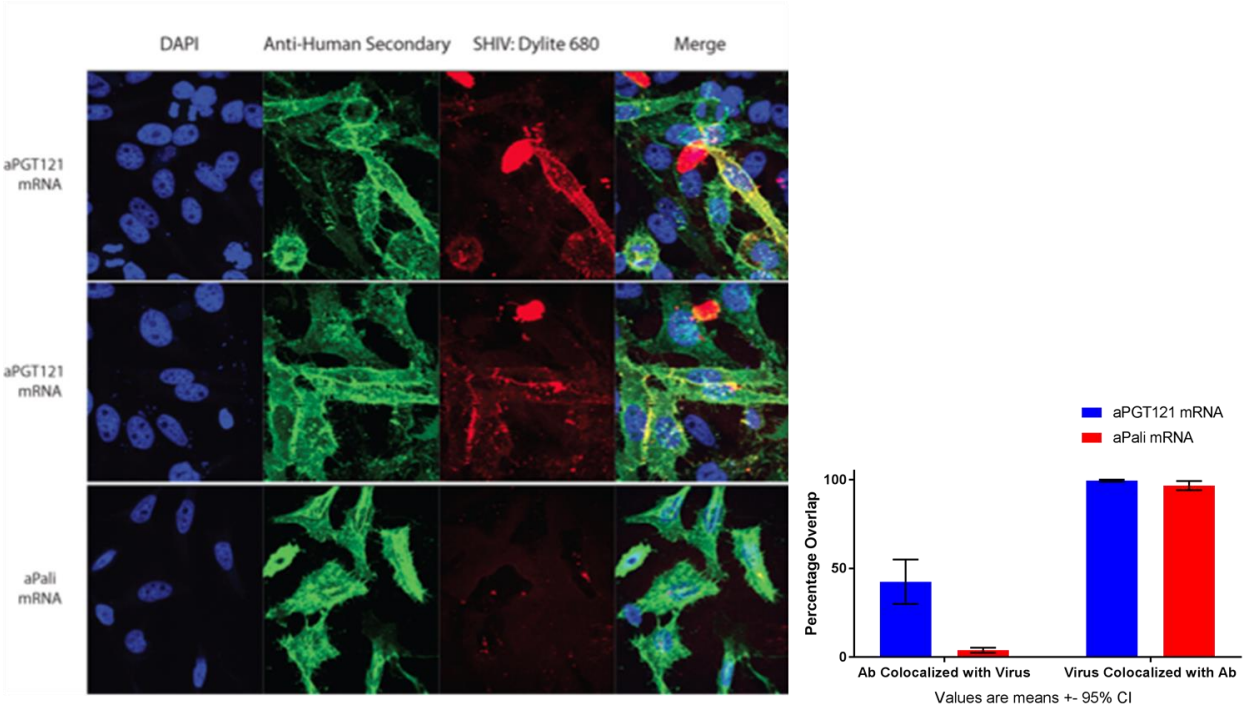

Figure 3.5: Transfected cells displaying aPGT121 on their surface are able to bind SHIV virions. Cells were transfected with PGT121 mRNA and 24 hours later dye labeled SHIV was added to the cultures. RSV neutralizing aPalivizumab (aPali) antibody, also displayed on the cell surface, did not bind SHIV.

Visualizing mRNA transfection through PGT121:NanoLuc Fusion protein

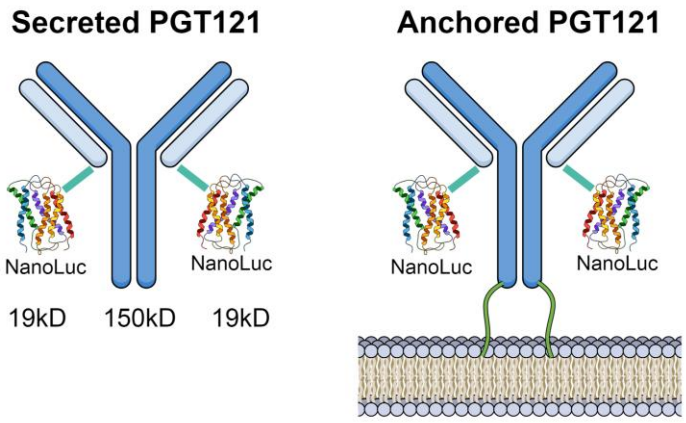

Figure 3.6: Schematic of the PGT121:NanoLuc fusion protein; in secreted and anchored forms. Total MW of anchored PGT121:NanoLuc is 195kD.

The primary aim of this project was to express PGT121 in the FRT epithelium. To ensure that experimentally relevant epithelium tissue was being examined for protein quantification, a real-time method was needed to screen for positive tissue during necropsy and tissue processing. The luminescence reporter NanoLuc was fused to the LC of PGT121 on the 3' end. NanoLuc is 100x more sensitive, does not use ATP during reaction with its substrate, and is only 19kD in size, as compared to Firefly Luciferase (Figure 4.6). Secreted PGT121:NanoLuc was isolated by gentle protein A/G purification of the supernatant after transient transfection of adherent cells. The dynamic range for PGT121:NanoLuc was found to be nearly 6 orders of magnitude from serial dilutions. In an adapted gp120 ELISA assay (consisting of all regular ELISA steps, with the substitution of NanoLuc substrate in lieu of detection antibodies), a sensitivity of around 500 pg/mL

was observed, on par with ELISA readouts, but with a greatly expanded dynamic range (Figure 3.7).

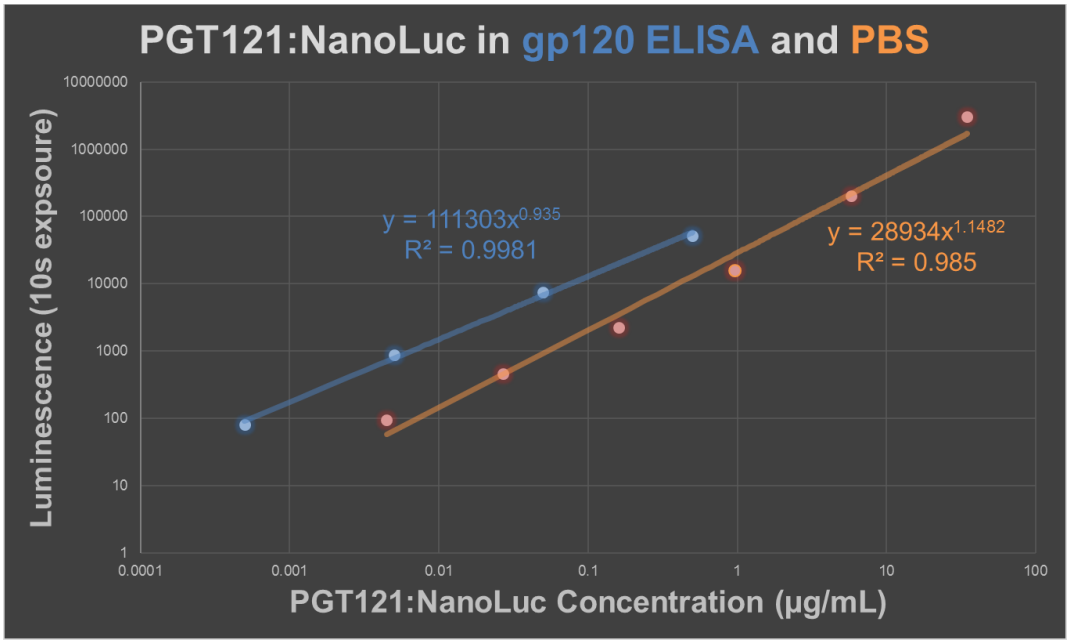

Figure 3.7: Luminescence output from serial dilutions of secreted PGT121:NanoLuc in PBS (green) and a modified HIV gp120 ELISA (blue line). A high dynamic range and reasonable sensitivity is observed. The relationship between luminescence output and protein concentration follows a power model.

Determining the optimal dose of PGT121:NanoLuc mRNA in the FRT

To determine if sheep FRT epithelium is amenable to higher doses of mRNA during aerosolized transfection, a single 300uL spray of base modified 1-methyl-psuedoUridine mRNA transcripts, one for the heavy chain and the other for the light chain of PGT121, was delivered to the cervix of sheep. Three animals received 250ug of mRNA, and another three received 750ug of total mRNA. 24 hours after delivery, the entire sheep FRT was extracted. 2mLs of NanoLuc substrate was applied to entire vaginal, cervix, and uterus. IVIS imaging was used to measure the location and amount of luminescence in each animal (Figure 3.8). Luminesce near the cervix is higher in all 750ug animals

(Figure 3.8 A&B). Interestingly, the average radiance for each dosing group is fitted by a linear model (Figure 3.8C).

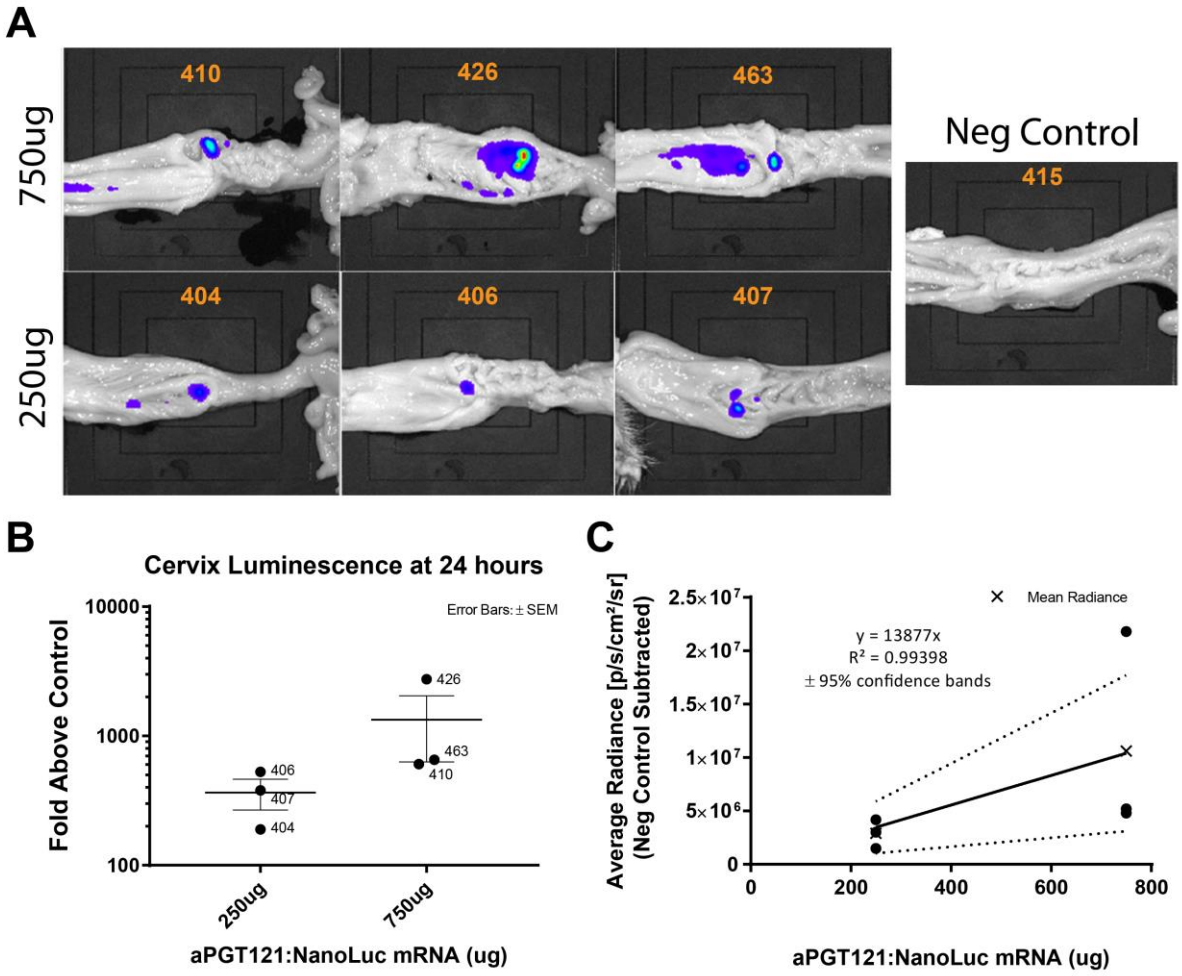

Figure 3.8: mRNA dose escalation in sheep FRT epithelium. (A) IVIS images of the FRT epithelium after a single mRNA dose at the cervix, 24 hours after transfection. All images are equally contrasted. (B) The average radiance at the cervix over the average radiance in the control animal. (C) A simple linear regression models the relationship between mRNA dose and radiance.

Cervical and vaginal epithelium can be transfected by aerosol

Now that we established that 750ug of mRNA is the minimum amount of mRNA that we should deliver, we wondered if both vagina and cervix are equally receptive to transfection. Two sprays, 750ug each, were delivered sequentially: one dose to the cervix, followed by a 3-4cm retraction of the speculum and spraying of the vagina. The signal was evaluated via IVIS imaging 24 hours after delivery in two animals. In both animals, protein expression was detected throughout the vagina and cervix. Collectively, 34% and 53% of the entire lower FRT was successfully transfected, using two sprays. The luminescence intensities in the vagina and cervix were also similar (Figure 3.9). This data suggests that both the vagina and cervix can be transfected via aerosol mRNA transfection.

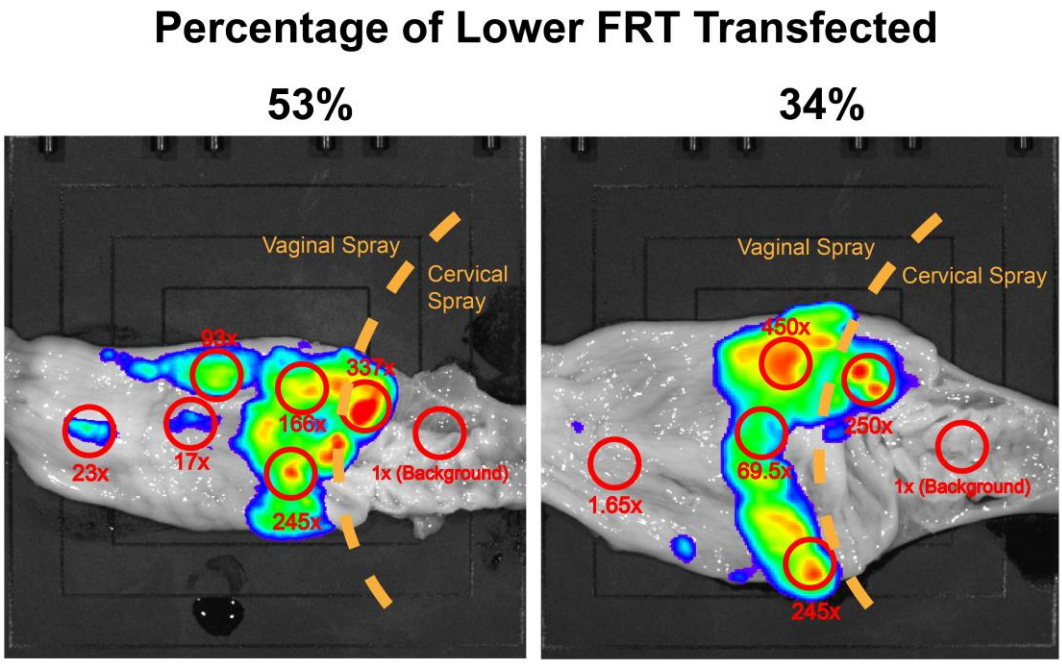

Figure 3.9: Sheep vagina and cervix are transfected with similar effectiveness. PGT121:NanoLuc mRNA was sprayed in two consecutive 750ug doses - one at the cervix, then after a 3-4cm retraction, a second dose at the vagina. Red circles indicate the fold radiance above uterus tissue for each region of interest.

Anchored antibody is retained in FRT tissue for at least 28 days

Our next goal was to quantify and compare the tissue and secretion distribution of the anchored (aPGT121) and secreted forms (sPGT121) of PGT121 over time. ***Our hypothesis was that anchored PGT121 would remain in the mucosal epithelium longer than wild type secreted antibody.*** We compared secreted and anchored PGT121 constructs at 14 days and 28 days post transfection. 1.5mgs in total was delivered to each animal, 1x 750ug dose at the cervix, followed with 1x 750ug dose in the vagina. Genital secretions were collected longitudinally on a weekly basis to assess the amount of PGT121 that accumulated in the lumen.

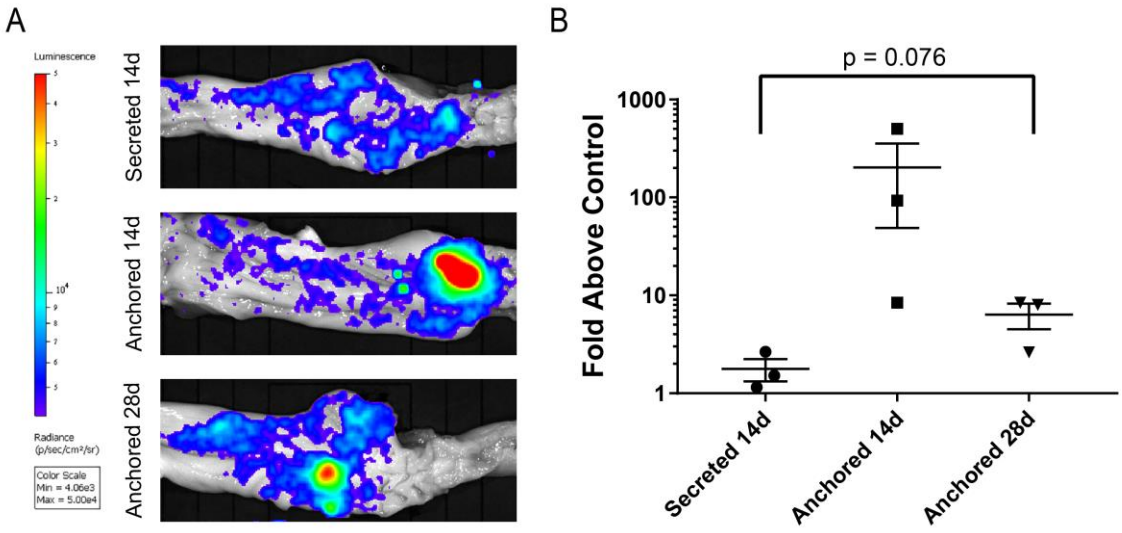

Figure 3.10: Anchored antibody remains in the FRT mucosal epithelium at 28 days post-transfection. (A) IVIS imaging of the extracted lower FRT at 14 days and 28 days. (B) The average radiance relative to a control animal. Error bars represent ± SEM.

IVIS was used following FRT removal to assess the retention of PGT121 for anchored and secreted constructs out to 1 month (Figure 3.10). Representative images for each time point and group are displayed (Figure 3.10A), along with quantification of the average

radiance relative to a naive control animal (Figure 3.10B). The luminescence signal in all aPGT121 tissues (n = 6), even at 28 days, is higher than sPGT121 tissues. These results support the notion that anchoring the antibody to the membrane surface differentially retains the antibody in the epithelium, at least for 1-month post-transfection. It also appears that the strongest source of signal is near the cervix, perhaps due to epithelial shedding differences between the vagina and cervix. Note that although sPGT121 28-day animals were originally scheduled, after assessing the low signal results at 14 days, it was determined that the animals could be repurposed.

Quantitative western blot was the assay used to determine the exact amount of PGT121 in the FRT epithelium (Figure 3.11). A standard curve using purified PGT121:NanoLuc was included in each blot. From each FRT explant, regions of caudal vagina, rostral vagina, cervix, and uterus were removed, using the IVIS signal as applicable. The tissue was dissociated using physical pulverization, homogenized with a bead mill, then lysed in RIPA buffer. Detection antibody against NanoLuc were used to quantify, in lieu of antibodies targeting human Fc, as apparent alterations in the Fc of sheep expressed PGT121 abrogated epitope binding. We speculate that glycosylation differences between sheep and humans Fc domains resulted in hiding of the target epitope of anti-human Fc antibodies. Another rationale for using western blot to quantify is that it seems the enzyme NanoLuc lost activity over time after processing of tissue. This became apparent upon downstream assays to measure PGT121:NanoLuc concentrations via luminescence (data not shown). This diminishing activity is either due to factors located within the *in vivo* microenvironment of the FRT, or during tissue homogenization and processing.

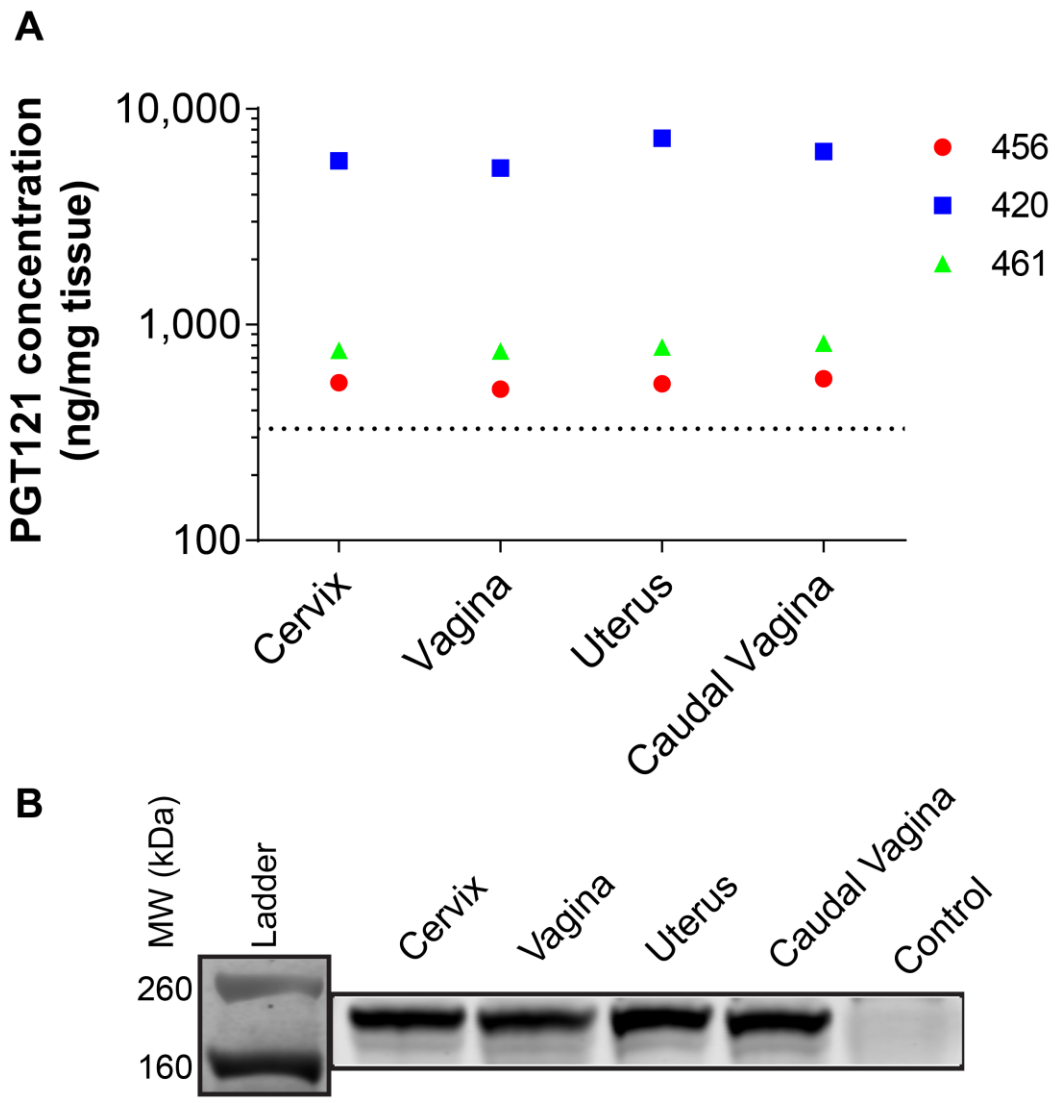

Figure 3.11: aPGT121 is present at high concentrations in all regions of the FRT at 28 days post-transfection. (A) aPGT121 concentrations in excised cervix, vagina, uterus, and caudal vagina were estimated using quantitative western blot (B) Western blot demonstrating the characteristic aPGT121 band at 195kD for all regions of the FRT, compared to control cervix.

Surprisingly, similar quantities of antibody appear to be in each section of the FRT, for a given animal (Figure 3.11A). Considering that only rostral vagina and cervix were targeted with the 2 doses of mRNA, this data suggests that free aPGT121:NanoLuc is localizing to these other regions of the FRT. It should also be noted that the rank order from highest to

lowest of animal 420, 461, and lastly 456, is the same rank order observed from the IVIS imaging of Figure 3.10B (although the differences weren't nearly as large as that observed via western blot).

Membrane anchoring results in increased concentrations of PGT121 in vaginal secretions over time

Quantitative western blots were also used to quantify the amount of PGT121 present in the vaginal secretions of sheep (Figure 3.12 – please note that the colors used in the anchored animals align to the same animal colors used in Figure 3.11). Anchored PGT121 was detectable out to 28 days post transfection, with average concentrations of 40ug/mL. Secreted PGT121, meanwhile, was only barely above the level of detection at 14 days post transfection. The maximum mean concentration of PGT121 was achieved at 24 hours, with 210ug/mL and 80ug/mL, for anchored and secreted PGT121, respectively. A limitation of this longitudinal sampling however is that we removed a given amount of protein each time we sampled, from a source that was finite (since mRNA encoded protein production should be completed within 48 hours or so).

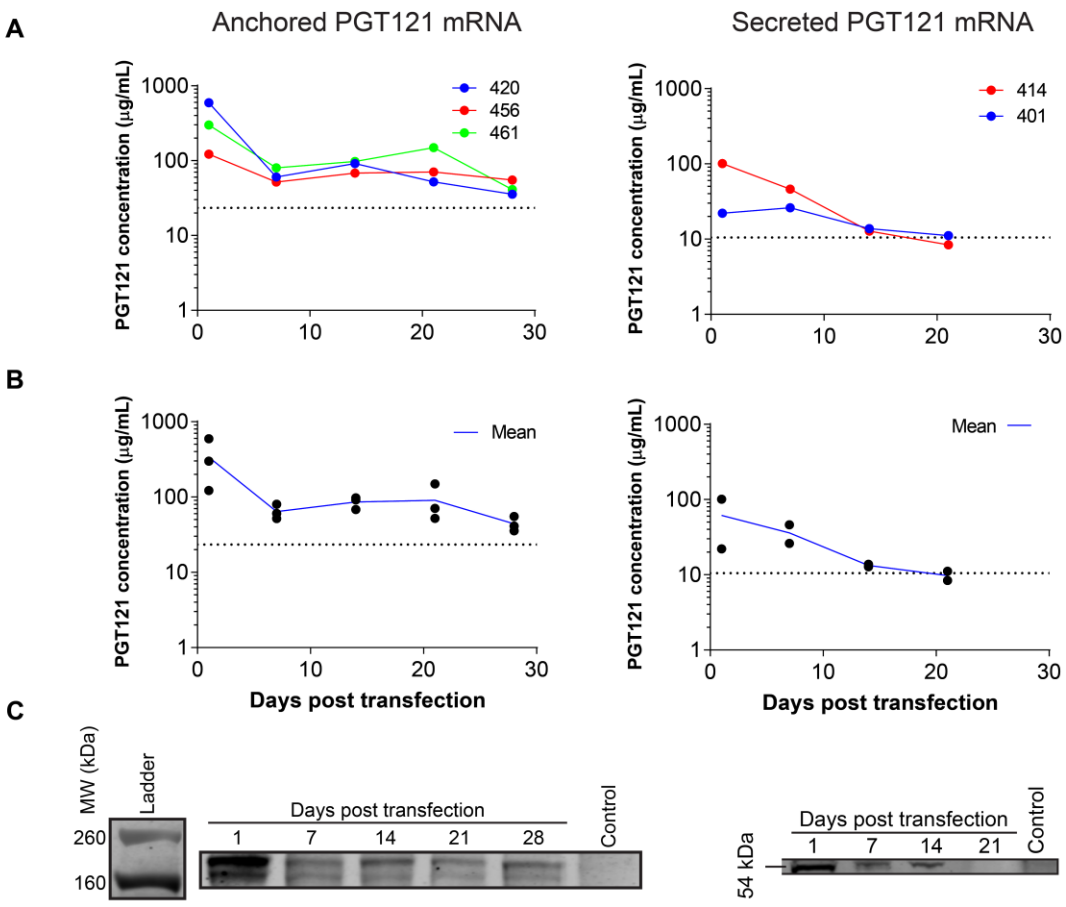

Figure 3.12: aPGT121 is present in vaginal secretions up to 28 days post transfection. Three sheep were transfected with two doses of 750ug of mRNA encoding for aPGT121. Secretions were collected at 1, 7, 14, 21, and 28 days post-transfection. (A) Longitudinal sampling of PGT121 concentrations over time, for all animals. (B) The mean concentration of PGT121 at each timepoint. (C) Antibody concentration was quantified via Western Blot analysis, using a standard curve of purified PGT121:NanoLuc protein. The expected size of aPGT121:NanoLuc was confirmed to be around 195kDa. The representative image displayed is for animal 420. For secreted antibody, the LC was more prone to uncouple from the HC, resulting in a 45kDa fragment.

Rhesus Macaque Studies

Up to this point, we have characterized the spatiotemporal patterns of mRNA transfection and the kinetics of protein expression *in vivo*. The expressed bNAb PGT121 was detectable at relatively high concentrations, up to 28 days using the anchored construct. This robust expression was demonstrated in sheep, which is relevant due the geometric similarities between sheep and human FRTs. The device used was an off-the-shelf aerosolizer, which sells for less than $10. The transfection medium consists of RNA in water.

The next logical step is to study protection from SHIV challenge in rhesus macaques. However, the number of animals needed to power such a study will require additional funding. In the meantime, we decided to perform appropriate *ex vivo* assays that could provide preliminary evidence indicating efficacy. The data that follows was conducted on three female rhesus macaques that were sprayed with 250ug of aPGT121 mRNA. Two of the monkeys (RWg13 and RVg13) received a 1:4 ratio of LC to HC, while RCo13 received only aPGT121 HC mRNA. It should be noted when interpreting the data, that heavy chain alone can still bind virus, so while a useful comparison, is not a true negative control.

PET/CT imaging reveals trafficking to systemic lymph nodes within 70 minutes

There is evidence that HIV/SHIV introduced into the FRT rapidly ‘seeds’ distal sites beyond the local mucosal tissue. Thus, any therapeutic delivery method would ideally also localize the intervention at the same local and systemic sites as the virus. To test whether aerosolized mucosal mRNA traffics to draining lymph nodes, we labeled PGT121 mRNA with the orthogonal ^{64}Cu labeled probes, as was described in Chapter 2. Radioactive mRNA was sprayed in two doses, once on the cervix and a second dose in the vagina, in

three rhesus macaques. PET/CT imaging was performed at 70 minutes, 4 hours, 24 hours, 48 hours, and 72 hours post administration (Figure 3.13)

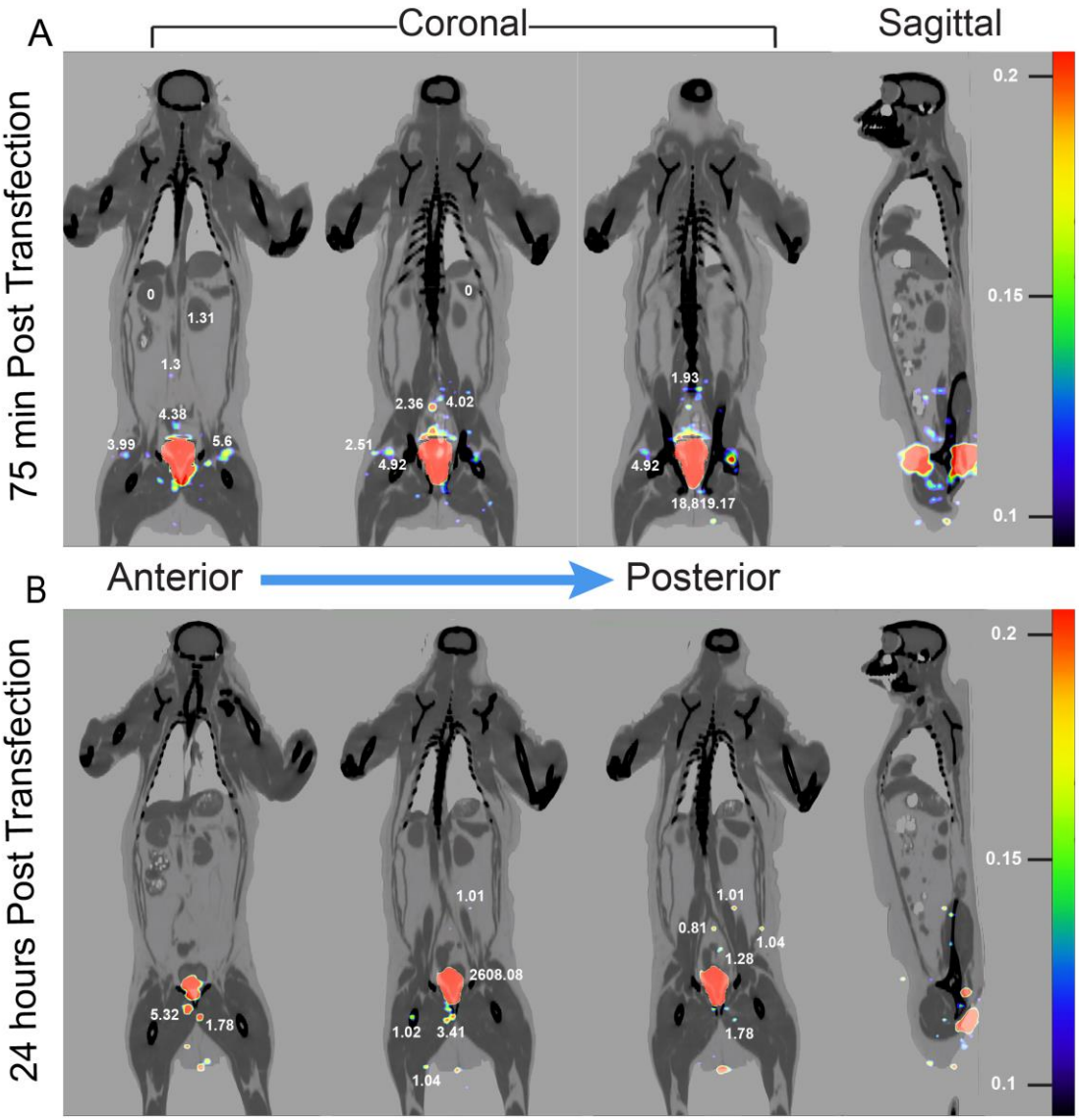

Figure 3.13: PET/CT imaging of rhesus macaque RVg13 after radioactive mRNA aerosolized transfection of the FRT. mRNA was labeled with 200uCi of radiation. (A) Representative PET images at 75 minutes and (B) 24 hours post transfection. Numbers in white next to organs represents the total SUV within that organ.

Trafficking to lymph nodes at the earliest imaging session, 75 minutes after aerosolized delivery, suggests mRNA is already leaving the cervicovaginal epithelium and reaching distal sites. Perhaps due to the large surface area of the FRT, these nodes are not confined to a single anatomical region. Rather, sacral, popliteal, inguinal and femoral, iliac, para-aortic, and mesenteric lymph nodes all contain detectable signal.

After 48 hours, the signal in the lymph nodes is no longer detectable, most likely due to 4 half-lives of radioactive decay. However, significant signal is still detected at the FRT mucosal surface at 72 hours (Figure 3.14), suggesting retention of mRNA transfected cells within the FRT. The mRNA is likely actively being degraded by RNA nucleases by 72 hours, but the chelated oligo probe is base modified and nuclease resistant, and thus should remain inside the cell.

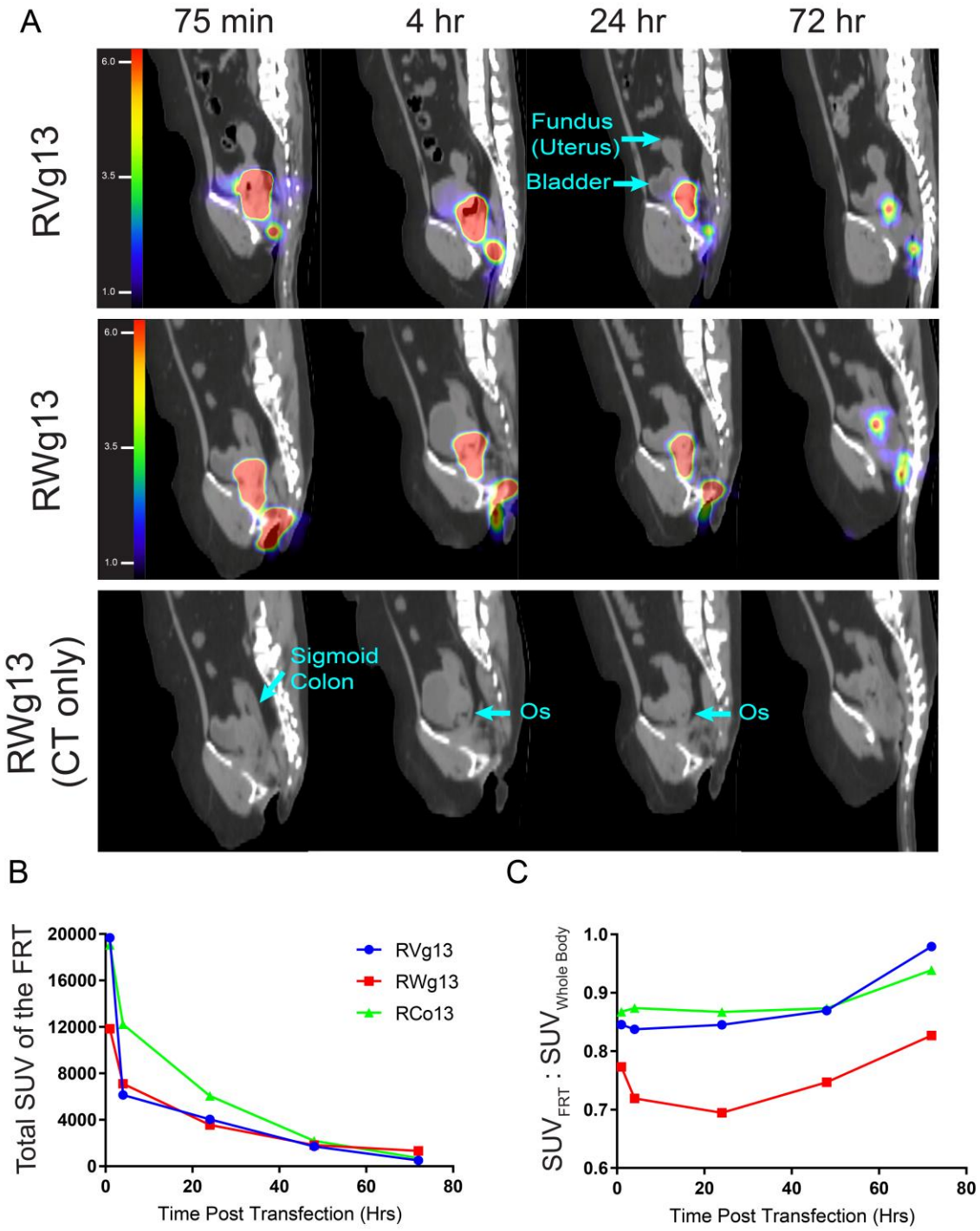

Figure 3.14: Radiolabeled mRNA is retained in the FRT following transfection. Two 125ug doses of ^{64}Cu labeled aPGT121 mRNA were delivered via aerosol to first the cervix, then ~ 3-4cm caudally in the vagina. PET/CT imaging over 3 days was used to monitor mRNA biodistribution. (A) representative PET/CT images from 75 minutes to 72 hours. (B) The total SUV in the FRT over time. (C) The ratio of the total SUV in the FRT to the total SUV contained within the entire body.

The cervical Os, which is our visualization target during speculum insertion, can also be resolved in the CT images. While not surprising, but nonetheless reassuring, the focal point of mRNA transfection appears to be the Os. Interestingly, using the radioactive signal also provides insight into gauging the efficiency (ie the amount of mRNA dose that is being 'wasted') of the current delivery method. Between 70 minutes and 4 hours, the amount of PET signal in the FRT space decreases by ½ to 2/3. After this initial rapid decrease, the SUV decrease from 4 hours to 72 hours is less drastic and resembles a more linear process. I believe the cause of the rapid decrease over the first 4 hours is due to excess mRNA that did not transfect the FRT epithelium. This suggests to me that using 350uL volume doses is simply too much in the much smaller confines of the rhesus macaque vagina. It is not suprising that aerosol parameters will need to be modified for future non-human primate studies and that the data that follows is not optimized (I will bring this optimization point again later on).

Cervicovaginal biopsy explants demonstrate protection from SHIV challenge

Secretions from the three animals were collected prior to transfection, and post-transfection at 4 hours, 24 hours, 48 hours, 72 hours, and 7 days. Biopsies were collected at 1 day and 3 days post transfection, with one sample taken from the cervix and two from the vagina, at each timepoint. Because of the uncertainty involved with performing biopsies (i.e. is the correct spot being sampled), the extracted explants were screened for transfection by adding NanoLuc substrate and measuring luciferase activity in each explant.

To provide some indication of protection, biopsy explants from aPGT121 transfected FRTs were challenged with SHIV162p3, which is a Clade B *Env* virus. $5.5x10^4$ $TCID_{50}$ (50% tissue culture infectious dose) of virus at a 1:1 ratio was added to each explant, incubated for 2 hours, washed, then cultured out to 10 days. Supernatant was collected at 4, 7, and 10 days post-challenge and assayed with a SIV p27 ELISA to determine if productive SHIV infection developed. With this assay workflow, we could determine both the transfection status of the explant and the ability of SHIV to infect that same tissue.

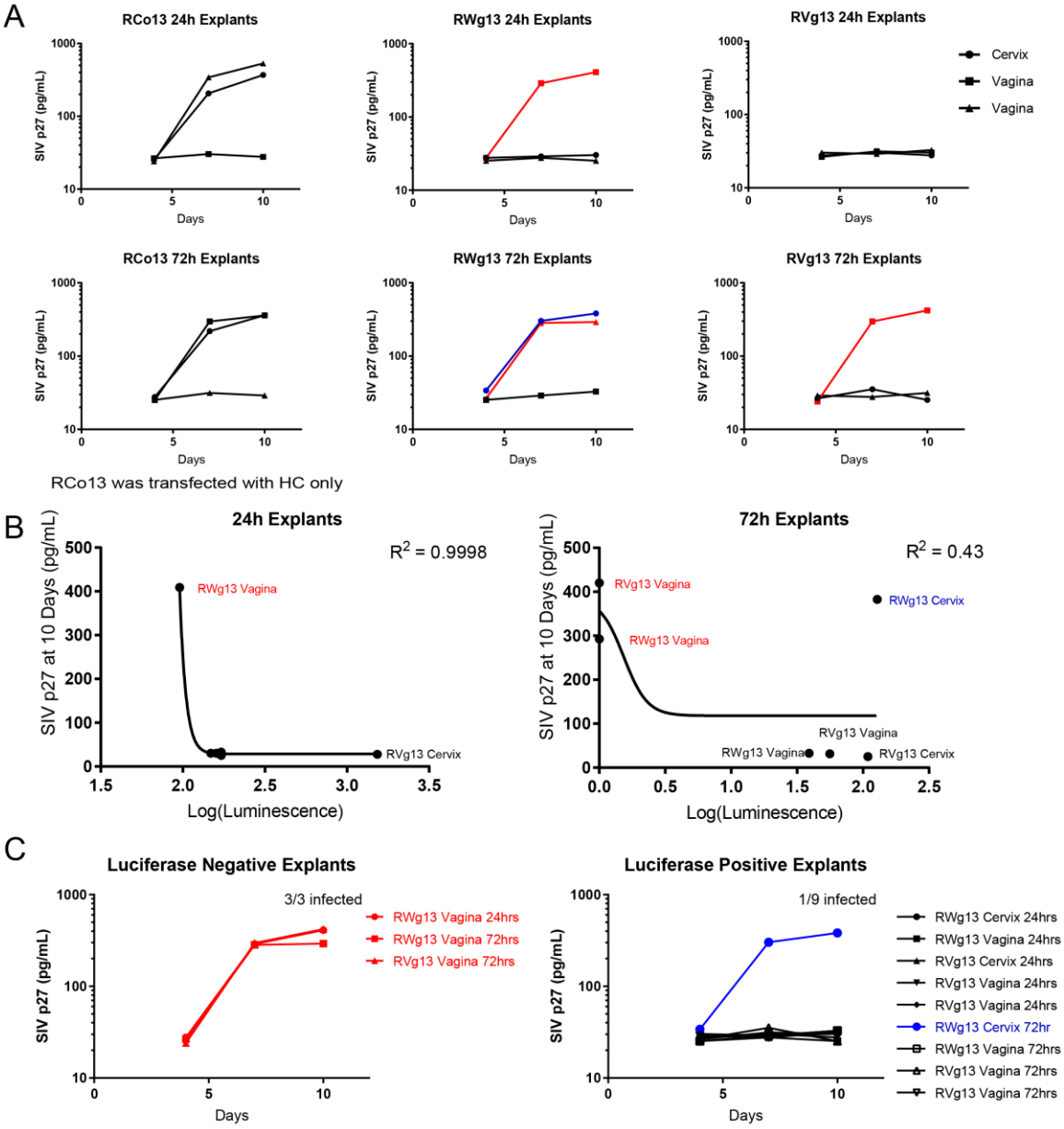

Figure 3.15: aPGT121 protects biopsy explants from SHIV162p3 challenge. 250ug of aerosolized aPGT121 mRNA was delivered to the cervix and rostral vagina of three rhesus macaques. Biopsy explants were removed from cervix and vagina at 24 and 72 hours post transfection, screened for luciferase activity, and then challenged with SHIV162p3. (A) p27 ELISA quantification of the explant supernatants, separated by animal and time point. A colored line indicates infected vaginal (red) or cervical (blue) tissue, and these colors remain designated throughout the other panels. (B) A logistic fit was used to model the relationship between infection status (p27) and transfection status (luciferase activity) for each explant, at 24 and 72 hours. (C) Separating explants based on transfection status indicates that 100% of non-transfected tissues became infected, while only 11.1% of transfected tissues were infected.

The main takeaway from Figure 3.15 is that the ability to separate explants based on transfection status, suggests that 100% (3 out of 3) of non-transfected vaginal samples became infected, while only 11.1% of transfected tissue were vulnerable to infection (1 out of 9 explants). It should be noted that the biopsy explant SHIV Challenge model is by design a 'worst-case scenario' that removes many natural barriers to infection, including mucus, secretions, and epithelium. In a natural *in vivo* infection setting, the virus is introduced in the lumen, and then must percolate through the epithelium to CD4+ cells that reside in the sub-mucosa. In the case of a biopsy *in vitro* challenge, the virus has direct access to CD4+ cells from all directions, theoretically being able to bypass the transfected surface epithelium.

Genital secretions from aPGT121 transfected animals neutralize SHIV in vitro

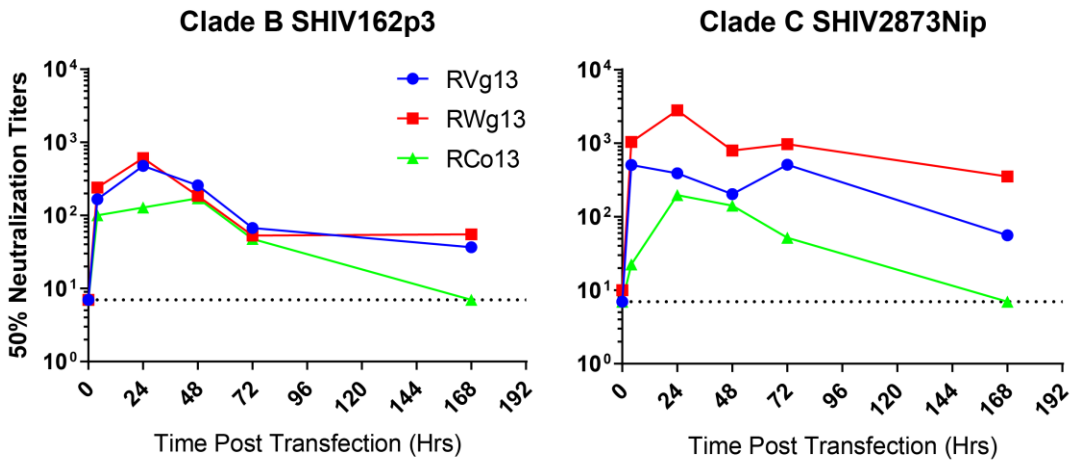

Figure 3.16: Genital secretions from aPGT121 transfected animals neutralize SHIV within 4 hours

Next, genital secretions collected over the course of a week were evaluated for their ability to neutralize SHIV through the TZM-bl Neutralization assay (Figure 3.16). Secretions demonstrated an ability to neutralize SHIV162p3 (Clade B) and SHIV2873Nip (Clade C)

at all time points measured, out to 1 week. Critically, secretions at 4 hours post-transfection contained substantial neutralizing activity. The kinetics over time for the heavy chain only (RCo13) construct suggest that without association of the constant regions of the HC and LC, retention of antibody in the secretions is attenuated.

This monkey data should be interpreted with some context, due to study constraints. First, dose and delivery optimization, as was performed in the sheep, was not possible the rhesus macaques due to the low animal numbers. Dose, speculum design, and dose volume are all variables that would need to be optimized. Nevertheless, the positive results indicated from explant challenge and secretion neutralization bode well for future SHIV challenge, especially if one considers the two would act in concert in an *in vivo* setting. As the dose escalation data suggests with the sheep, exploring the maximum dose and parameters for optimum antibody expression in rhesus monkeys remains to be investigated.

Conclusion

The vaginal mucosal has been explored in vaccination and therapeutic contexts to deliver drugs both locally and systemically. The lower FRT displays beneficial properties for drug delivery, including a large surface area, a high degree of vascularization, avoidance of first pass metabolism of the liver, good drug permeability, and is accessible enough to allow self-application[5]. Intra-vaginal application has been used to deliver hormones, anti-microbials, and spermicides, packaged in the form of creams and gels, tablets and suppositories, vaginal rings, and mucoadhesives. For local treatment of FRT conditions, however, the high tissue permeability and vascularization likely lowers the resident half-life of applied drugs.

The amount of PGT121 required in the cervicovaginal mucosa to provide protection is unknown. Previous studies measured the amount of bNAb in the genital secretions, but did not ascertain FRT tissue concentrations, and how these levels relate to secretion concentrations and correlate with protection. Since the source of PGT121 in genital secretions are mRNA transfected epithelial cells, the amount of aPGT121 contained within the FRT mucosa will contribute to virus neutralization.

In sheep, genital secretion aPGT121 concentrations remained well above the predicted IC_{50} concentration of 30ng/mL for 28 days, peaking at 200ug/mL by 24 hours, and remaining above 30ug/mL 28 days post-transfection. Epithelial aPGT121 was detected ubiquitously throughout the FRT at 28 days, although the significance of these amounts is hard to comment upon without *in vivo* challenge data.

In this aerosolized mRNA transfection platform, the localized production of transgene protein by the native epithelium ensures that high tissue and secretion concentrations are achieved quickly, while also ensuring host glycosylation and other post-translational motifs are preserved. The addition of a membrane anchor retains the expressed protein in the epithelium. The formulation used in these experiments was a simple mixture of mRNA in water. The hypotonicity of water relative to host secretions may assist with fluid uptake into the FRT epithelium[126]. When stored lyophilized, mRNA is extremely stable and is not dependent on cold chain storage conditions[128]. The robust transfections we observed, simplicity of the aerosolizer, low cost of IVT mRNA, and stability of lyophilized mRNA, all support the potential for a use-on-needed, patient self-applied platform. This transient, spray based approach also holds *social promise* because of its 'invisible' nature - a third party or partner would never know that the woman was using this as a prophylactic, increasing women's autonomy and privacy.

The FRT epithelium structure varies spatially in regard to thickness, immune cell types[99,129], and frequencies of susceptible cells, and thus have differential probabilities of a productive infection developing. However, once surface area is considered, all areas of the lower female reproductive tract can be considered vulnerable to infection. Thus, it is favorable if prophylactic approaches protect the entirety of the lower FRT. In this study, we detected high concentrations of anchored PGT121 28 days after transfection in the uterus, cervix, and the vagina. The DAF GPI membrane anchor is not a permanent tether and proteins can be released from the surface of transfected cells by endogenous glycolipidases[130].

Parenteral administration of antibodies post-exposure can reduce downstream viral load setpoints[131]. The rapid expression times observed in sheep and rhesus macaque models (less than 4 hours) suggests that this aerosolized mRNA transfection platform could be used as an acute therapeutic measure at the site of infection. Assuming that cervicovaginally expressed bNAbs have the potential to follow the same diffusion and trafficking routes as cell free virions, the possibility exists for it to be used in combination with parenteral bNAbs to prevent or attenuate initial virus seeding. PET/CT tracking of mRNA further suggests that mRNA reaches systemic lymph nodes within 70 minutes; whether this mRNA is translated to protein in these secondary lymphoid organs is unknown.

Packaging multiple drugs into a single formulation can prove tricky for nanoparticles, due to varying physical and chemical properties that impact stability[132]. Using mRNA provides flexibility, as any theoretical combination of neutralizing or non-neutralizing antibodies can be expressed simultaneously. Because we delivered the light chain and heavy chain encoding mRNAs as separate transcripts, we have already demonstrated expression of

two mRNA transcripts simultaneously, suggesting the potential for multiplexing during delivery.

Combining bNAbs that target non-overlapping gp120 and gp41 epitopes results in additive effects on neutralization breadth[133,134], and thus lower the effective concentrations required for neutralization. There is some evidence that chronic controllers do this naturally and develop multiple bNAbs targeting different, non-overlapping sites on Env[110] to suppress virus. To prevent possible escape mutation strains, using optimal CD4bs, V3, and MPER targeting antibodies simultaneously could result in IC50's as low as 0.01ug/mL, with 100% breadth[135]. Alternatively, bispecific and trispecific ScFv's consisting of the binding domains of multiple bNAbs, increase the breadth of coverage and display high binding affinities, and can be expressed from a single mRNA transcript that is comparable in size to the ones used in this study[136]. Other sexually transmitted infections that correlate with HIV, such as herpes, hepatitis, and genital warts (HPV), could also be targeted with relevant antibodies or anti-microbial peptides.

This study suggests a complementary approach to large dose systemic antibody injection to achieve rapid (less than 4 hours) and long lasting (at least 28 days) neutralizing antibody concentrations within the lower female reproductive tract of sheep and non-human primates. The entire lower FRT was conducive to transfection, but demonstrates differential retention of encoded antibody, most likely reflective of differential rates of epithelial shedding. Further, we demonstrate that although the majority of mRNA remains in the FRT, aerosolized mRNA transports to distal lymph nodes quickly, albeit at low amounts. Tethering PGT121 to the transfected cell surface using a GPI anchor promoted genital secretion and tissue concentrations to remain well above neutralizing concentrations at 28 days post transfection. Ex vivo challenge of RM FRT biopsy explants

with SHIV demonstrates tissue level protection due to aPGT121 tissue expression, as well as antibody neutralization activity in secretions. These data provide a firm basis and rationale for *in vivo* SHIV challenge in non-human primates.

Methods

IVT mRNA Synthesis

The anchored and secreted PGT121 sequences were ordered as a DNA gBlock from IDT containing a 5' UTR with Kozak sequence, a 3' UTR derived from the mouse alpha globin sequence, and extensions to allow for Gibson assembly. The sequences were human codon optimized on the IDT website. The gBlock was cloned into a PCR amplified pMA7 vector through Gibson assembly using NEB Builder with 3x molar excess of insert. All reaction transcripts were 0.8% agarose gel purified prior to assembly reaction. Subsequent plasmids from each colony were Sanger sequenced to ensure desired sequence fidelity.

Plasmids were linearized with NotI-HF (New England BioLabs) overnight at 37 °C. Linearized templates were purified by sodium acetate (Thermo Scientific) precipitation before being rehydrated with nuclease free water. IVT was performed overnight at 37 °C using the HiScribe T7 kit (NEB) following the manufacturer's instructions. RNA product was treated with DNase I (Aldevron) for 30 minutes to remove template and purified using lithium chloride precipitation (Thermo Scientific). RNA was heat denatured at 65 °C for 10 minutes before being capped with a Cap-1 structure using guanylyl transferase (Aldevron) and 2'-O-methyltransferase (Aldevron). Transcripts were then polyadenylated enzymatically (Aldevron). mRNA was then purified by lithium chloride precipitation, treated with alkaline phosphatase (NEB), and purified again. Concentrations were measured using a Nanodrop. Quality control measures include RNA agorose

electrophoresis to confirm purify, size distributions and poly(A) tail length, and in vitro transfection to confirm efficient translation of delivered mRNA. Transfection methods included aerosolized delivery to a monolayer of cells and Lipofectamine 3000 (Thermofisher, CA) based transfection. Confirmation of protein production depended on the particular protein being expressed, but generally involved luminescence reading on a plate reader and/or immunofluorescence detection via microscopy at least 4 hours post transfection (substantial protein is present by 3 hours).

***In vitro* Aerosol Transfection**

Adherent cells were plated in 24 well plates the day prior to transfection so as to be 80% confluent at the time of aerosol transfection. Media was removed directly prior to application of spray. A total volume of 50uL (MicroSprayer) or 200uL (Teleflex) of mRNA in water was applied to the cells, at a nozzle to cell surface distance of 2 inches (MicroSprayer) or 4.5 inches (Teleflex) ; these distances are required to prevent cell dissociation from the plate surface during spraying. 500uL of media was reapplied to the cells. For fixation, cells were washed 1x with PBS, incubated with 4% PFA at room temperature for 10 minutes and washed again with PBS. Permeabilization was carried out using 0.1% Triton X in PBS for 5 minutes at RT. Blocking was performed using 5% BSA in PBS at RT for 30 minutes. Primary antibodies were diluted in PBST and incubated at RT for 30 minutes. After washing 3x, secondaries were added at RT for 30 minutes. After DAPI counterstaining, coverslips were mounted with prolong gold medium and the edges sealed the following day with nail polish.

Sheep:
6 – 18 month old female sheep (weighing 80-110 lbs) were housed at the Mississippi State University College of Veterinary Medicine.

Speculum and Sprayer Equipment
The MADgic Teleflex (referred to as Teleflex from here on out) pediatric atomizer is purchased individually contained within sterile packages. The dead space on the devices was determined to be ~170uL. mRNA solutions at the desired concentrations were loaded into a high pressure 1mL catheter syringe (MedLine). The end of the syringe was outfitted with a stopper plug. Teleflex and syringes were then attached via Luer Lock. A washer was attached to the end of the Teleflex tip to ensure proper centralization of the nozzle within the barrel of speculum. Using this setup, the Teleflex nozzle remains situated 5mm away from the distal end of the speculum.

Aerosolized mRNA delivery
Sheep were sedated using 500uL i.m. injections of Xylazine. After 3-5 minutes, animals were positioned in a supine position on a flat table. A polyethelene speculum, with an internal diameter of 3mm, was positioned by a Theorongolist until the cervical Oss was visible. Mucus was cleared away by brief surface cleaning with a Qtip applicator. The Teleflex, with dosing syringe, was then inserted into the tube until the distal nozzle of the aerosolizer was 5mm from the distal opening of the speculum. Hand pressure was then used to spray the mRNA. If vagina was also being sprayed in the same animal, the speculum was removed in a caudal direction by 1.5-2 inches, surface cleaning was performed, and vagina sprayed with a freshly loaded dose of mRNA. Average volumes delivered ranged from 300-450uL, based on the particular experiment. Speculums were sterilized in between animals, to minimize potential cross contamination. All controlled substance doses, mRNA doses, times of administration, and other experimental notes were recorded, as required by IACUC at MS State.

Secretion Collection

Weck-cell sponges (Beaver Visitech) were presoaked with 50uL of 1x PBS. If multiple sites within the lower FRT were sampled simultaneously, the sponges were connected together using surgical suture. With the animals upright and non-sedated, vaginal secretions were collected by positioning the sponge in the desired location and waiting for 3 minutes. Sponges were placed into 1.5mL ependorfs and frozen at -80°C until analysis. To extract secretions from the sponges, the sponges were first placed into pre-weighed Qiashredder filters and centrifuged at 20,000xg for 10 minutes at 4°C. 200uL of extraction solution (IGEPAL, protease inhibitor in PBS) was added to the sponge and placed on ice for 15 minutes. The sponge was then spun at 20,000xg for a further 30 minutes. Secretions were alliquoted and stored at -80°C.

IVIS Imaging

The excised female reproductive tract was cut along a single edge so the entire surface area of the vagina and cervix lay flat. 2mLs of a fresh 1:40 solution of NanoGlo Substrate (Promega) in 1x PBS was added to the entire vagina and uterus. After 1 minute at room temperature, the organ was imaged with an IVIS. The positive portions were identified from the images, and carefully excised. The tissues were then either snap frozen in liquid nitrogen if protein analysis was the goal, or for microscopic analysis the tissues were placed in 4% PFA overnight at 4°C.

Western Blot

Tissues were weighed and snap frozen on liquid nitrogen before being crushed using a BioPulverizer (BioSpec Products). Radioimmunoassay (RIPA) buffer (Thermo Scientific) was then added at a ratio of 2 µL to 1 mg. This solution was then further homogenized using a bead mill (Next Advance) before being centrifuged at 16,000 xg for 20 minutes. Lysate supernatants were then aliquoted and stored frozen at -80 °C. Lysate protein concentrations were determined using a bicinchoninic acid assay (BCA, Pierce). 50 µg of

tissue lysates or a known amount of purified PGT121 were heat denatured for 10 minutes at 70 °C in 4x Loading Buffer (Li-Cor). Lysates and a Chameleon Duo ladder (Li-Cor) were loaded into wells of a 4-12% bis-tris polyacrylamide gel (Thermo Scientific) and separated at 200 V for 32 minutes on a Mini Gel Tank (Thermo Scientific). Proteins were transferred onto nitrocellulose with 0.45 µm pore size (Thermo Scientific) for 1 hour at 12 V. Membranes were blocked for 1 hour in Odyssey Blocking Solution (LiCor) before being incubated with primary antibodies, diluted in blocking buffer with 0.1% Tween-20 (VWR) overnight at 4 °C. Membranes were washed 3 times for 5 minutes each at RT with PBS containing 0.1% Tween-20 (PBST). Membranes were then incubated in secondary antibodies, diluted in the primary antibody diluent, before being washed again in the same manner. Membranes were then imaged on a LiCor Odyssey Cx imager and analyzed using the Image Studio software.

gp120 ELISAs

Recombinant $gp120_{JR\text{-}FL}$ (MyBioSource) was coated into 96 well microtiter, high binding plates (CoStar) at a concentration of 2 ug/mL, overnight at 4°C. The plates were washed 4x with PBS-Tween 20 (0.05 %). Blocking was carried at room temperature for 2 hours with 2.5% BSA in PBS-T. Samples and standards were diluted appropriately in PBS-T and incubated overnight at 4°C. A standard curve was ran using Protein A purified whole PGT121-NanoLuc antibody from transient mRNA transfected *in vitro* transfection of adherent cells. After washing, goat anti-human IgG Fc conjugated with alkaline phosphatase (Thermo) was added to the plates at 1:1500 and incubated at 37°C for 90 minutes. A final 4x washing was performed using TBS-T (as phosphate can inhibit the alkaline phosphatase reaction), and detection performed using *p*-nitrophenyl phosphate substrate (Sigma). The plates were read at 405nm after 30 minutes.

Rhesus Macaque Studies

Spraying
300uL sprays were delivered to the FRT, with a shortened 3mL syringe acting as the speculum.

Radioactive labeling and PET/CT imaging
Radioactive labeling was carried out, as described in the Chapter 2 methods section. The sprayed dose was 0.200 mCu per animal. Imaging sessions occurred at 1 hour, 4 hours, 24 hours, 48 hours, and 72 hours post administration.

Explant challenge with SHIV
24 and 72 hours post transfection, biopsies from cervical and vaginal mucosa were removed. To mitigate the potential for sampling error, the extracted tissue was screened for the presence of PGT121-NanoLuc by reading the luminescence after NanoLuc substrate addition. Tissues were then washed 3x with 1x PBS, incubated with SHIV at a 1:1 dilution for 2 hours at 37°C, washed a further 3x, then cultured on collagen sponges in 10% FBS supplemented DMEM media. Supernatant from the cultures was collected at the indicated timepoints and frozen, until p27 ELISA results could be attained.

Ethics
All sheep work was conducted with the written approval of the IACUC at Mississippi State University College of Veterinary Medicine and the Georgia Institute of Technology. All non-human primate work was completed and with the written consent of the IACUC at the New Iberia Research Center, at the University of Louisiana Lafayette.

CHAPTER 4

PERSPECTIVES

A long-term goal of the PET/CT vaccine tracking platform (Chapter 2 and 3) would be in developing a model by which the acute trafficking patterns of a vaccine could predict the development of vaccine correlates of protection and efficacy. A successful vaccine will stimulate the innate immune system and this theoretically should increase the amount of mRNA that reaches secondary lymphoid organs because of active cell transport, assuming that active cellular transport of mRNA correlates with immune cell stimulation and development of adaptive immune responses. In our study, we did observe the development of immune responses (see below for more information). In these same animals, we also observed the majority of mRNA that trafficked to draining lymph nodes at 24 hours had already done so at 4 hours. This fast trafficking of mRNA from the injection site is most likely due to passive transport by convective forces (as the cellular APCs take on the order of hours to be recruited to the injection site), but the time point of 4 hours is a bit nebulous.

The transport of vaccine components to secondary lymphoid tissue can occur in a passive manner that is driven by convective forces or in an active, cell mediated manner by antigen presenting cells that infiltrate the tissue due to cytokine and chemokine signaling gradients brought about by inflammation. Passive convection occurs minutes to hours after delivery, while active transport is on the order of hours to days. In the next animal we perform this experimental approach with, we will image via PET/CT at 20 minutes, 1 hour, and 2 hours after administration. This quick series of images should help elucidate the contribution of

passive trafficking to the overall accumulation of mRNA at draining lymph nodes, as immune cell migration should not occur within the first 2 hours of vaccine administration.

Correlating the downstream development of correlates of protection with the acute trafficking patterns after administration would be a powerful tool for vaccine development. Performing a study to examine whether PET/CT could be used to predict vaccine efficacy, would require a large number of animals. In the study of chapter 2, we monitored whether we could detect a humoral response to prME yellow fever antigen after boosting the 2 non-human primates that remained alive after PET imaging. No antibodies were detected up to three months after giving the mRNA boost. The primary goal of the experiment was not to examine or evaluate vaccine efficacy. In fact, using similar doses in other studies has not elicited adaptive immune responses either. This is most likely the result of the low amount of mRNA that we used (200ug), the possibility that the antigen prME is not the most immunogenic, and perhaps due to the carrier CholK itself, which might not contain enough intrinsic innate stimulation to promote the development of adaptive immune responses with this antigen.

By using specifically chosen vaccines that have differential efficacy when different routes of administration and/or adjuvants are used, we could examine how each parameter impacts: vaccine trafficking after administration, vaccine efficacy, and ultimately the relationship between the two. The results of the study could prove useful in elucidating mechanisms of successful vaccines, save resources and animals, and provide a fast indication as to whether the vaccine will prove effective in that patient, instead of having to rely on blood titers months after the vaccine administration.

FUTURE DIRECTIONS

Our immediate goal is to ascertain funding for a non-human primate mRNA-expressed PGT121 challenge study with SHIV. While quantifying antibody concentrations over time is useful from a scientific standpoint, the definitive test is to try to infect monkeys at different time points post FRT transfection with a combination of secreted and anchored PGT121 mRNA. If such a challenge demonstrates efficacy, then further studies can go back attempt to optimize parameters such as antibody type and the nature of the GPI membrane anchor. At the same time, an optimal sprayer can be specifically designed for use in rhesus macaques.

The Bill and Melinda Gates Foundation has expressed interest in the FRT mRNA transfection platform for the purposes of contraception. This option will be explored through the use of antibody based binding to sperm and peptide-based spermicides.

I am excited for the translational potential of this FRT platform – demonstrating expression in both sheep and rhesus macaques suggests that such an approach might also work on human tissue. The work presented in this thesis paves the way for numerous avenues of future research. While not all were enumerated here, numerous grants will be written in the Fall of 2018 regarding this work.

Future Work

Future funding submissions will address the following:

1. Aerosolized mRNA vaccine against HIV using gp120 mutational library
2. Peripartum transmission of infectious diseases from mother to child
3. Gene editing of the cervix for latent virus removal and cancer prevention

I will address each of these concepts, briefly, in turn.

1. Aerosolized mRNA vaccine against HIV using gp120 mutational library

The coalescing of each chapter of my thesis points towards a fundamental framework with which to study the development of an mRNA based HIV vaccine. In Chapter 2, I described an approach to adjuvant naked mRNA vaccines by directly tethering the adjuvant to the mRNA molecule in an orthogonal manner. This resulted in antigen specific humoral and cellular responses in a mouse model to the protein encoded by the mRNA, in this case, the model antigen OVA. In Chapter 3, we developed a non-invasive means to monitor mRNA biodistribution after delivery. Using an orthogonal oligo based method to radioactively label mRNA, we followed mRNA via PET/CT imaging in non-human primates as it aggregated in draining lymph nodes. As the mRNA was labeled directly, this approach is flexible, and is in fact currently being investigated for use in lipid nanoparticles to assay nucleic acid delivery and expression kinetics.

In the first two chapters, the mRNA was delivered I.M., the most common route for vaccine administration worldwide. Chapter 4 presented an off the shelf, cost effective, and robust cervicovaginal aerosolized mucosal mRNA transfection platform that resulted in stable expression of the protein of interest in the lower FRT epithelium and genital secretions. We decided to utilize the PET/CT mRNA tracking approach described in Chapter 3, and the data suggests that at 1-hour post administration, mRNA is already exiting the region of the FRT and travelling to secondary lymphoid organs. Notably, mRNA was retained in the epithelial tissue, as evidenced by positive mRNA signal in the lower FRT at 72 hours.

With these tools at our disposal, we believe it is worth pursuing the use of an adjuvanted aerosolized mRNA vaccine based HIV vaccine. Vaginally delivered mRNA should mirror the early stages of HIV infection: diffusion through the epithelium, protein expression locally, and systemic 'seeding' of regional lymphoid organs. The innate immune sensors that detect viral mRNA (see Chapter 2) are many of the same that respond to IVT mRNA. Additionally, host mRNA translation will result in native glycosylation patterns and protein folding, as would occur during natural HIV infection.

Our approach aims to address the huge problem in HIV vaccination of rapid virus evolution that HIV undergoes as it responds to host selective pressures. All broadly neutralizing antibodies tested *in vivo* demonstrate escape mutations from the virus. As the host immune response evolves to fight HIV, it remains one step behind the virus.

We propose to create an mRNA library of all possible gp120 amino acid mutations. This early exposure of HIV envelope permutations could allow the development of rapid memory responses against potential HIV mutations during the course of early infection, or founder virus variants. After repeated dosing regimens, cellular and humoral immunity will be assessed.

2. Peripartum transmission of infectious diseases from mother to child

Our data demonstrates that within 4 hours post aerosol transfection, genital secretions of rhesus macaques contain neutralizing concentrations of PGT121. This **acute expression** opens up the possibility for *urgent and emergency purposes*. One such application is the prevention of peripartum transmission of infectious diseases. During labor, viral and bacterial pathogens within the FRT can inoculate the newborn through penetration of orifices and skin. Over the following week (and varying by pathogen), the pathogens are

able replicate until disease manifestations become clinically apparent. In the worst cases (HSV and Group B strep), encephalitis can lead to death of the newborn. If the infection status is suspected in the mother, the risk of peripartum transmission is almost nullified by appropriate antiviral and antibiotic regimens. The catch is that these approaches take on the order of days before these systemic drugs are able to reach the mucosal tissue where they can reduce pathogen burden in time for delivery. The current therapy standard also involves actively monitoring the newborn for signs of disease and delivering appropriate medicines, but this also requires prior awareness of motherly infection. Relevant pathogens in this regard are HIV, HSV, Group B strep, Dengue, and Hepatitis B.

It is also feasible that our approach could be incorporated in the context of an emergency 'rape kit'. In such a use, the administered mRNA could encode a cocktail of sexual transmitted infection diseases (ie HSV, Hep B, HIV, HPV) and include a spermicide to prevent fertilization.

3. Gene editing of the cervix for latent virus removal and cancer prevention

The recent advent of CRISPR/Cas9 as a flexible gene-editing platform has led to rapid scientific developments. The system is modular and does not require molecular evolution, as was the case with previous gene editing techniques, such as zinc fingers nucleases and TALENs. The platform is comprised of two components: 1) a set of core nucleases, the most popular being spCas9 (streptococcus pyogenes), that were discovered within bacteria as an adaptive means to combat phages; and 2) guideRNAs (gRNAs) that are complementary to specific sequences of genomic DNA. The Cas9 nuclease associates with gRNAs to form active ribonucleoproteins (RNP). These RNPs translocate to the nuclease. Once in the nucleus, complementary gRNA annealing allows Cas9 to create double stranded breaks in the genome. Subsequent inherent repair mechanisms lead to

insertions and deletions from the wild type genome. As a result, output from gene editing experiments is reported as % of InDels (standing for insertion-deletions).

We believe gene editing of the FRT mucosal could be leveraged to protect the cervix from *tumor developing mutations and/or remove latent virus* (HPV, HSV2, HIV). We will explore the use of aerosolized delivery as a gene-editing platform. As a topical note, CRISPR induced genetic mutations in rhesus macaques have been presented, but not published, to date.

REFERENCES

1. Wolff, J. A. *et al.* Direct gene transfer into mouse muscle in vivo. *Science* **247,** 1465–1468 (1990).
2. Geall, A. J. & Ulmer, J. B. Introduction to RNA-based vaccines and therapeutics. *Expert Rev. Vaccines* **14,** 151–152 (2015).
3. Sahin, U., Karikó, K. & Türeci, Ö. mRNA-based therapeutics — developing a new class of drugs. *Nat. Rev. Drug Discov.* **13,** 759–780 (2014).
4. Deering, R. P., Kommareddy, S., Ulmer, J. B., Brito, L. A. & Geall, A. J. Nucleic acid vaccines: prospects for non-viral delivery of mRNA vaccines. *Expert Opin. Drug Deliv.* **11,** 885–899 (2014).
5. Geall, A. J., Mandl, C. W. & Ulmer, J. B. RNA: The new revolution in nucleic acid vaccines. *Semin. Immunol.* **25,** 152–159 (2013).
6. Petsch, B. *et al.* Protective efficacy of in vitro synthesized, specific mRNA vaccines against influenza A virus infection. *Nat. Biotechnol.* **30,** 1210–1216 (2012).
7. Pardi, N. *et al.* Zika virus protection by a single low-dose nucleoside-modified mRNA vaccination. *Nature* **543,** 248–251 (2017).
8. DeFrancesco, L. The ‘anti-hype’ vaccine. *Nat. Biotechnol.* **35,** 193–197 (2017).
9. Alexopoulou, L., Czopik, A., Medzhitov, R. & Flavell, R. Recognition of double-stranded RNA and activation of NF-B by Toll-like receptor 3. *Nature* **413,** 732–8 (2001).
10. Karikó, K., Ni, H., Capodici, J., Lamphier, M. & Weissman, D. mRNA Is an Endogenous Ligand for Toll-like Receptor 3. *J. Biol. Chem.* **279,** 12542–12550 (2004).
11. Yoneyama, M. & Fujita, T. *Recognition of viral nucleic acids in innate immunity*. **20,** (2010).

12. Kindt, T. J., Goldsby, R. A., Osborne, B. A. & Kuby, J. *Kuby Immunology*. (Macmillan, 2007).
13. Pollard, C. *et al.* Type I IFN counteracts the induction of antigen-specific immune responses by lipid-based delivery of mRNA vaccines. *Mol. Ther. J. Am. Soc. Gene Ther.* **21,** 251–259 (2013).
14. De Beuckelaer, A. *et al.* Type I Interferons Interfere with the Capacity of mRNA Lipoplex Vaccines to Elicit Cytolytic T Cell Responses. *Mol. Ther. J. Am. Soc. Gene Ther.* **24,** 2012–2020 (2016).
15. Kirschman, J. L. *et al.* Characterizing exogenous mRNA delivery, trafficking, cytoplasmic release and RNA–protein correlations at the level of single cells. *Nucleic Acids Res.* **45,** e113 (2017).
16. Anderson, B. R. *et al.* Incorporation of pseudouridine into mRNA enhances translation by diminishing PKR activation. *Nucleic Acids Res.* **38,** 5884–5892 (2010).
17. Karikó, K. *et al.* Incorporation of pseudouridine into mRNA yields superior nonimmunogenic vector with increased translational capacity and biological stability. *Mol. Ther. J. Am. Soc. Gene Ther.* **16,** 1833–1840 (2008).
18. Andries, O. *et al.* N1-methylpseudouridine-incorporated mRNA outperforms pseudouridine-incorporated mRNA by providing enhanced protein expression and reduced immunogenicity in mammalian cell lines and mice. *J. Controlled Release* **217,** 337–344 (2015).
19. Svitkin, Y. V. *et al.* N1-methyl-pseudouridine in mRNA enhances translation through eIF2α-dependent and independent mechanisms by increasing ribosome density. *Nucleic Acids Res.* **45,** 6023–6036 (2017).

20. Verbeke, R. *et al.* Co-delivery of nucleoside-modified mRNA and TLR agonists for cancer immunotherapy: Restoring the immunogenicity of immunosilent mRNA. *J. Controlled Release* **266,** 287–300 (2017).

21. Reed, S. G., Orr, M. T. & Fox, C. B. Key roles of adjuvants in modern vaccines. *Nat. Med.* **19,** 1597–1608 (2013).

22. Fotin-Mleczek, M. *et al.* Messenger RNA-based Vaccines With Dual Activity Induce Balanced TLR-7 Dependent Adaptive Immune Responses and Provide Antitumor Activity: *J. Immunother.* **34,** 1–15 (2011).

23. Scheel, B. *et al.* Toll-like receptor-dependent activation of several human blood cell types by protamine-condensed mRNA. *Eur. J. Immunol.* **35,** 1557–1566 (2005).

24. Santangelo, P. J. *et al.* Single molecule-sensitive probes for imaging RNA in live cells. *Nat. Methods* **6,** 347–349 (2009).

25. Lifland, A. W., Zurla, C. & Santangelo, P. J. Single molecule sensitive multivalent polyethylene glycol probes for RNA imaging. *Bioconjug. Chem.* **21,** 483–488 (2010).

26. Lifland, A. W., Zurla, C., Yu, J. & Santangelo, P. J. Dynamics of native β-actin mRNA transport in the cytoplasm. *Traffic Cph. Den.* **12,** 1000–1011 (2011).

27. Alonas, E. *et al.* Combining single RNA sensitive probes with subdiffraction-limited and live-cell imaging enables the characterization of virus dynamics in cells. *ACS Nano* **8,** 302–315 (2014).

28. Jung, J., Lifland, A. W., Alonas, E. J., Zurla, C. & Santangelo, P. J. Characterization of mRNA-Cytoskeleton Interactions In Situ Using FMTRIP and Proximity Ligation. *PLoS ONE* **8,** (2013).

29. Jung, J., Lifland, A. W., Zurla, C., Alonas, E. J. & Santangelo, P. J. Quantifying RNA–protein interactions in situ using modified-MTRIPs and proximity ligation. *Nucleic Acids Res.* **41,** e12 (2013).

30. Zurla, C., Lifland, A. W. & Santangelo, P. J. Characterizing mRNA interactions with RNA granules during translation initiation inhibition. *PloS One* **6,** e19727 (2011).

31. Lifland, A. W. *et al.* RSV glycoprotein and genomic RNA dynamics reveal filament assembly prior to the plasma membrane. *Nat. Commun.* **8,** 667 (2017).

32. Loomis, K. H., Kirschman, J. L., Bhosle, S., Bellamkonda, R. V. & Santangelo, P. J. Strategies for modulating innate immune activation and protein production of in vitro transcribed mRNAs. *J. Mater. Chem. B* **4,** 1619–1632 (2016).

33. Groves, B. *et al.* Computing in mammalian cells with nucleic acid strand exchange. *Nat. Nanotechnol.* **11,** 287–294 (2016).

34. Halliday, A., Turner, J. D., Guimarães, A., Bates, P. A. & Taylor, M. J. The TLR2/6 ligand PAM2CSK4 is a Th2 polarizing adjuvant in Leishmania major and Brugia malayi murine vaccine models. *Parasit. Vectors* **9,** 96 (2016).

35. Cottalorda, A. *et al.* TLR2 engagement on CD8 T cells lowers the threshold for optimal antigen-induced T cell activation. *Eur. J. Immunol.* **36,** 1684–1693 (2006).

36. Geng, D. *et al.* Amplifying TLR-MyD88 signals within tumor-specific T cells enhances antitumor activity to suboptimal levels of weakly immunogenic tumor antigens. *Cancer Res.* **70,** 7442–7454 (2010).

37. Mercier, B. C., Cottalorda, A., Coupet, C.-A., Marvel, J. & Bonnefoy-Bérard, N. TLR2 engagement on CD8 T cells enables generation of functional memory cells in response to a suboptimal TCR signal. *J. Immunol. Baltim. Md 1950* **182,** 1860–1867 (2009).

38. Yang, Q. *et al.* TLR7 promotes Th1 polarization in immune thrombocytopenia. *Thromb. Res.* **128,** 237–242 (2011).

39. Misiak, A. *et al.* Addition of a TLR7 agonist to an acellular pertussis vaccine enhances Th1 and Th17 responses and protective immunity in a mouse model. *Vaccine* **35,** 5256–5263 (2017).

40. Hung, I. F. N. *et al.* Immunogenicity of intradermal trivalent influenza vaccine with topical imiquimod: a double blind randomized controlled trial. *Clin. Infect. Dis. Off. Publ. Infect. Dis. Soc. Am.* **59,** 1246–1255 (2014).

41. Van Hoeven, N. *et al.* A Formulated TLR7/8 Agonist is a Flexible, Highly Potent and Effective Adjuvant for Pandemic Influenza Vaccines. *Sci. Rep.* **7,** 46426 (2017).

42. Bagnoli, F. *et al.* Vaccine composition formulated with a novel TLR7-dependent adjuvant induces high and broad protection against Staphylococcus aureus. *Proc. Natl. Acad. Sci. U. S. A.* **112,** 3680–3685 (2015).

43. Wille-Reece, U. *et al.* HIV Gag protein conjugated to a Toll-like receptor 7/8 agonist improves the magnitude and quality of Th1 and CD8+ T cell responses in nonhuman primates. *Proc. Natl. Acad. Sci. U. S. A.* **102,** 15190–15194 (2005).

44. Berghaus, L. J. *et al.* Innate immune responses of primary murine macrophage-lineage cells and RAW 264.7 cells to ligands of Toll-like receptors 2, 3, and 4. *Comp. Immunol. Microbiol. Infect. Dis.* **33,** 443–454 (2010).

45. Warren, L. *et al.* Highly efficient reprogramming to pluripotency and directed differentiation of human cells using synthetic modified mRNA. *Cell Stem Cell* **7,** 618–630 (2010).

46. Sioud, M. Single-stranded small interfering RNA are more immunostimulatory than their double-stranded counterparts: A central role for 2′-hydroxyl uridines in immune responses. *Eur. J. Immunol.* **36,** 1222–1230 (2006).

47. Judge, A. *et al.* Potent and persistent *in vivo* anti-HBV activity of chemically modified siRNAs. *Nat. Biotechnol.* **23,** 1002 (2005).

48. Söderberg, O. *et al.* Characterizing proteins and their interactions in cells and tissues using the in situ proximity ligation assay. *Methods* **45,** 227–232 (2008).

49. Bhosle, S. M. *et al.* Unifying in vitro and in vivo IVT mRNA expression discrepancies in skeletal muscle via mechanotransduction. *Biomaterials* (2018). doi:10.1016/j.biomaterials.2018.01.010

50. Schett, G., Dayer, J.-M. & Manger, B. Interleukin-1 function and role in rheumatic disease. *Nat. Rev. Rheumatol.* **12,** 14–24 (2016).

51. Kanneganti, T.-D. *et al.* Critical Role for Cryopyrin/Nalp3 in Activation of Caspase-1 in Response to Viral Infection and Double-stranded RNA. *J. Biol. Chem.* **281,** 36560–36568 (2006).

52. Kumar, S., Anselmo, A. C., Banerjee, A., Zakrewsky, M. & Mitragotri, S. Shape and size-dependent immune response to antigen-carrying nanoparticles. *J. Controlled Release* **220,** 141–148 (2015).

53. Toy, R. & Roy, K. Engineering nanoparticles to overcome barriers to immunotherapy. *Bioeng. Transl. Med.* **1,** 47–62 (2016).

54. Pulendran, B. & Ahmed, R. Immunological mechanisms of vaccination. *Nat. Immunol.* **131,** 509–517 (2011).

55. Qin, L., Gilbert, P. B., Corey, L., McElrath, M. J. & Self, S. G. A Framework for Assessing Immunological Correlates of Protection in Vaccine Trials. *J. Infect. Dis.* **196,** 1304–1312 (2007).

56. Gilbert, P. B., Qin, L. & Self, S. G. Evaluating a surrogate endpoint at three levels, with application to vaccine development. *Stat. Med.* **27,** 4758–4778 (2008).

57. DeFrancesco, L. The ‘anti-hype’ vaccine. *Nature Biotechnology* (2017). doi:10.1038/nbt.3812

58. Lonez, C., Vandenbranden, M. & Ruysschaert, J.-M. Cationic lipids activate intracellular signaling pathways. *Adv. Drug Deliv. Rev.* **64,** 1749–1758 (2012).

59. Pollard, C. *et al.* Type I IFN counteracts the induction of antigen-specific immune responses by lipid-based delivery of mRNA vaccines. *Mol. Ther. J. Am. Soc. Gene Ther.* **21,** 251–259 (2013).

60. Petsch, B. *et al.* Protective efficacy of in vitro synthesized, specific mRNA vaccines against influenza A virus infection. *Nat. Biotechnol.* **30,** 1210–1216 (2012).

61. Pardi, N. *et al.* Zika virus protection by a single low-dose nucleoside-modified mRNA vaccination. *Nature* **543,** 248–251 (2017).

62. Benteyn, D., Heirman, C., Bonehill, A., Thielemans, K. & Breckpot, K. mRNA-based dendritic cell vaccines. *Expert Rev. Vaccines* **14,** 161–176 (2015).

63. Diken, M. *et al.* Selective uptake of naked vaccine RNA by dendritic cells is driven by macropinocytosis and abrogated upon DC maturation. *Gene Ther.* **18,** 702–708 (2011).

64. Broos, K. *et al.* Particle-mediated Intravenous Delivery of Antigen mRNA Results in Strong Antigen-specific T-cell Responses Despite the Induction of Type I Interferon. *Mol. Ther. - Nucleic Acids* **5,** e326 (2016).

65. Stoll, S., Delon, J., Brotz, T. M. & Germain, R. N. Dynamic Imaging of T Cell-Dendritic Cell Interactions in Lymph Nodes. *Science* **296,** 1873–1876 (2002).

66. van Aalst, S. *et al.* Routing dependent immune responses after experimental R848-adjuvated vaccination. *Vaccine* **36,** 1405–1413 (2018).

67. Frey, S. E. *et al.* Comparison of lyophilized versus liquid modified vaccinia Ankara (MVA) formulations and subcutaneous versus intradermal routes of administration in healthy vaccinia-naïve subjects. *Vaccine* **33,** 5225–5234 (2015).

68. Desigaux, L. *et al.* Self-assembled lamellar complexes of siRNA with lipidic aminoglycoside derivatives promote efficient siRNA delivery and interference. *Proc. Natl. Acad. Sci.* **104,** 16534–16539 (2007).

69. Habrant, D. *et al.* Design of Ionizable Lipids To Overcome the Limiting Step of Endosomal Escape: Application in the Intracellular Delivery of mRNA, DNA, and siRNA. *J. Med. Chem.* **59,** 3046–3062 (2016).

70. Colombani, T. *et al.* Self-assembling complexes between binary mixtures of lipids with different linkers and nucleic acids promote universal mRNA, DNA and siRNA delivery. *J. Controlled Release* **249,** 131–142 (2017).

71. Kirschman, J. L. *et al.* Characterizing exogenous mRNA delivery, trafficking, cytoplasmic release and RNA–protein correlations at the level of single cells. *Nucleic Acids Res.* **45,** e113–e113 (2017).

72. Alonas, E., Vanover, D., Blanchard, E., Zurla, C. & Santangelo, P. J. Imaging viral RNA using multiply labeled tetravalent RNA imaging probes in live cells. *Methods* **98,** 91–98 (2016).

73. Moses, W. W. Fundamental limits of spatial resolution in PET. *Nucl. Instrum. Methods Phys. Res. Sect. Accel. Spectrometers Detect. Assoc. Equip.* **648,** S236–S240 (2011).

74. Lu, F. & HogenEsch, H. Kinetics of the inflammatory response following intramuscular injection of aluminum adjuvant. *Vaccine* **31,** 3979–3986 (2013).

75. Calabro, S. *et al.* Vaccine adjuvants alum and MF59 induce rapid recruitment of neutrophils and monocytes that participate in antigen transport to draining lymph nodes. *Vaccine* **29,** 1812–1823 (2011).

76. Thomas, S. N., Rohner, N. A. & Edwards, E. E. Implications of Lymphatic Transport to Lymph Nodes in Immunity and Immunotherapy. *http://dx.doi.org.prx.library.gatech.edu/10.1146/annurev-bioeng-101515-014413* (2016). doi:10.1146/annurev-bioeng-101515-014413

77. Wood, K. J., Bushell, A. & Hester, J. Regulatory immune cells in transplantation. *Nat. Rev. Immunol.* **12,** nri3227 (2012).

78. Ford, M. L., Adams, A. B. & Pearson, T. C. Targeting co-stimulatory pathways: transplantation and autoimmunity. *Nat. Rev. Nephrol.* **10,** 14–24 (2014).

79. Liang, F. & Loré, K. Local innate immune responses in the vaccine adjuvant-injected muscle. *Clin. Transl. Immunol. Lond.* **5,** e74 (2016).

80. Liang, F. *et al.* Vaccine priming is restricted to draining lymph nodes and controlled by adjuvant-mediated antigen uptake. *Sci. Transl. Med.* **9,** eaal2094 (2017).

81. Fact sheet - Latest statistics on the status of the AIDS epidemic. Available at: http://www.unaids.org/en/resources/fact-sheet. (Accessed: 26th May 2018)

82. Brandenberg, O. F. *et al.* Predicting HIV-1 transmission and antibody neutralization efficacy in vivo from stoichiometric parameters. *PLOS Pathog.* **13,** e1006313 (2017).

83. Miller, W. C., Rosenberg, N. E., Rutstein, S. E. & Powers, K. A. Role of acute and early Hiv infection in the sexual transmission of Hiv. *Curr. Opin. Hiv Aids* **5,** 277–282 (2010).

84. Zimmerman, P. A. *et al.* Inherited Resistance to HIV-1 Conferred by an Inactivating Mutation in CC Chemokine Receptor 5: Studies in Populations with Contrasting Clinical Phenotypes, Defined Racial Background, and Quantified Risk. 14

85. Parrish, N. F. *et al.* Phenotypic properties of transmitted founder HIV-1. *Proc. Natl. Acad. Sci.* **110,** 6626–6633 (2013).

86. Asmal, M. *et al.* A Signature in HIV-1 Envelope Leader Peptide Associated with Transition from Acute to Chronic Infection Impacts Envelope Processing and Infectivity. *PLOS ONE* **6,** e23673 (2011).

87. Liu, A. *et al.* Differential Compartmentalization of HIV-Targeting Immune Cells in Inner and Outer Foreskin Tissue. *PLOS ONE* **9,** e85176 (2014).

88. Pandrea, I. *et al.* Paucity of CD4+ CCR5+ T Cells May Prevent Transmission of Simian Immunodeficiency Virus in Natural Nonhuman Primate Hosts by Breast-Feeding. *J. Virol.* **82,** 5501–5509 (2008).

89. Li, Q. *et al.* Glycerol monolaurate prevents mucosal SIV transmission. *Nature* **458,** 1034–1038 (2009).

90. Zhang, Z.-Q. *et al.* Roles of substrate availability and infection of resting and activated CD4+ T cells in transmission and acute simian immunodeficiency virus infection. *Proc. Natl. Acad. Sci.* **101,** 5640–5645 (2004).

91. Stieh, D. J. *et al.* Vaginal Challenge with an SIV-Based Dual Reporter System Reveals That Infection Can Occur throughout the Upper and Lower Female Reproductive Tract. *PLOS Pathog.* **10,** e1004440 (2014).

92. Monaco, D. C., Ende, Z. & Hunter, E. Virus-Host Gene Interactions Define HIV-1 Disease Progression. in *Viruses, Genes, and Cancer* 31–63 (Springer, Cham, 2017). doi:10.1007/82_2017_33

93. Barouch, D. H. *et al.* Rapid Inflammasome Activation following Mucosal SIV Infection of Rhesus Monkeys. *Cell* **165,** 656–667 (2016).

94. Shen, R. *et al.* Vaginal Myeloid Dendritic Cells Transmit Founder HIV-1. *J. Virol.* **88,** 7683–7688 (2014).

95. Banchereau, J. & Steinman, R. M. Dendritic cells and the control of immunity. *Nature* **392,** 245–252 (1998).

96. Yoshida, M. *et al.* Human Neonatal Fc Receptor Mediates Transport of IgG into Luminal Secretions for Delivery of Antigens to Mucosal Dendritic Cells. *Immunity* **20,** 769–783 (2004).

97. Bouvet, J. P., Bélec, L., Pirès, R. & Pillot, J. Immunoglobulin G antibodies in human vaginal secretions after parenteral vaccination. *Infect. Immun.* **62,** 3957–3961 (1994).

98. Rudin, A., Johansson, E.-L., Bergquist, C. & Holmgren, J. Differential Kinetics and Distribution of Antibodies in Serum and Nasal and Vaginal Secretions after Nasal and Oral Vaccination of Humans. *Infect. Immun.* **66,** 3390–3396 (1998).

99. Crowley-Nowick, P. A. *et al.* Normal Uterine Cervix: Characterization of Isolated Lymphocyte Phenotypes and Immunoglobulin Secretion. *Am. J. Reprod. Immunol.* **34,** 241–247

100. Zeng, M. *et al.* Mucosal Humoral Immune Response to SIVmac239Δnef Vaccination and Vaginal Challenge. *J. Immunol.* **196,** 2809–2818 (2016).

101. Drayton, D. L., Liao, S., Mounzer, R. H. & Ruddle, N. H. Lymphoid organ development: from ontogeny to neogenesis. *Nat. Immunol.* **7,** 344–353 (2006).

102. Fahrbach, K. M., Malykhina, O., Stieh, D. J. & Hope, T. J. Differential Binding of IgG and IgA to Mucus of the Female Reproductive Tract. *PLOS ONE* **8,** e76176 (2013).

103. Choi, R. Y. *et al.* Cervicovaginal HIV-1 Neutralizing IgA Detected among HIV-1-Exposed Seronegative Female Partners in HIV-1-Discordant Kenyan Couples. *AIDS Lond. Engl.* **26,** 2155–2163 (2012).

104. Tudor, D. *et al.* HIV-1 gp41-specific monoclonal mucosal IgAs derived from highly exposed but IgG-seronegative individuals block HIV-1 epithelial transcytosis and neutralize CD4+ cell infection: an IgA gene and functional analysis. *Mucosal Immunol.* **2,** 412–426 (2009).

105. Wang, Y.-Y. *et al.* IgG in cervicovaginal mucus traps HSV and prevents vaginal Herpes infections. *Mucosal Immunol.* **7,** 1036–1044 (2014).

106. Astronomo, R. D. *et al.* Neutralization Takes Precedence Over IgG or IgA Isotype-related Functions in Mucosal HIV-1 Antibody-mediated Protection. *EBioMedicine* **14,** 97–111 (2016).

107. Horwitz, J. A. *et al.* Non-neutralizing Antibodies Alter the Course of HIV-1 Infection In Vivo. *Cell* **170,** 637-648.e10 (2017).

108. Hessell, A. J. *et al.* Reduced Cell-Associated DNA and Improved Viral Control in Macaques following Passive Transfer of a Single Anti-V2 Monoclonal Antibody and Repeated Simian/Human Immunodeficiency Virus Challenges. *J. Virol.* **92,** e02198-17 (2018).

109. Lewis, G. K. *et al.* Beyond Viral Neutralization. *AIDS Res. Hum. Retroviruses* **33,** 760–764 (2017).

110. Freund, N. T. *et al.* Coexistence of potent HIV-1 broadly neutralizing antibodies and antibody-sensitive viruses in a viremic controller. *Sci. Transl. Med.* **9,** eaal2144 (2017).

111. Caskey, M. *et al.* Viraemia suppressed in HIV-1-infected humans by broadly neutralizing antibody 3BNC117. *Nature* **522,** 487–491 (2015).

112. Caskey, M. *et al.* Antibody 10-1074 suppresses viremia in HIV-1-infected individuals. *Nat. Med.* **23,** 185–191 (2017).

113. Scheid, J. F. *et al.* HIV-1 antibody 3BNC117 suppresses viral rebound in humans during treatment interruption. *Nature* **535,** 556–560 (2016).

114. Schoofs, T. *et al.* HIV-1 therapy with monoclonal antibody 3BNC117 elicits host immune responses against HIV-1. *Science* **352,** 997–1001 (2016).

115. Julg, B. *et al.* Protection against a mixed SHIV challenge by a broadly neutralizing antibody cocktail. *Sci. Transl. Med.* **9,** eaao4235 (2017).

116. Julg, B. *et al.* Protective Efficacy of Broadly Neutralizing Antibodies with Incomplete Neutralization Activity against Simian-Human Immunodeficiency Virus in Rhesus Monkeys. *J. Virol.* **91,** e01187-17 (2017).

117. Hessell, A. J. *et al.* Broadly Neutralizing Human Anti-HIV Antibody 2G12 Is Effective in Protection against Mucosal SHIV Challenge Even at Low Serum Neutralizing Titers. *PLOS Pathog.* **5,** e1000433 (2009).

118. Julg, B. *et al.* Virological Control by the CD4-Binding Site Antibody N6 in Simian-Human Immunodeficiency Virus-Infected Rhesus Monkeys. *J. Virol.* **91,** e00498-17 (2017).

119. Barouch, D. H. *et al.* Therapeutic efficacy of potent neutralizing HIV-1-specific monoclonal antibodies in SHIV-infected rhesus monkeys. *Nature* **503,** 224–228 (2013).

120. Shingai, M. *et al.* Antibody-mediated immunotherapy of macaques chronically infected with SHIV suppresses viraemia. *Nature* **503,** 277–280 (2013).

121. Nishimura, Y. *et al.* Early antibody therapy can induce long-lasting immunity to SHIV. *Nature* **543,** 559–563 (2017).

122. Gaudinski, M. R. *et al.* Safety and pharmacokinetics of the Fc-modified HIV-1 human monoclonal antibody VRC01LS: A Phase 1 open-label clinical trial in healthy adults. *PLOS Med.* **15,** e1002493 (2018).

123. Parren, P. W. H. I. *et al.* Antibody Protects Macaques against Vaginal Challenge with a Pathogenic R5 Simian/Human Immunodeficiency Virus at Serum Levels Giving Complete Neutralization In Vitro. *J. Virol.* **75,** 8340–8347 (2001).

124. Veazey, R. S. *et al.* Prevention of virus transmission to macaque monkeys by a vaginally applied monoclonal antibody to HIV-1 gp120. *Nat. Med.* **9,** 343–346 (2003).

125. Sherwood, J. K. Residence half-life of IgG administered topically to the mouse vagina. *Biol. Reprod.* **54,** 264–269 (1996).

126. Ensign, L. M., Hoen, T. E., Maisel, K., Cone, R. A. & Hanes, J. S. Enhanced vaginal drug delivery through the use of hypotonic formulations that induce fluid uptake. *Biomaterials* **34,** 6922–6929 (2013).

127. Acartürk, F. Mucoadhesive vaginal drug delivery systems. *Recent Pat. Drug Deliv. Formul.* **3,** 193–205 (2009).

128. Bonnet, J. *et al.* Chain and conformation stability of solid-state DNA: implications for room temperature storage. *Nucleic Acids Res.* **38,** 1531–1546 (2010).

129. Misset, J. Mucosal immunity of the female genital tract after HPV infection and vaccination. 28

130. Sharom, F. J. & Radeva, G. GPI-anchored Protein Cleavage in the Regulation of Transmembrane Signals. in *Membrane Dynamics and Domains* 285–315 (Springer, Boston, MA, 2004). doi:10.1007/978-1-4757-5806-1_9

131. Hessell, A. J. *et al.* Early short-term treatment with neutralizing human monoclonal antibodies halts SHIV infection in infant macaques. *Nat. Med.* **22,** 362–368 (2016).

132. Ensign, L. M., Cone, R. & Hanes, J. Nanoparticle-based drug delivery to the vagina: A review. *J. Controlled Release* **190,** 500–514 (2014).

133. Kong, R. *et al.* Improving Neutralization Potency and Breadth by Combining Broadly Reactive HIV-1 Antibodies Targeting Major Neutralization Epitopes. *J. Virol.* **89,** 2659–2671 (2015).

134. Doria-Rose, N. A. *et al.* HIV-1 Neutralization Coverage Is Improved by Combining Monoclonal Antibodies That Target Independent Epitopes. *J. Virol.* **86,** 3393–3397 (2012).

135. Bouvin-Pley, M. *et al.* Drift of the HIV-1 Envelope Glycoprotein gp120 toward Increased Neutralization Resistance over the Course of the Epidemic: a Comprehensive Study Using the Most Potent and Broadly Neutralizing Monoclonal Antibodies. *J. Virol.* **88,** 13910–13917 (2014).

136. Steinhardt, J. J. *et al.* Rational design of a trispecific antibody targeting the HIV-1 Env with elevated anti-viral activity. *Nat. Commun.* **9,** (2018).